Structures Research Report 2010/68901

University of Florida
Civil and Coastal Engineering

University of Florida
Civil and Coastal Engineering

UF

GATOR Engineering

University of Florida
Civil and Coastal Engineering

Final Report

Revised: **November 2010**
Original: **November 2009**

A Static Analysis Method for Barge-Impact Design of Bridges with Consideration of Dynamic Amplification

Principal investigators:
Gary R. Consolazio, Ph.D.

Research assistants:
Daniel J. Getter
Michael T. Davidson

Department of Civil and Coastal Engineering
University of Florida
P.O. Box 116580
Gainesville, Florida 32611

Sponsor:
Florida Department of Transportation (FDOT)
Marcus H. Ansley, P.E. – Project manager

Contract:
UF Project No. 00068901
FDOT Contract No. BD-545-85

DISCLAIMER

The opinions, findings, and conclusions expressed in this publication are those of the authors and not necessarily those of the State of Florida Department of Transportation.

Technical Report Documentation Page

1. Report No.	2. Government Accession No.	3. Recipient's Catalog No.

4. Title and Subtitle	5. Report Date
A Static Analysis Method for Barge-Impact Design of Bridges with Consideration of Dynamic Amplification	Original Nov. 2009; Revised Nov. 2010
	6. Performing Organization Code
	8. Performing Organization Report No.
7. Author(s) G. R. Consolazio, D. J. Getter, Michael T. Davidson	Original 2009/68901; Revised 2010/68901
9. Performing Organization Name and Address University of Florida Department of Civil & Coastal Engineering P.O. Box 116580 Gainesville, FL 32611-6580	10. Work Unit No. (TRAIS)
	11. Contract or Grant No. BD-545 RPWO 85
	13. Type of Report and Period Covered Final Report
12. Sponsoring Agency Name and Address Florida Department of Transportation Research Management Center 605 Suwannee Street, MS 30 Tallahassee, FL 32399-0450	14. Sponsoring Agency Code

15. Supplementary Notes

This report was originally published in November 2009 and was revised in November 2010. Included in the 2010 revisions are corrections to equation typesetting errors in Chapter 5 (report pgs. 55-58, 60-61, 63) and Appendix B (report pgs. B-3, B-4), and the addition of Appendices C and D. All 2010 revisions are indicated with a vertical bar in the left margin.

16. Abstract

Current practice with regard to designing bridge structures to resist impact loads associated with barge collisions relies upon the use of the American Association of State Highway and Transportation Officials (AASHTO) bridge design specifications. The AASHTO barge impact design provisions, which were developed from pendulum impact-hammer testing of reduced-scale barge models, employ a static analysis approach. However, recent studies have revealed that significant dynamic amplifications of structural demands (pier design forces) are produced as the result of mass-related inertial forces associated with the bridge superstructure. These same studies have also demonstrated that currently employed static analysis procedures fail to capture or account for such amplification effects.

In the present study, an equivalent static analysis procedure is developed for use in barge impact design and assessment of bridge structures. In contrast to the AASHTO static analysis procedure, the new method proposed here, called the static bracketed impact analysis (SBIA) method, employs static loading conditions and static structural analyses, but produces bridge design forces that conservatively approximate dynamic amplification effects associated with superstructure mass. Alternatively stated, the SBIA method produces bridge design forces that are equivalent to—or greater than—those that would be predicted using more refined dynamic time-domain methods such as the previously developed coupled vessel impact analysis (CVIA) method. Due to its simplicity, SBIA is particularly appropriate for situations involving preliminary design of bridges or the design of relatively regular bridge structures for which time-domain dynamic analysis is not warranted.

In this report, a detailed discussion of mass-related dynamic amplifications in bridges subjected to barge impact loading is presented. Based on insights gained through characterization of dynamic amplification modes, the static bracketed impact analysis (SBIA) method is developed and described in detail. A parametric study is then conducted using the SBIA method to demonstrate that conservative, dynamically amplified bridge design forces are produced.

17. Key Words	18. Distribution Statement
Barge, impact, collision, bridge pier, finite element analysis, dynamic analysis, time-domain analysis, equivalent static analysis, bridge design specifications, dynamic amplification	No restrictions.

19. Security Classif. (of this report)	20. Security Classif. (of this page)	21. No. of Pages	22. Price
Unclassified	Unclassified	126	

Form DOT F 1700.7 (8-72). Reproduction of completed page authorized

ACKNOWLEDGEMENTS

The authors would like to thank the Florida Department of Transportation (FDOT) for providing the funding that made this research project possible.

EXECUTIVE SUMMARY

Current practice with regard to designing bridge structures to resist impact loads associated with barge collisions relies upon the use of the American Association of State Highway and Transportation Officials (AASHTO) bridge design specifications. The AASHTO barge impact design provisions, which were developed from pendulum impact-hammer testing of reduced-scale barge models, employ a static analysis approach. However, recent studies have revealed that significant dynamic amplifications of structural demands (pier design forces) are produced as the result of mass-related inertial forces associated with the bridge superstructure. These same studies have also demonstrated that currently employed static analysis procedures fail to capture or account for such amplification effects.

In the present study, an equivalent static analysis procedure is developed for use in barge impact design and assessment of bridge structures. In contrast to the AASHTO static analysis procedure, the new method proposed here, called the static bracketed impact analysis (SBIA) method, employs static loading conditions and static structural analyses, but produces bridge design forces that conservatively approximate dynamic amplification effects associated with superstructure mass. Alternatively stated, the SBIA method produces bridge design forces that are equivalent to—or greater than—those that would be predicted using more refined dynamic time-domain methods such as the previously developed coupled vessel impact analysis (CVIA) method. Due to its simplicity, SBIA is particularly appropriate for situations involving preliminary design of bridges or the design of relatively regular bridge structures for which time-domain dynamic analysis is not warranted.

In this report, a detailed discussion of mass-related dynamic amplifications in bridges subjected to barge impact loading is presented. Based on insights gained through characterization of dynamic amplification modes, the static bracketed impact analysis (SBIA) method is developed and described in detail. A parametric study is then conducted using the SBIA method to demonstrate that conservative, dynamically amplified bridge design forces are produced.

TABLE OF CONTENTS

LIST OF FIGURES

LIST OF TABLES

CHAPTER 1
INTRODUCTION

1.1 Introduction

Design provisions such as the American Association of State Highway and Transportation Officials (AASHTO) *LRFD Bridge Design Specifications and Commentary* (2008) prescribe loading conditions that bridge structures must be adequately designed to resist. For bridges spanning over waterways that are navigable by barge traffic, design calculations and vulnerability assessment calculations must consider the combined effects of lateral barge impact loading and vertical gravity loading. Barge impact loading occurs when a moving barge flotilla (possessing initial kinetic energy) strikes a stationary bridge component (frequently a pier) and is rapidly redirected or brought to a stop. Given that kinetic energy affects the magnitudes of loads generated, barge collision events are fundamentally dynamic in nature. Dynamic sources of structural loading such as barge collision and earthquake loading are frequently assessed through the use of equivalent static loading conditions and static structural analysis. In the case of barge collision loading, the AASHTO bridge design provisions permit designers to use a simplified static analysis procedure to assess structural response in lieu of more complex fully dynamic methods.

As detailed in past research reports (Consolazio et al. 2006, Consolazio et al. 2008), the vessel collision components of the AASHTO bridge design provisions include a static barge impact load prediction procedure that is based on tests conducted by Meier-Dörnberg (1983). In the Meier-Dörnberg study, both static and dynamic-drop-hammer tests were performed on reduced scale models of barge bows to quantify impact loads. A key finding of the study was that no significant differences were observed between static and dynamic load tests. However, because the test procedures failed to include a moving barge striking a deformable bridge structure, dynamic amplification effects related to characteristics of the impacted bridge were omitted from the study.

To overcome the limitations of the Meier-Dörnberg study (i.e., reduced scale and omission of pier characteristics) a full-scale barge impact test program (Consolazio et al. 2006) was carried out on piers of the old St. George Island Causeway Bridge. The St. George Island test program involved impacting a full-scale tanker barge into three different bridge pier configurations, each having different structural characteristics. Over a series of eighteen (18) tests, conducted over a range of impact speeds, direct measurements of impact loads and corresponding bridge responses were made. Subsequently, detailed dynamic structural analyses were conducted, using the same impact conditions as those that were generated experimentally, on models of the bridge structure. The experimental test results and dynamic structural analysis results revealed that significant dynamic amplifications of bridge pier design forces were produced resulting from mass-related inertial restraint from the bridge superstructure. It was also demonstrated in this study that currently employed static analysis procedures do not capture amplification effects caused by the weight (mass) of the bridge superstructure.

In response to the discovery of superstructure-induced dynamic amplification effects, a follow-up study was conducted (Consolazio et al. 2008) to develop dynamic barge-bridge collision analysis procedures capable of accounting for such dynamic phenomena. A key result of this study was the development of a dynamic time-domain analysis procedure called coupled vessel impact analysis (CVIA) which numerically couples models of a barge, bridge

pier, foundation, soil, and superstructure. Dynamic amplifications due to inertial superstructure restraint are directly accounted for in this method through the inclusion of both superstructure (bridge deck) mass and stiffness. Used in conjunction with newly formulated barge crush curves (Consolazio et al. 2009) and a simplified bridge modeling procedure (Consolazio and Davidson 2008), both developed in the same research study, coupled vessel impact analysis permits bridge design forces to be quantified using a rational and accurate dynamic structural analysis procedure.

However, while the CVIA method balances accuracy with numerical efficiency, it is still a *time-history* analysis procedure. As such, analysis results such as impact loads, bridge displacements, and member forces are all functions of time that must be post-processed in order to identify maximum design values of interest. If a transient dynamic assessment of structural adequacy is needed, CVIA is an ideal solution. However, in many cases, a simpler, yet conservative, analysis method involving a small number of discrete load cases (as opposed to hundreds or thousands of time steps) is more desirable.

1.2 Objectives

The objectives of this study center on the development of an equivalent static analysis procedure for barge impact design and assessment of bridge structures. In contrast to the AASHTO static barge impact analysis procedure, the equivalent static method developed here employs static loading conditions and static structural analyses, but produces structural demands (design forces) that conservatively approximate dynamic amplification effects associated with superstructure mass. The new method is intended to produce design forces that are *equivalent* to—or greater than—those that would be predicted using more refined dynamic methods such as CVIA. Key objectives of this study are to ensure that the newly developed equivalent static analysis method is both simple to use, conservative, and capable of accounting for dynamic amplification. Such a method will be particularly appropriate for situations involving preliminary design of bridges (during which few structural details are available) or the design of relatively regular (non-lifeline) bridge structures for which the additional effort involved in conducting a time-history analysis is not warranted. An ideal bridge design process might involve the use of equivalent static analysis for preliminary design, followed by more refined time-history analysis (e.g., CVIA) to maximize safety and minimize costs.

1.3 Scope of work

- Development of bridge models: Finite element bridge models are developed for a representative set of bridges sampled from throughout the state of Florida. Each bridge model incorporates all necessary information that is needed to permit nonlinear static and nonlinear dynamic analyses to be performed. Nonlinearities are incorporated into the pier components, piles, soil, and the barge (in the case of dynamic analysis).
- Characterization of dynamic amplification effects: Each model in the bridge inventory is analyzed under both static and dynamic impact conditions. Dynamic amplification levels are then numerically quantified by comparing dynamic to static predictions of pier design forces.

- Development of an equivalent static analysis method: Using insights gained through characterization of dynamic amplification effects, an equivalent static analysis procedure called static bracketed impact analysis (SBIA) is developed. The SBIA method utilizes two static analysis load cases to bracket (envelope) pier element design forces in such a manner that dynamic amplification effects are conservatively approximated.
- Demonstration parametric study: A comprehensive parametric study is conducted using the SBIA method and two types of superstructure modeling. Parametric study results demonstrate the level of conservatism of the simplified static method relative to more refined dynamic CVIA analyses.

CHAPTER 2
BACKGROUND

2.1 Review of the current AASHTO load determination procedure

For bridges that span over navigable waterways, the design specifications used in the United States include the *American Association of State Highway and Transportation Officials* (AASHTO) *Guide Specification and Commentary for Vessel Collision Design of Highway Bridges* (AASHTO 2009) and the *AASHTO* Load and Resistance Factor Design (*LRFD) Bridge Design Specifications and Commentary* (AASHTO 2008). These documents, collectively referred to as the "AASHTO provisions" in this report, use an empirical load calculation procedure based upon an experimental study conducted by Meier-Dörnberg (1983).

Meier-Dörnberg conducted both static and dynamic impact tests on reduced-scale European Type IIa barge bow sections. The European type IIa barge is similar in size and configuration to the jumbo hopper barges widely used throughout the United States. Two dynamic tests, using 2-ton pendulum hammers and two different shapes of impact head, were conducted on 1:4.5-scale stationary (i.e., fixed) barge bows. One dynamic test involved three progressive impacts using a cylindrical hammer with a diameter of 67.0 in., whereas the other involved three progressive impacts using a 90° pointed hammer. A static test was also conducted on a 1:6 scale barge bow using a 90.6 in. hammer. Results obtained from the dynamics tests are shown in Figures 2.1a-b and results from the static test are shown in Figure 2.1c.

Using the experimental data collected, Meier-Dörnberg developed mathematical relationships between kinetic energy (E_B), inelastic barge deformation (a_B), and dynamic and static force (P_B and $\overline{P}_B$ respectively). These relationships are illustrated in Figure 2.2. As the figure suggests, no major differences were found between the magnitude of dynamic and static impact force. However, this observation was strongly influenced by the stationary barge bow configuration used in the testing. Omission of a flexible impact target and the corresponding barge-pier interaction necessarily precludes the ability to measure and capture dynamic amplification effects.

Also, inelastic barge bow deformations were measured in the Meier-Dörnberg study. Results showed that once barge bow yielding was initiated, at approximately 4 in. of deformation (a_B), the stiffness of the bow diminishes significantly (see Figure 2.2). Additionally, Meier-Dörnberg recognized that inelastic bow deformations represent a significant form of energy dissipation during collision events.

In the development of the AASHTO barge impact design provisions, the relationships between initial barge kinetic energy (KE), barge deformation (a_B) and equivalent static force (P_B) developed by Meier-Dörnberg, were adopted with minimal modifications:

$$KE = \frac{C_H W V^2}{29.2} \tag{2.1}$$

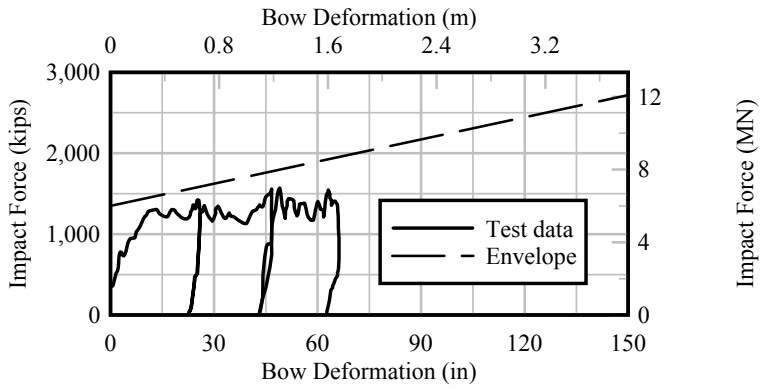

(a)

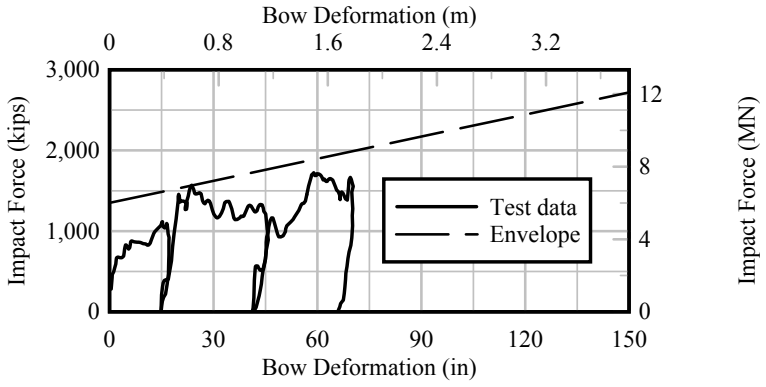

(b)

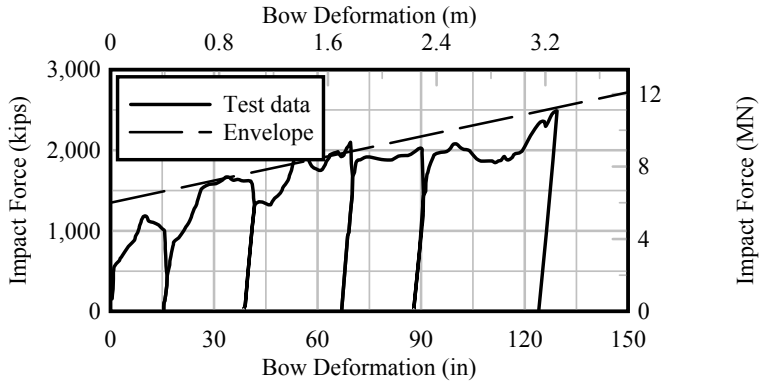

(c)

Figure 2.1 Force-deformation results obtained by Meier-Dörnberg (Adapted from Meier-Dörnberg 1983): a) Results from dynamic cylindrical impact hammer test, b) Results from dynamic 90° pointed impact hammer test, and c) Results from static impact hammer test

$$a_B = \left[\left(1 + \frac{KE}{5672}\right)^{1/2} - 1\right]\frac{10.2}{R_B} \tag{2.2}$$

$$P_B = \begin{cases} 4112 a_B R_B & \text{if } a_B < 0.34 \\ (1349 + 110 a_B) R_B & \text{if } a_B \geq 0.34 \end{cases} \tag{2.3}$$

In equations 2.1 - 2.2 KE is the barge kinetic energy (kip-ft), C_H is the hydrodynamic mass coefficient, W is the vessel weight (in tonnes where 1 tonne = 2205 lbs.), V is the impact speed (ft/sec), and $R_B = B_B/35$ where B_B is the width of the barge (ft). The only notable difference between the expressions developed by Meier-Dörnberg and the AASHTO expressions, given above as Eqn. 2.1 - 2.3, is the use of a barge width correction factor (R_B). While the AASHTO specification utilizes the R_B term to reflect the influence of barge width, no such factor has been included to account for variations in either the size (width) or geometric shape of the bridge pier being impacted.

Note that Eqn. 2.3 is a barge force-deformation relationship (i.e., a "crush curve") that relates static barge impact force P_B to barge deformation a_B. The AASHTO barge crush model (Eqn. 2.3) is illustrated graphically in Figure 2.3 for a hopper barge having a width B_B=35 ft and therefore an R_B= 1.

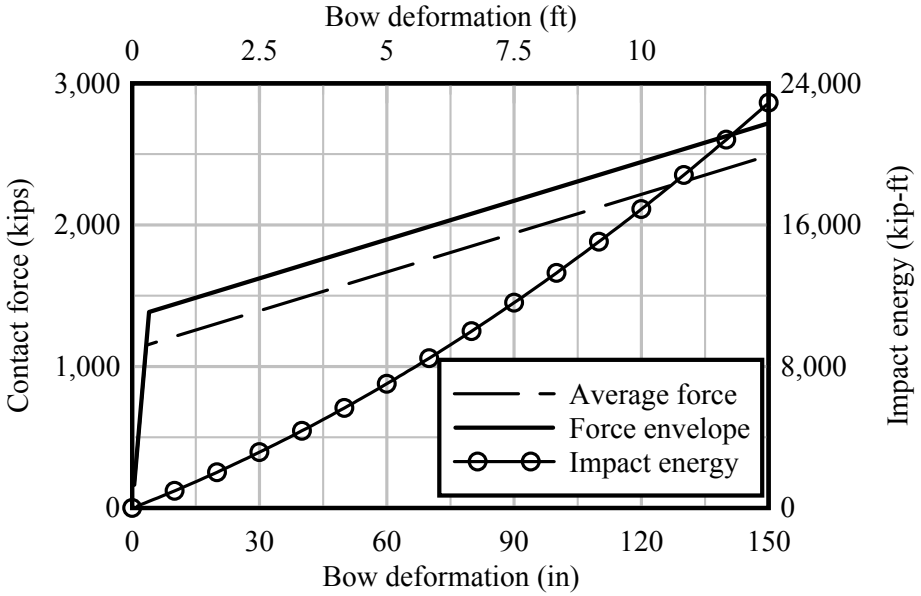

Figure 2.2 Relationships developed from experimental barge impact tests conducted by Meier-Dörnberg (1983) (Adapted from AASHTO 1991)

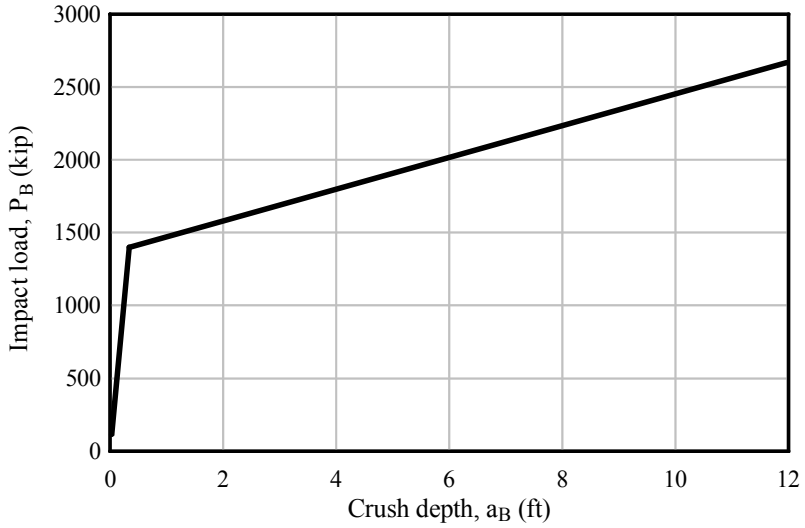

Figure 2.3 AASHTO relationship between barge crush depth and impact force

2.2 Updated barge bow force-deformation relationships

For dynamic structural analysis purposes, barge response during impact events may be characterized by appropriate force-deformation relationships (crush curves) that describe nonlinear stiffness of the affected vessel portions. As discussed above, development of the AASHTO crush curve (shown in Figure 2.3) relied upon scale model crushing tests. These experiments, however, were carried out using reduced-scale barge models of European, pontoon-style construction, not typical of vessels navigating waterways in the United States.

To address these limitations, a study was conducted (Consolazio et al. 2008, Consolazio et al. 2009) to characterize barge bow crushing behavior. High-resolution finite element models of the bow sections of two common U.S. barge types—a jumbo hopper barge and an oversize tanker barge—were developed using structural drawings. Over 120,000 elements were used to model each barge bow. During analysis, the barge bow models were subjected to crushing by a wide variety of impactor shapes and sizes. Specifically, both round and flat-faced impact surfaces were employed in the simulations, with impactor sizes ranging from 1 ft. to 35 ft.

Force-deformation relationships obtained from a multitude of simulations (a typical case is illustrated in Figure 2.4) were used to form an updated set of design force-deformation relationships for barge bows. The study yielded the following findings:

- For typical design scenarios (head-on impact conditions), barge bow force-deformation can be idealized as an elastic, perfectly-plastic relationship. Recall from Figure 2.3 that the AASHTO impact force continues to increase with increasing deformation. The simulations conducted by Consolazio et al. (2008) did not exhibit post-yield hardening behavior. The AASHTO curve and a typical UF curve are compared in Figure 2.5.
- Due to the high degree of uniformity in barge internal structural configurations (Cameron et al. 1997), impact forces are not sensitive to the width of the barge. The AASHTO provisions employ a barge width correction factor, R_B, to account for vessels with widths

other than 35 feet. However, for a given pier shape and width, the finite element crushing simulations revealed no substantial differences between forces produced by crushing a 35-foot wide jumbo hopper barge and crushing a 50-foot wide tanker barge.

- Maximum collision force is dependent, in part, on the shape of the impacted pier surface. The AASHTO crush model does not account for impact surface geometry; however, the finite element crushing simulations indicate that rounded pier surfaces, as opposed to flat-faced impact surfaces, provide an effective means of mitigating the forces generated during barge impact events.
- Maximum barge impact force is related to the width of the impacted pier surface, particularly for flat-faced rectangular piers.

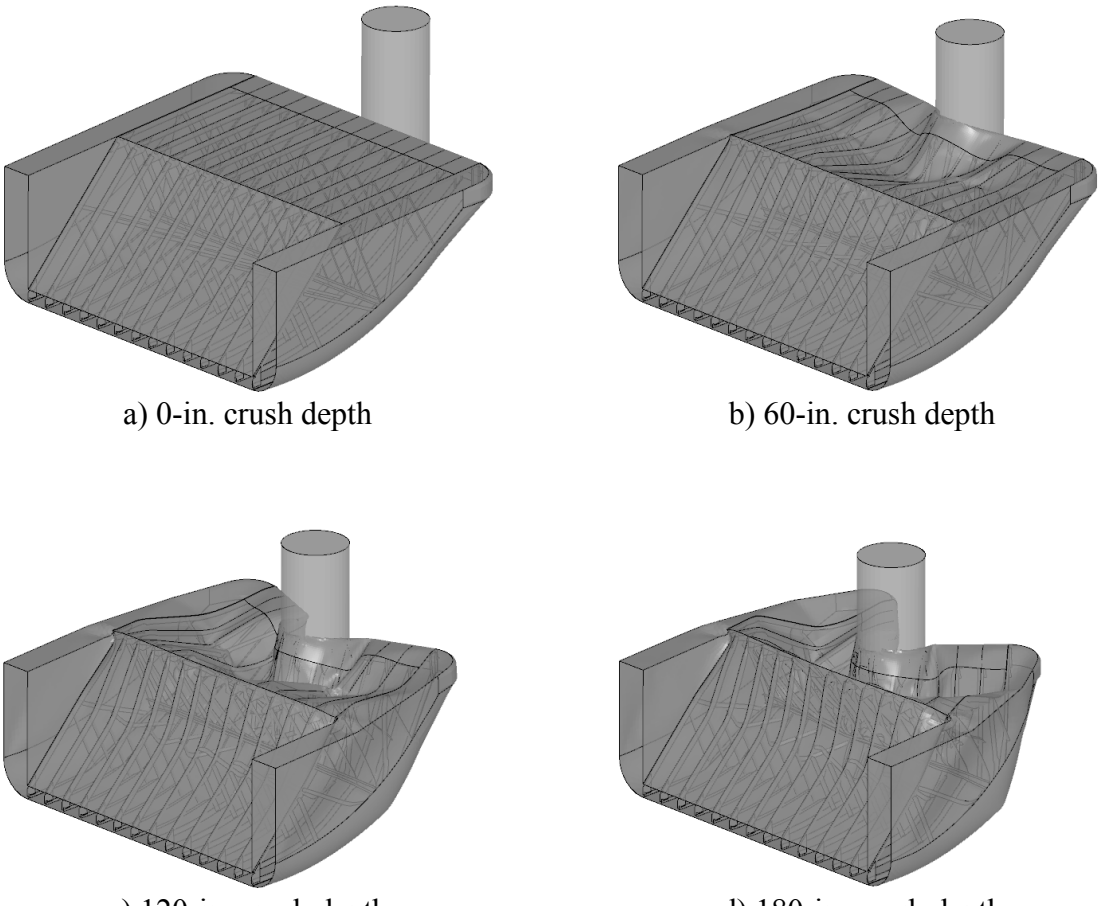

a) 0-in. crush depth

b) 60-in. crush depth

c) 120-in. crush depth

d) 180-in. crush depth

Figure 2.4 Finite element simulation of barge bow crushing:
6 ft diameter round impact with jumbo hopper barge bow

Based on these findings, design barge bow force-deformation relationships were developed (the formulation of these equations and an algorithm for determining the appropriate crush model for a given design scenario are detailed in Consolazio et al. 2008). Additional simulations that were subsequently conducted by Consolazio et al. (2009) resulted

in minor changes being made to the proposed crush curves. The revised barge crush-model (force-deformation behavior) is shown in Figure 2.6 and is used throughout the remainder of this study.

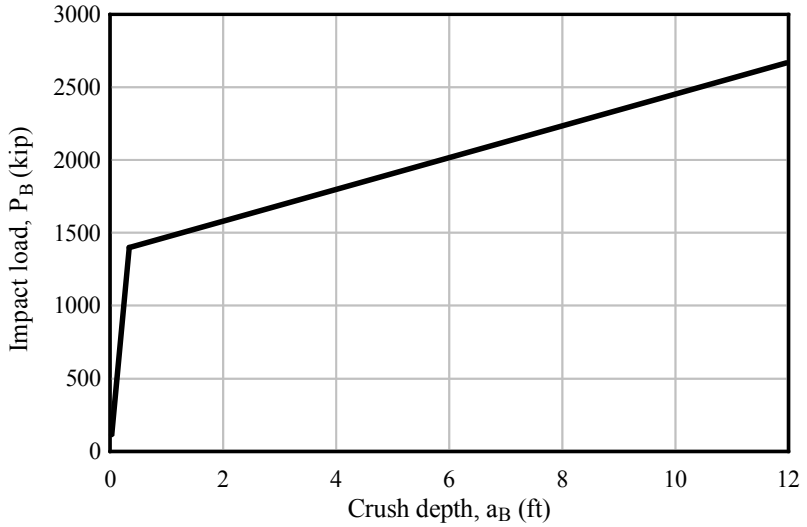

a) AASHTO crush curve (independent of impact surface characteristics)

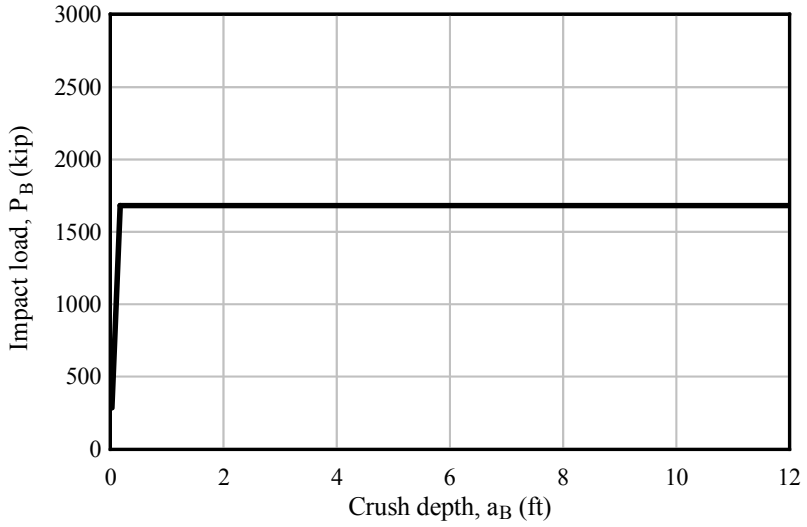

b) UF barge crush curve for 6-foot diameter round impact surface

Figure 2.5 Barge bow force-deformation relationships

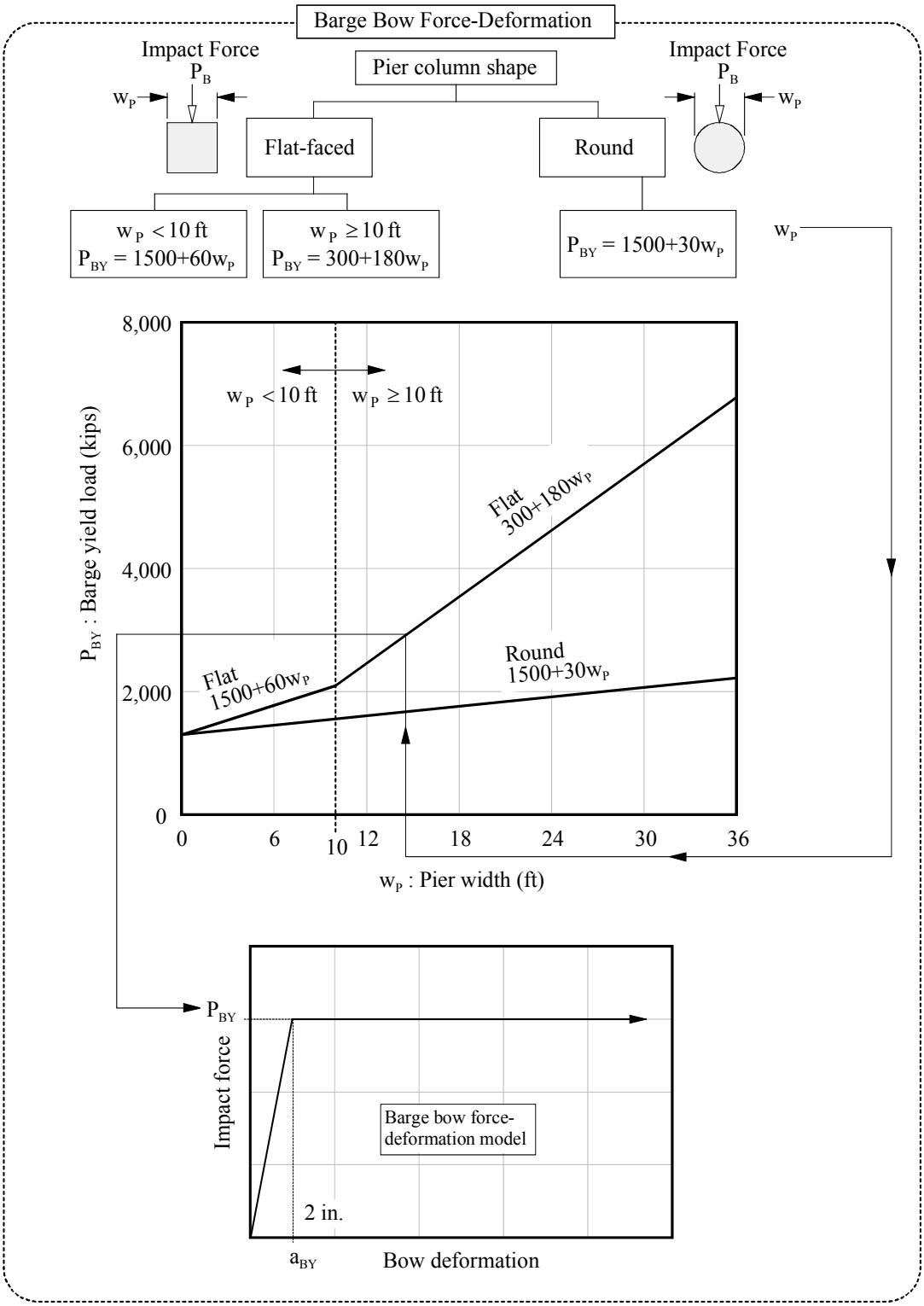

Figure 2.6 Barge bow force-deformation flowchart

2.3 Coupled vessel impact analysis (CVIA)

Coupled vessel impact analysis (CVIA) involves coupling (linking) a single degree of freedom (SDOF) nonlinear dynamic barge model to a multi-degree of freedom (MDOF) nonlinear dynamic bridge analysis code. The term coupled refers to the use of a shared contact force between the barge and impacted bridge structure (Figure 2.7). The impacting barge is defined by a mass, initial velocity, and bow force-deformation (crush) relationship. Traveling at a prescribed initial velocity, the barge impacts a specified location on the bridge structure and generates a time-varying impact force in accordance with the crush curve of the barge and the relative displacements of the barge and bridge model at the impact location. The MDOF bridge model (pier, superstructure, and soil) is subjected to the time-varying dynamic impact force and consequently displaces, develops internal forces, and interacts with the SDOF barge model through the shared impact force.

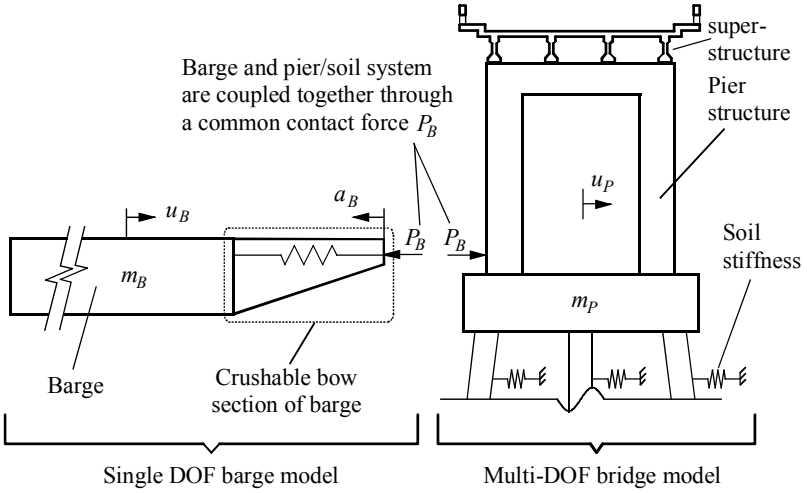

Figure 2.7 Coupling between barge and bridge in CVIA

The CVIA algorithm has been documented in detail in a number of previous publications (Consolazio and Davidson 2008; Consolazio and Cowan 2005; Consolazio et al. 2008) and has been implemented in the commercial pier analysis software package FB-MultiPier (2009). Since barge, pier, and superstructure stiffness and mass related forces are all included in CVIA, the method is able to accurately predict pier and substructure design forces under dynamic barge impact conditions. CVIA has been validated against full-scale experimental impact data (Consolazio and Davidson 2008) and presently constitutes a state-of-the-art computational tool for barge-bridge collision analysis when numerical efficiency is paramount. Because the CVIA procedure can accurately capture dynamic amplifications of pier design forces due to superstructure inertial effects, it is used throughout this study when dynamic assessments of structural demand are required.

CHAPTER 3
MODELING AND ANALYSIS PROCEDURES

3.1 Introduction

To maximize the accuracy and computational efficiency of the coupled vessel impact analyses conducted in this study, several modeling and analysis procedures were employed, and, in selected cases, new features were developed and implemented into the FB-MultiPier pier analysis code (FB-MultiPier 2007). FB-MultiPier can be used to perform linear or nonlinear, static or dynamic analyses on single pier models or full bridge (multi-pier, multi-span) models. As illustrated in Figure 3.1, FB-MultiPier bridge models generally contain the following components:

- Superstructure: Modeled using resultant frame elements with linear elastic material behavior (Section 3.2)
- Bridge pier: Modeled using cross-section integrated frame elements in conjunction with nonlinear kinematic and constitutive material models (Section 3.3.1)
- Pile cap: Modeled using thick shell elements with linear elastic material behavior
- Foundation: Modeled using cross-section integrated frame elements in conjunction with nonlinear kinematic and constitutive material models (Section 3.3.1)
- Soil: Modeled using nonlinear discrete spring elements, distributed along each embedded foundation element (Section 3.3.2)

Although FB-MultiPier has the ability to directly analyze full multi-span, multi-pier bridge structures, in this study, one-pier two-span (OPTS) bridge models were used instead to increase computational efficiency (Consolazio and Davidson 2008).

3.2 Superstructure

In an FB-MultiPier bridge model, the superstructure is represented using a series of linear-elastic resultant frame elements. As a result, the girders, deck, and other superstructure features are considered to act compositely during inter-pier force transmission. Rigid elements and multi-degree of freedom springs are used to connect the primary superstructure elements to each pier. The superstructure modeling capabilities of FB-MultiPier enable important dynamic interactions between bridge piers.

3.2.1 OPTS modeling

The most accurate numerical representation of a bridge structure involves analyzing a *full* bridge model with multiple-piers and multiple-spans. However, the required computation time for such an analysis can be prohibitive when transient dynamic analytical techniques are employed. Dynamic time-history analysis of barge-bridge collision events involves analyzing hundreds or thousands of time steps, which may require several hours using a typical desktop or notebook computer. Two potential strategies can be employed to reduce computation time:

a reduction of the number of time steps or a reduction of the number of model degrees-of-freedom (DOF).

Simulation duration and accuracy considerations dictate the number of time steps required for an analysis. Typically, a two to five-second simulation is necessary to capture barge collision loading and the ensuing bridge response. In addition, attempting to decrease computation time by increasing the time step size can lead to numerical instability or loss of accuracy (Tedesco et al. 1999). Thus, the number of time steps for a given collision simulation is effectively fixed.

For this study, improved computational efficiency was instead achieved by reducing the number of model DOF. Multiple-pier bridge representations were simplified into one-pier two-span (OPTS) models using a technique developed by Consolazio and Davidson (2008). The OPTS procedure involves removing all piers adjacent to the pier of interest (referred to as the left and right-flanking structures) and replacing these extraneous portions with a system of equivalent springs and lumped masses. The simplified, or OPTS, structure (shown in Figure 3.2) consists of a pier of interest (impact pier), two adjacent bridge spans, and a condensed representation of the flanking structures.

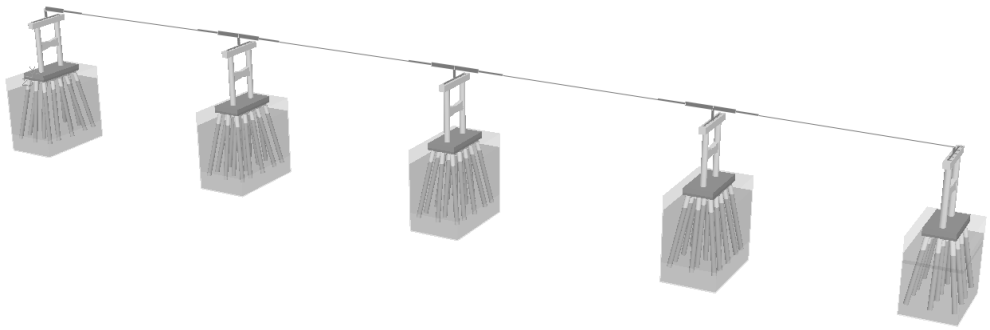

a) Rendering of physical structure

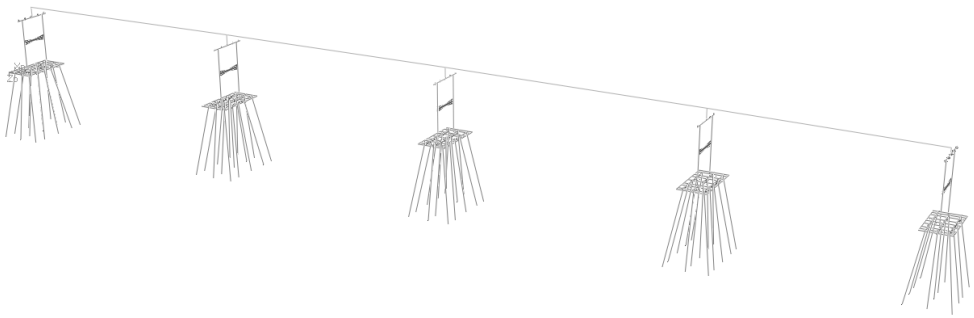

b) Finite element representation

Figure 3.1 Full-bridge modeling in FB-MultiPier

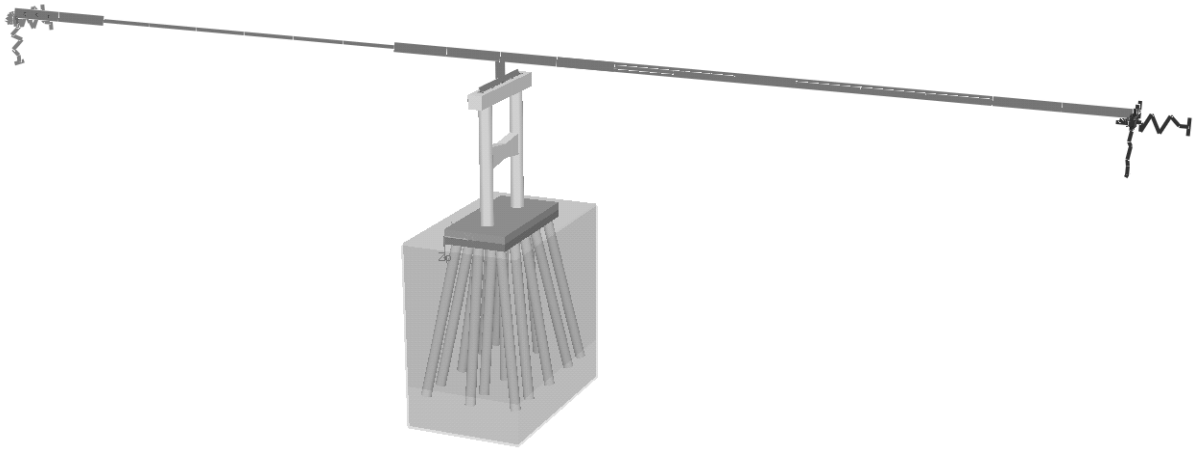

a) Rendering of physical structure

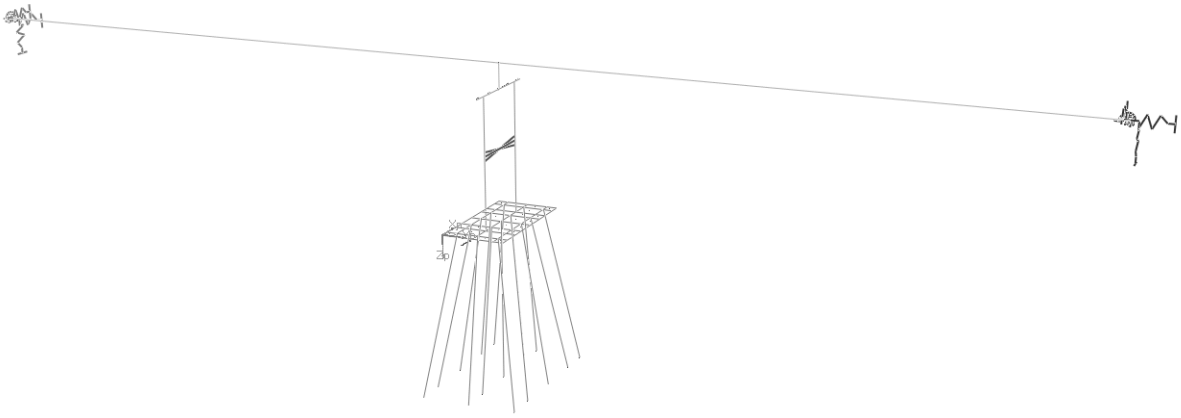

b) Finite element representation

Figure 3.2 One-pier two-span (OPTS) numerical modeling in FB-MultiPier

To condense piers and spans outside of the OPTS model, the left and right-flanking structures are first isolated from the OPTS system. In Figure 3.3, the left-flanking structure consists of piers P-1, P-2, and P-3, and the right-flanking structure consists of piers P-5, P-6, and P-7. Once isolated, a shear load is applied to the piers directly adjacent to the impact pier (piers P-3 and P-5 in Figure 3.3) at each point of disconnect between the flanking structures and the OPTS model. To account for potential nonlinearity in the flanking structures, the applied shear loads should be similar in magnitude to the total bearing shears expected from the vessel collision event being considered (Consolazio et al. 2008).

The stiffness condensation procedure proposed by Consolazio et al. (2008) involves applying loads (or moments) in all six DOF to form a full 6x6 flexibility matrix. A stiffness matrix is formed by inverting the flexibility matrix, and then diagonalized by discarding the off-diagonal terms. However, it was observed that the DOF commonly exhibit linear independence, making a full matrix inversion unnecessary, hence stiffness values were calculated by direct inversion for the purposes of this study.

The transverse stiffness of each flanking structure is calculated by dividing the applied shear force by the resulting transverse displacement of the loaded pier at the same DOF. Similarly, the rotational stiffness of each flanking structure is assessed by applying a unit moment (in a separate load case) and dividing the moment by its corresponding rotation. The condensed stiffness at other degrees of freedom (i.e., longitudinal stiffness) is obtained in a similar fashion—a unit force or moment is applied, and then the load is divided by the corresponding displacement. Once each stiffness value is quantified, the stiffness contribution of each flanking structure can be replaced by a combination of translational and rotational linear springs. In this study, equivalent springs were developed for all six DOF (translations and rotations).

In addition to the stiffness considerations, mass-related inertial effects of the flanking structures must also be incorporated into the OPTS model. Consolazio and Davidson (2008) assumed that the mass of only one-half of each of the bridge spans flanking the OPTS system contribute to the dynamic response of the impacted pier. As a result, the mass of each of these half-spans is lumped at the ends of the OPTS model spans. The lumped mass formulation procedure is illustrated in Figure 3.4.

Since the resulting OPTS model contains significantly fewer degrees of freedom than the corresponding full-bridge model, the required analysis time is greatly reduced. Consolazio et al. (2008) showed that OPTS-CVIA simulation of typical bridges required between 15 and 30 minutes of analysis time, less than 15% of the time required for respective full-resolution (full-bridge) simulations. In addition, the accuracy of design force predictions was maintained. Using OPTS models, pier member demands (shears and moments) generally differed by less than 3% when compared to multiple-pier analyses. Since the OPTS technique can dramatically reduce computation time while maintaining accurate response predictions, this modeling procedure was used throughout the current study.

3.2.2 Modeling substructure-superstructure interface

The use of linear resultant frame elements for superstructure modeling in FB-MultiPier necessitates the inclusion of additional elements to correctly distribute forces to the bearing locations of underlying piers. More specifically, intermediate superstructure elements are employed to approximate the effect of the physical footprint of the superstructure and its interaction with the pier.

As illustrated in Figure 3.5, the superstructure-substructure interface model consists of four primary parts—a rigid vertical link, a rigid horizontal transfer beam, bearing springs, and horizontal bearing offset rigid links. The vertical link is used to produce the correct relative height between the superstructure center of gravity and centerline of the pier cap beam. This distance can be quite large (reaching heights greater than 10 ft), especially for bridges with long-span haunched girders or box-girder superstructures. A horizontal transfer beam, connected to the vertical link, serves to distribute superstructure load to physical bearing pad positions. For piers with two bearing rows, additional horizontal rigid elements act to offset the bearing locations from the pier cap centerline.

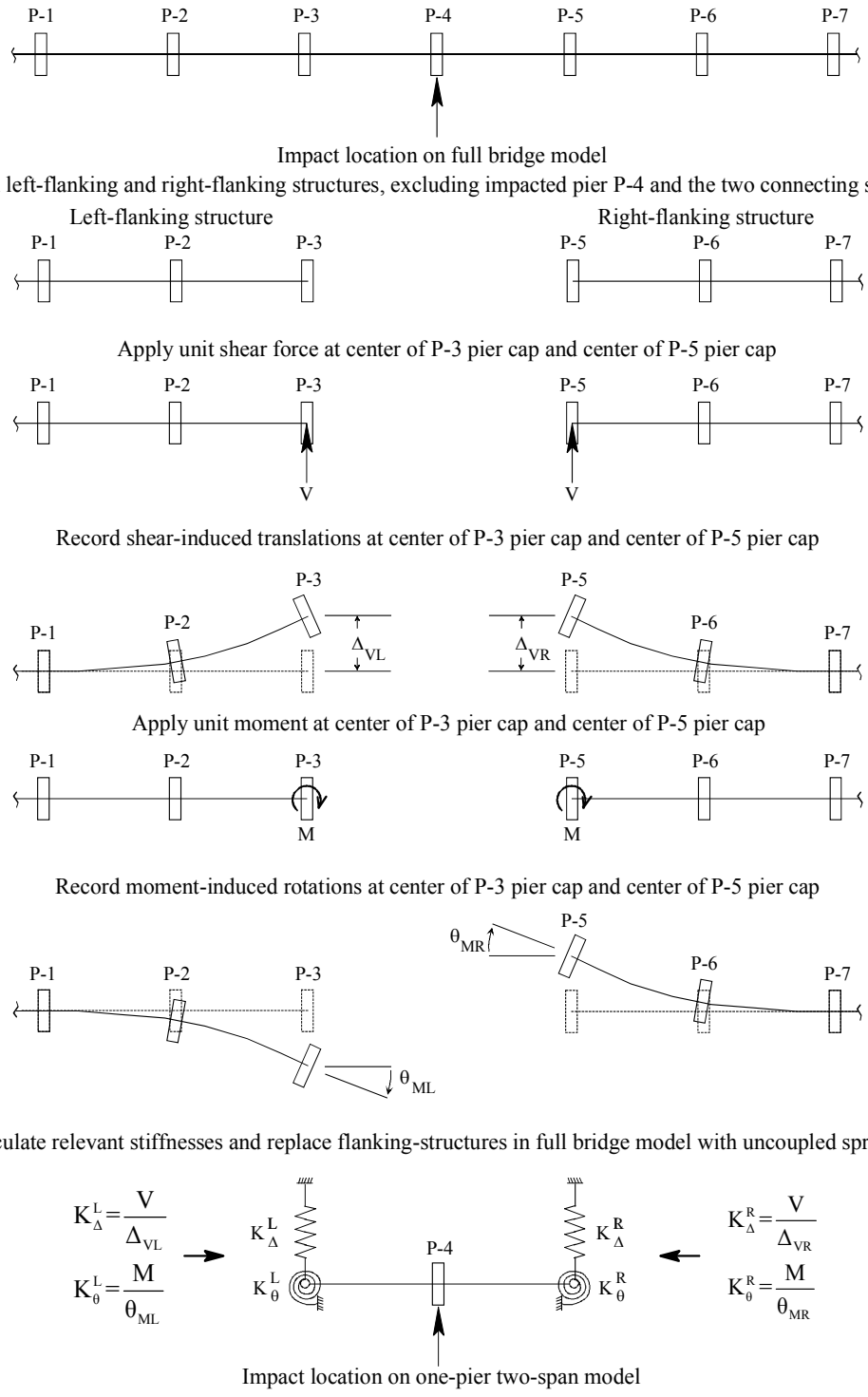

Figure 3.3 Plan view of multiple-pier numerical model and formulation of equivalent springs for OPTS model

Bearing pad elements are modeled as discrete stiffnesses. Arbitrary, nonlinear load-deformation relationships can be associated with each bearing DOF, providing the ability to model complex hyperelastic material behavior or finite-width gapping. For the purposes of this research, this level of model sophistication was unwarranted. However, the use of non-rigid load-deformation relationships for these elements did provide a more realistic representation of bearing behavior when compared to constraint-based pin or roller supports. Therefore, empirical load-deformation relationships, as opposed to infinitely stiff bearing conditions, were employed for these model components.

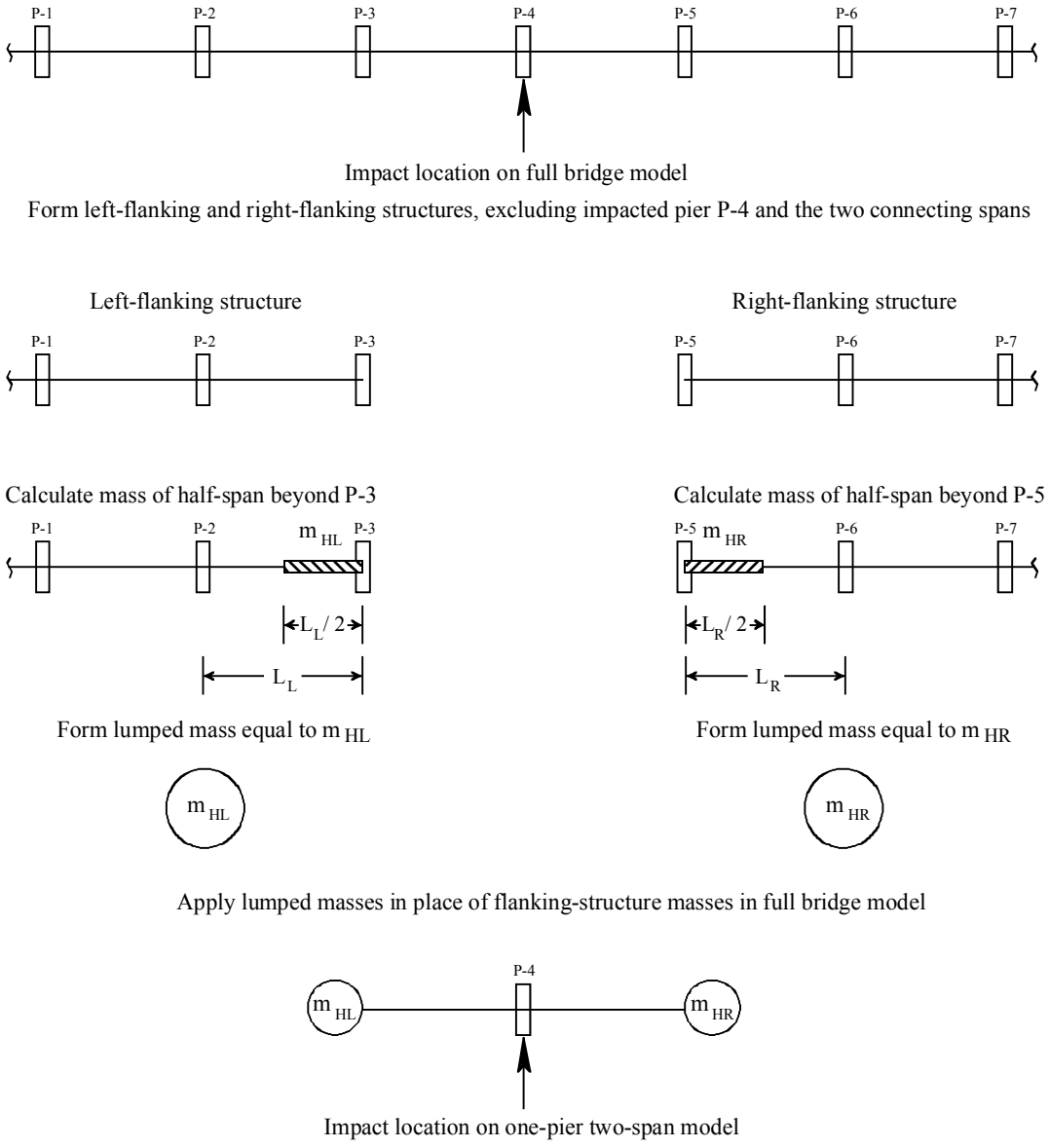

Figure 3.4 Plan view of multiple-pier numerical model and location of lumped masses for OPTS model

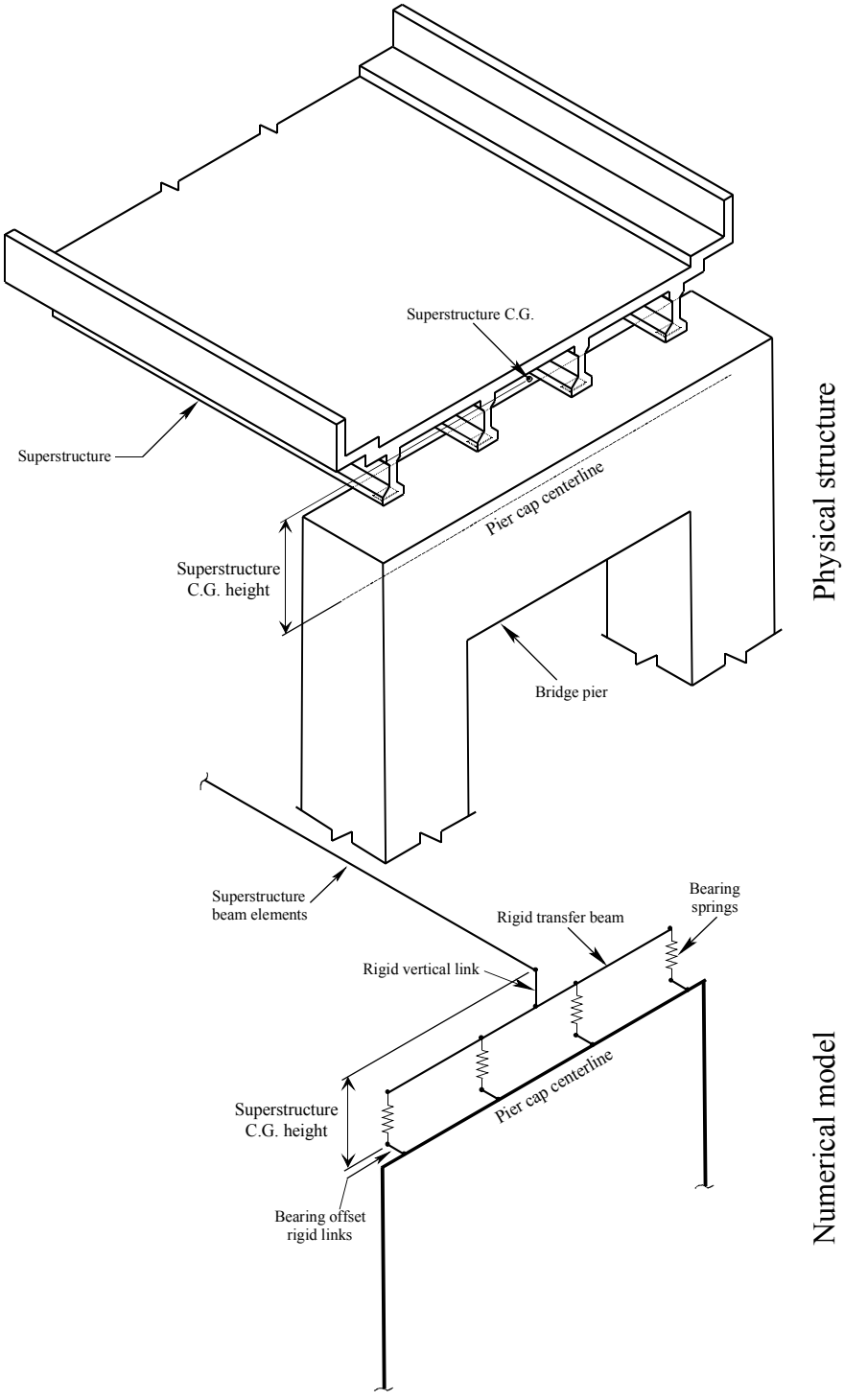

Figure 3.5 Overview of superstructure model configuration in FB-MultiPier

In the course of conducting this study, it was observed that constraint-based (pin or roller) bearing conditions led to erratic distribution of bearing loads. For example, when constraints were employed, vertical bearing reactions under gravity loading could consist of widely varying compression and tension forces. For analysis cases where constraint-based bearing conditions were employed, the sum of vertical bearing reactions was consistently found to be statically equal to the superstructure dead load, however, the conspicuous load distribution led to undesired localized member force concentrations and erroneous deformation patterns.

To alleviate this problem, finite stiffness values were prescribed for each bearing spring DOF to simulate more realistic bearing conditions. To accomplish this, bridge models with constrained bearing conditions were first statically subjected to loading conditions similar to those associated with respective vessel impact events of interest. The stiffness of the rigid springs was incrementally reduced until the total bearing reaction was evenly distributed among the bearing elements. During this process, care was taken not to overly soften the bearing springs, as this would reduce the overall rigidity of the superstructure-substructure interface. Reducing the relative stiffness of the superstructure system could cause a larger portion of the vessel impact load to travel through the foundation, as opposed to the superstructure, resulting in unconservative pier column demand predictions. With this concern in mind, it was confirmed that the sum of the non-rigid bearing forces compared well with the sum of the constraint-associated bearing forces. Consequently, it was observed that the softened bearings afforded a uniform distribution of bearing forces to the pier while maintaining comparable superstructure rigidity.

3.3 Substructure

Bridge substructures, as modeled in this study, consist of an OPTS superstructure model combined with one or more pier columns, a pier cap beam, a pile cap, multiple driven piles or drilled shafts, and a numerical representation of the soil. Horizontal and vertical soil stiffness is modeled using nonlinear spring elements. Linear elastic, thick-formulation shell elements are used to model the pile cap.

3.3.1 Pier modeling

Flexural substructure elements—pier columns, pier cap beam, and either piles or drilled shafts—are modeled using nonlinear cross-section integrated frame elements. For relatively light loading, such as that associated with certain service loading conditions, bridge structural components are typically assumed to remain effectively linear. As such, accurate predictions of pier behavior under this type of loading can be obtained using resultant frame elements with gross cross-sectional properties and linear-elastic material models.

However, barge-bridge collision is an extreme event scenario, potentially resulting in permanent damage or even collapse of the bridge structure. As a result, robust nonlinear analytical tools are necessary to capture the effects of widespread concrete cracking, plastic hinge formation, and permanent member deformation. Furthermore, bridge structural elements are commonly composed of multiple materials (i.e., reinforced or prestressed concrete). To address the composite nature of concrete pier elements, FB-MultiPier employs cross-section integrated frame elements that permit the cross-sectional shape and the locations of reinforcing bars or prestressing tendons to be modeled explicitly. When such elements are employed, the cross section is discretized into multiple regions of integration

and relevant material models (stress-strain relationships) are assigned to each discrete area (integration point) as illustrated in Figure 3.6.

As the section flexes in general biaxial bending and deforms axially, a planar (linear) strain field is generated across the section. Nonlinear stress-strain relationships for each material (Figure 3.7) lead to a non-uniform distribution of stresses over the cross-section. Section axial force and moments are then computed by integrating (summing) the force and moment contributions from each integration point.

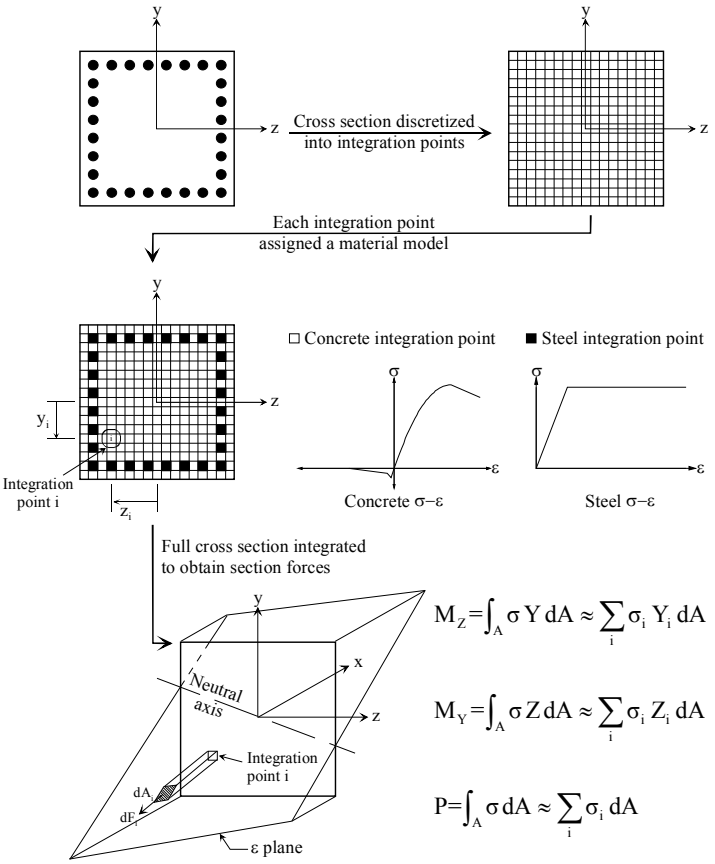

Figure 3.6 Cross section integration scheme for nonlinear frame elements

FB-MultiPier can employ either built-in stress-strain relationships or user-defined stress-strain relationships for concrete and steel. In Figure 3.7, built-in FB-MultiPier stress-strain relationships for typical bridge pier materials are illustrated. Concrete is modeled using a modified Hogenstead parabola in compression, with strain softening described by a straight line. It is important to note that the maximum compressive stress (f_c'') is 0.85 times the specified cylinder compressive strength (f_c'). In tension, concrete is treated as linear until the cracking stress (f_r) is reached. After cracking, a bilinear model is employed to account for tension stiffening. For 270-ksi high-strength prestressing tendons, the stress-strain model proposed by the Precast/Prestressed Concrete Institute (PCI 2004) is employed. Mild reinforcing steel is treated as elastic, perfectly plastic with a yield stress of 60 ksi. When combined with the cross-section integration scheme, these material models provide accurate

predictions of moment-curvature and plastic hinging behavior for reinforced and prestressed concrete members.

3.3.2 Soil modeling

With regard to representing soil-structure interaction, FB-MultiPier utilizes empirical soil-strength models, where these models correlate pertinent soil parameters (e.g., internal friction angle, subgrade modulus) to deformation behavior under loading. Three primary modes of soil-structure interaction are considered: lateral resistance (P-y), axial skin friction along the pile or shaft (τ-z), and tip bearing resistance (Q-z). For each mode, nonlinear curves define relationships between resistance and displacement. Example soil resistance curves are illustrated in Figure 3.8.

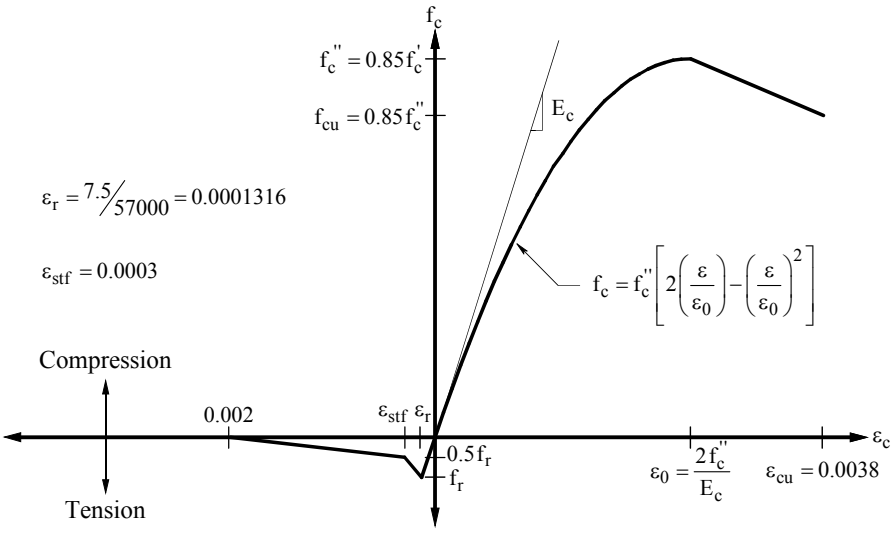

a) Concrete material model
Source: FB-MultiPier (2007)

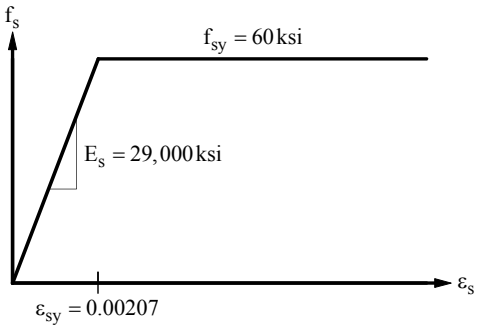

b) Mild steel material model

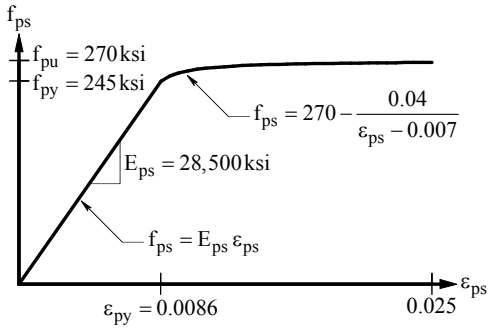

c) Prestressing steel material model
Source: PCI (2004)

Figure 3.7 Nonlinear material models as implemented in FB-MultiPier

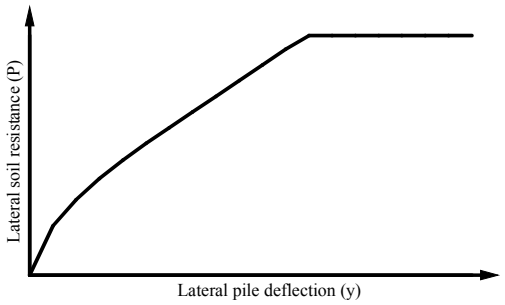

a) Lateral soil resistance (P-y) curve

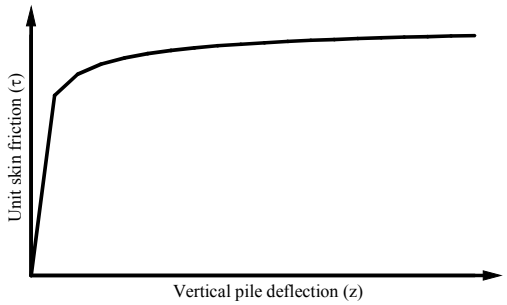

b) Skin friction (τ-z) curve

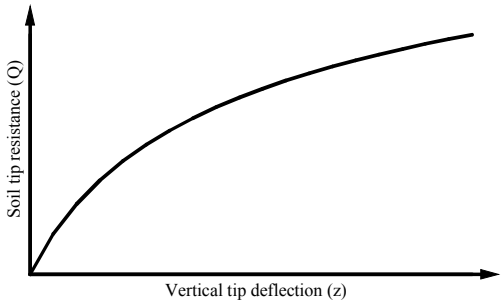

c) Tip resistance (Q-z) curve

Figure 3.8 Typical soil resistance curves employed by FB-MultiPier

Due to the continuous nature of soil resistance, soil-structure interaction in each orthogonal direction is represented using nonlinear spring elements distributed along the embedded pile (or drilled shaft) length. One vertical spring at each nodal location models the tributary skin friction (τ-z). Additional spring elements are placed at each pile tip node to represent the tip resistance (Q-z).

Modeling lateral (horizontal) soil resistance requires a slightly more refined approach. FB-MultiPier incorporates user-defined pile row multipliers (p-y multipliers) to account for pile group behavior. Each row of piles is assigned a factor by which the lateral resistance is scaled, depending on pile spacing and position within the group (Figure 3.9). However, these factors are dependent on the direction of pile group motion. For example, a pile on the leading row may be assigned a factor of 0.8. However, if the foundation motion reverses direction, the pile becomes part of a trailing row, for which a row multiplier of 0.3 is applied. Similarly, when group motion occurs in the transverse direction, unique multipliers are used. Consequently, four horizontal spring elements define the lateral soil resistance in each orthogonal direction, at every node. The nonlinear stiffness of each spring is scaled by the applicable p-y multiplier, providing a realistic representation of lateral pile group behavior.

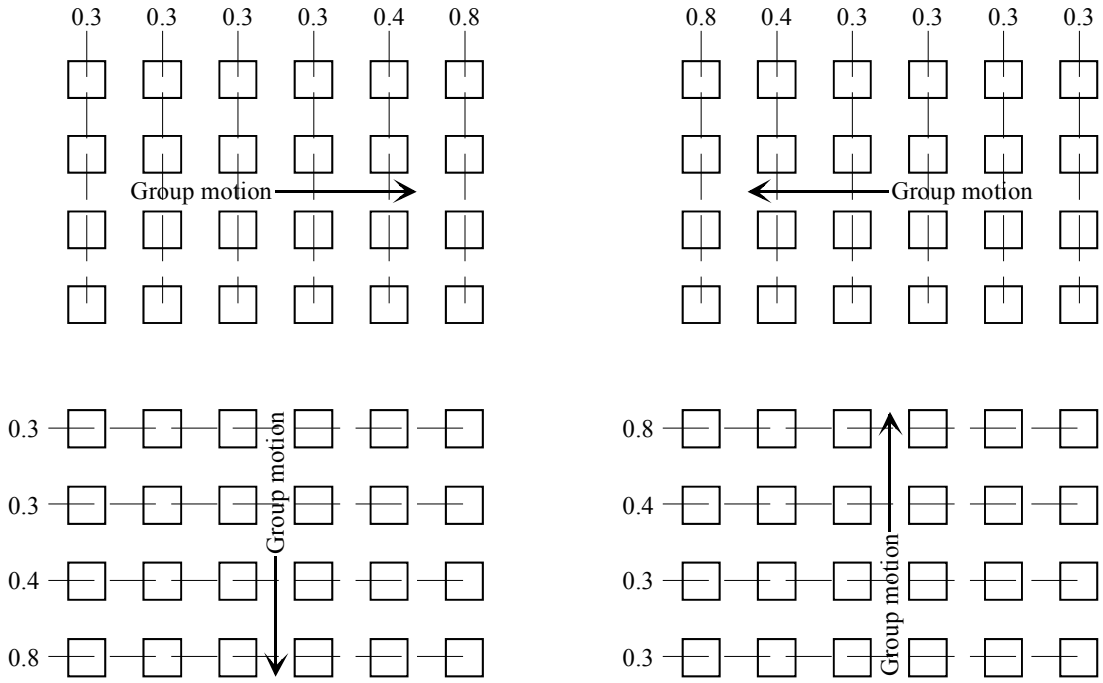

Figure 3.9 Variation of row multipliers for differing pile group motion
(Note: Specific multiplier values will vary based on pile spacing)

Behavior of soil-spring elements under cyclic lateral loading can be considered either nonlinear-elastic or nonlinear-inelastic, depending on the soil type. Typically, for cohesionless soils, such as sands, the material exhibits nonlinear-elastic behavior, returning to the original undeformed state when load is removed. In contrast, cohesive soils (e.g, clay) are often considered nonlinear-inelastic and gaps may form between soil and pile surfaces during cyclic loading. FB-MultiPier soil models can account for this type of behavior; however, a lack of available, dynamic soil data for many of the bridges studied precluded the direct incorporation of such effects in the current study.

It is important to note that FB-MultiPier has the ability to automatically compute all of the soil parameters noted above—lateral resistance (P-y), axial skin friction (τ-z), tip bearing resistance (Q-z), and row-multipliers—from the soil layering information specified by the designer. Hence, explicit calculation of each of these parameters by the designer is not necessary if the fundamental properties of each soil layer are provided to FB-MultiPier.

3.4 Barge bow modeling considerations

As noted in the previous chapter, all dynamic barge collision simulations conducted in this study were performed using the coupled vessel impact analysis (CVIA) technique. CVIA simulations were conducted both to quantify dynamic amplifications of pier member forces and to calibrate the equivalent static bracketed impact analysis (SBIA) method that is described later in this report. In a CVIA simulation, the barge is represented by a SDOF system linked to a MDOF bridge representation by means of a force-deformation relationship

(crush curve). For this study, elastic-perfectly-plastic relationships for barge bow crushing behavior were adopted, as recommended by Consolazio et al. (2009).

The barge bow force-deformation relationships proposed by Consolazio et al. (2009) were developed by conducting high-resolution finite element simulations of head-on collision events using the LS-DYNA finite element code (LSTC 2008). However, a *perfectly* head-on collision between an aberrant barge flotilla and a flat pier surface is statistically improbable. It is much more likely that the vessel will strike the bridge pier at an oblique angle. In fact, during the full-scale barge collision tests conducted by Consolazio et al. in 2004, perfectly head-on collisions were extremely difficult to achieve, even when this was the intention.

Furthermore, Consolazio et al. (2009) found that barge collision forces are dictated primarily by internal truss engagement in the bow structure. Consequently, forces generated by perfectly head-on impacts with flat surfaces are much larger those generated from impacts with similarly-sized round surfaces. This difference is due to the simultaneous engagement of internal trusses by the flat surface, as opposed to the gradual engagement by a similarly-sized round surface. However, given the unlikely nature of a perfectly head-on impact event, the inclusion of such conditions can result in the generation of overly conservative impact loads and member design forces. Slightly oblique impact is much more likely, and would engage the internal barge trusses in a relatively more gradual manner, resulting in reduced overall impact forces. The topic of oblique barge impact forces is presently being investigated as part of a concurrent study by the University of Florida (UF) and Florida Department of Transportation (FDOT). Selected preliminary findings from that concurrent study, presented below, were incorporated into the formulation of the proposed equivalent static analysis method.

3.4.1 Simulation of oblique barge impact scenarios

To assess the effect of oblique impact conditions on vessel collision forces, a series of high-resolution finite element barge bow crushing simulations were conducted using the LS-DYNA finite element code. For this investigation, detailed finite element barge bow models developed by Consolazio et al. (2008) were subjected to varying oblique impact conditions (for further details regarding the development of the barge models, refer to Consolazio et al. 2008 and Consolazio et al. 2009).

Bow crushing simulations were performed for the two most common barge types navigating U.S. waterways: the jumbo hopper barge, and oversize tanker barge. Each barge bow model was fixed at the rear, and then subjected to quasi-static crushing with an angled impact surface (Figure 3.10). As illustrated in Figure 3.11, each barge bow was crushed to a depth of 16 ft with an impact surface equal to the width of the barge (35 ft for the jumbo hopper, and 50 ft for the oversize tanker). Crushing was achieved by pushing the impactor into the bow at a constant rate.

A total of 12 crushing simulations were conducted, with the impact surface positioned at angles (θ) of 1°, 2°, 5°, 10°, 15°, and 20° relative to the barge bow surface. Throughout each simulation, the contact force generated between the barge bow and oblique impact surface was monitored and associated with the crush depth to form the corresponding barge bow force-deformation relationship (crush curve).

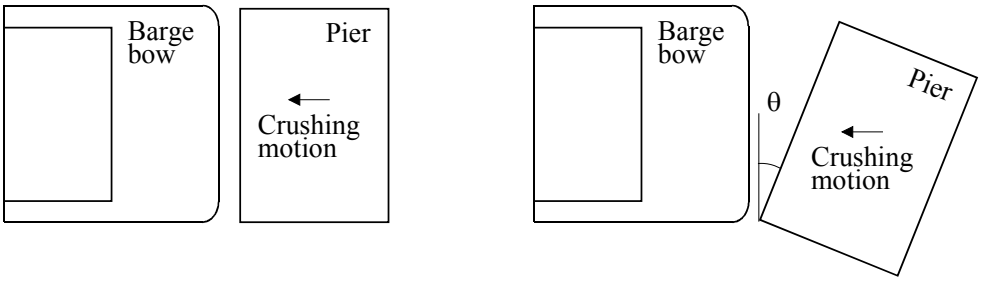

Figure 3.10 Direction of motion and oblique angle for barge crushing simulations

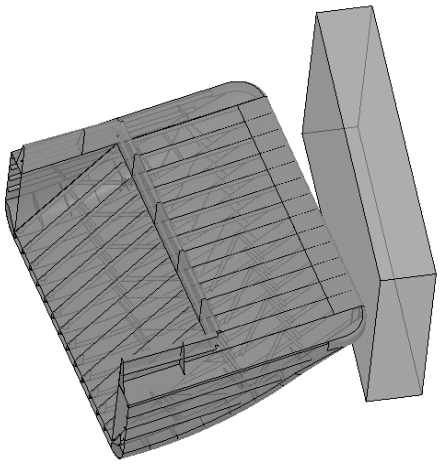

a) 0 ft crush depth

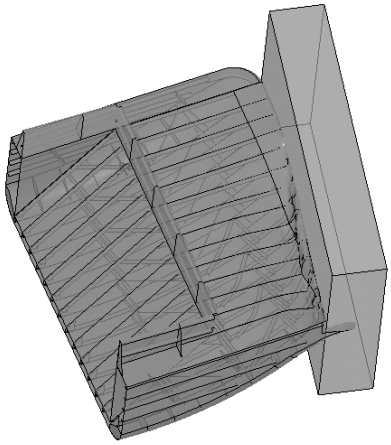

b) 5 ft crush depth

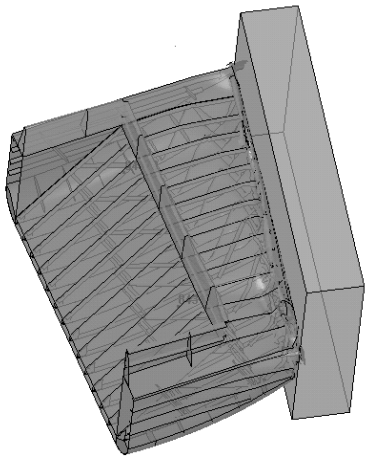

c) 10 ft crush depth

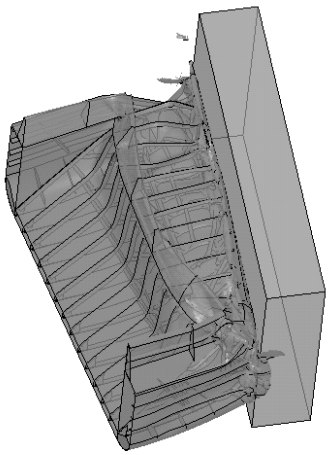

d) 15 ft crush depth

Figure 3.11 Finite element simulation of wide-faced oblique bow crushing of the jumbo hopper barge bow (10° impact angle shown)

The maximum impact force generated during each oblique crushing scenario was compared to the corresponding collision angle. These data were used to form preliminary nonlinear equations (Figure 3.12) to predict the maximum barge crush force (P_{by}), based on the angle of impact (θ). The prediction equations will be finalized as part of the concurrent UF-FDOT study.

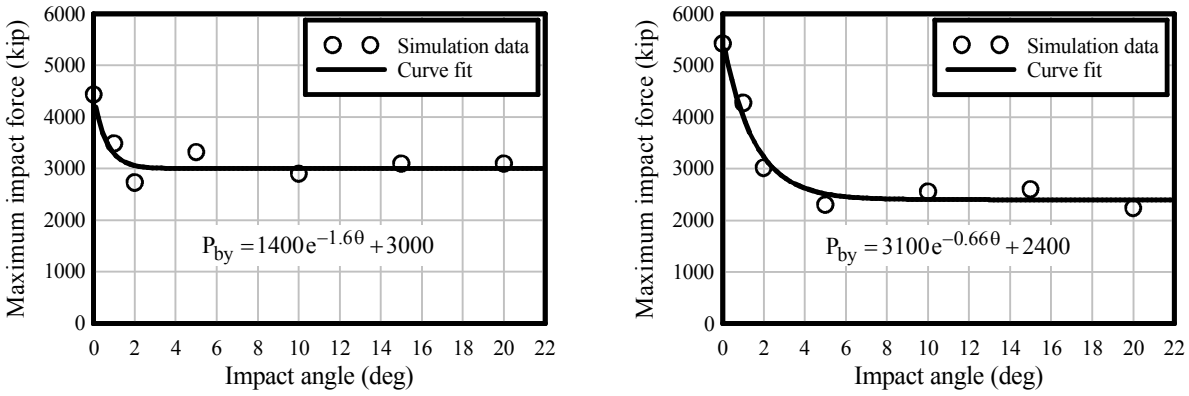

a) Jumbo hopper barge

b) Oversize tanker barge

Figure 3.12 Impact force variation for oblique impact conditions

The impact forces (P_{by}) from the equations shown in Figure 3.12 were normalized by the corresponding head-on collision force (4400 kips for the jumbo hopper barge, and 5500 kips for the oversize tanker barge) to form normalized impact force ratios (Figure 3.13). The resulting expressions illustrate how oblique impact angles—even small angles—can result in sizeable reductions in impact force (relative to a head-on collision). For the jumbo hopper barge, an impact angle of only 2° leads to a 30% impact force reduction (relative to a perfectly head-on collision). For the oversize tanker barge, the corresponding reduction is much larger, at 55%. However, an oblique impact of approximately 8° is necessary to attain the full reduction.

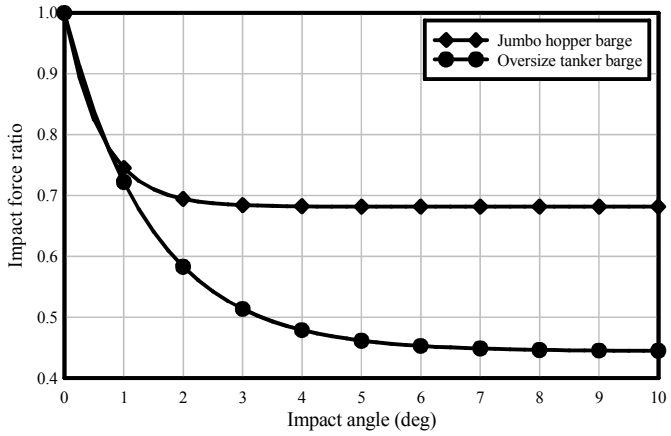

Figure 3.13 Force-ratio versus impact angle for oblique impact conditions

These preliminary results suggest that obliquity of the impact surface leads to gradual engagement of internal bow trusses, thus reducing the maximum impact force. This mode of bow crushing is similar in nature to that observed in Consolazio et al. (2009) for impact simulations involving round pier surfaces, reaffirming the dependency between impact surface geometry and collision force. These findings also suggest that the maximum crush forces proposed by Consolazio et al. (2009) may be overly conservative for wide, flat-faced surfaces, given that perfectly head-on collision is improbable.

3.4.2 Incorporation of force reduction due to oblique impact

Bridges with large waterline footings (pile caps) are common in the United States, and, due to footing placement, barge collision with the pile cap itself is likely. Using the perfectly head-on impact barge crush curves proposed by Consolazio et al. (2009), barge impact forces can be very large for bridges with wide, waterline footings, despite the fact that there is a very low statistical probability of being subjected to a perfectly head-on impact.

For this reason, impact forces used in this study were reduced by 30% when considering waterline pile cap impact conditions. As illustrated in Figure 3.13, impact forces for both barge types are diminished by at least 30% (more than 40% for oversize tanker barges) for oblique impacts of 2° or greater. For purposes of this study, it was assumed that aberrant barges or barge flotillas are very likely to strike bridge piers at an angle of at least 2°. Therefore, a 30% reduction of crush force for cases of waterline footing collision was warranted.

For these cases, the barge bow yield force (P_{by}) was reduced by 30%, forming a revised elastic, perfectly-plastic crush curve as shown in Figure 3.14. Consolazio et al. (2009) found that the yield crush depth (a_{by}) was relatively insensitive to barge type, location of impact (center or corner of bow), or impact surface geometry. Consequently, the yield crush depth for the idealized crush curve was not altered in the present study.

To date, the concurrent barge crushing simulation study has only addressed oblique impact scenarios that engage the full barge bow width. As such, reduced crush forces were (conservatively) not employed for impact conditions involving narrow (relative to the barge bow) flat-faced pier surfaces (such as those involving a rectangular pier column).

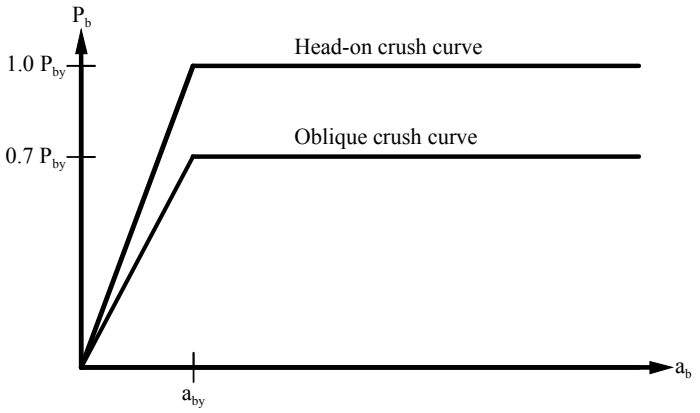

Figure 3.14 Reduced elastic, perfectly-plastic barge crush curve for oblique flat-faced impacts on waterline pile caps, as compared to head-on collision

3.5 Gravity preloading through static pre-analysis

All vessel collision analyses conducted as part of this study included structural member self-weight (dead) load due to gravity (with buoyancy effects included). When conducting a static impact analysis, the application of gravity loading is trivial. During the analysis, the structure achieves static equilibrium under the combination of self-weight and lateral loading. However, to analyze the structure dynamically, careful consideration of non-transient loads, such as self-weight, is important.

Figure 3.15 demonstrates the simplest way to conduct a coupled vessel impact analysis (CVIA) with the pier self-weight included. In this scenario, both the barge impact loading (P_{by}) and pier gravity loading (W) occur simultaneously, at the beginning of the simulation—i.e., immediately prior to collision, the pier is stress free. In contrast, during an actual barge collision event, the pier stresses due to self-weight and other static loading are present before and during impact. Consequently, the loading scheme in Figure 3.15 is unrealistic.

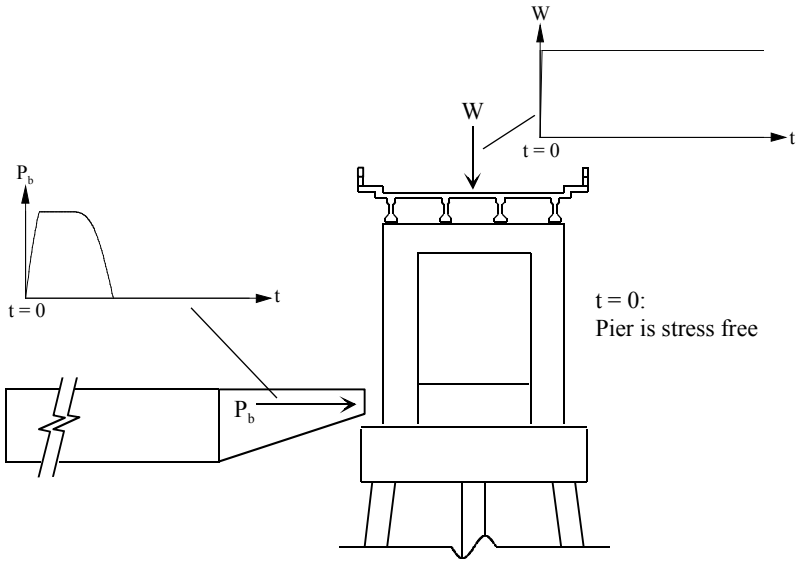

Figure 3.15 CVIA with instantaneous dynamic application of self-weight

In addition to being unrealistic, the abrupt application of self-weight loading leads to undesired dynamic pier response. Figure 3.16 illustrates, in a simplified way, how the instantaneous application of loads can lead to an amplified response. Inertial forces caused by motion of the single-degree of freedom (SDOF) mass push the system far beyond the static displacement. By applying the load abruptly, the maximum dynamic displacement is 100% larger—in the absence of damping—than that predicted by a static analysis. Additionally, the excessive displacement leads to amplified internal forces and unwarranted inelastic deformations, especially in vertical soil springs.

When a bridge structure is loaded in this manner, vertical oscillations result in amplified axial forces in the pier columns and piles. Furthermore, during vessel collision, vertical oscillations combine with lateral sway to amplify flexural demands throughout the pier. The erratic pier behavior caused by instantaneous self-weight application makes assessing load-moment interaction (with any level of physical confidence) nearly impossible.

One way to alleviate modeling issues associated with instantaneous dynamic application of self-weight is to apply these loads gradually, prior to vessel collision. This process is demonstrated in Figure 3.17 where gravity loads are applied over some duration of time, Δt. The duration, Δt, of the gravity loading phase must be sufficiently long for the structure to achieve static equilibrium under self-weight prior to barge impact. For typical bridge structures, gradual application of gravity over duration Δt can require more simulation time than the barge collision event itself, thereby more than doubling the overall computation time. While this scenario is a possible means of mitigating undesired dynamic amplifications of gravity loading, the additional computational time is undesirable.

Alternatively, for this study, self-weight stresses were initialized by means of a static gravity pre-analysis (Figure 3.18). Two distinct analyses were conducted—one static analysis (with only gravity and buoyancy loading), and one dynamic analysis, including both the initialized gravity loading and vessel collision loading. As part of this study, this two-stage analysis feature was implemented into the FB-MultiPier analysis engine.

To perform static gravity pre-analysis, the bridge is analyzed statically, with only the self-weight in place. Once the structure reaches static equilibrium, the stiffness matrix and displacement vector are stored. These quantities are then used as initial conditions for a time-domain vessel collision analysis (CVIA). As before, the self-weight is imposed instantaneously in the dynamic analysis. However, because statically-induced gravity stresses are already present, the abrupt loading does not cause undesired dynamic oscillations.

A demonstration case is presented to illustrate the effectiveness of the static pre-analysis procedure for mitigating structural response amplification. A model of the New St. George Island Causeway Bridge (located in northwestern Florida) channel pier is shown in Figure 3.19. The model was analyzed (with only self-weight loading) using three methods: static analysis, dynamic analysis with instantaneous gravity loading, and dynamic analysis with static pre-analysis.

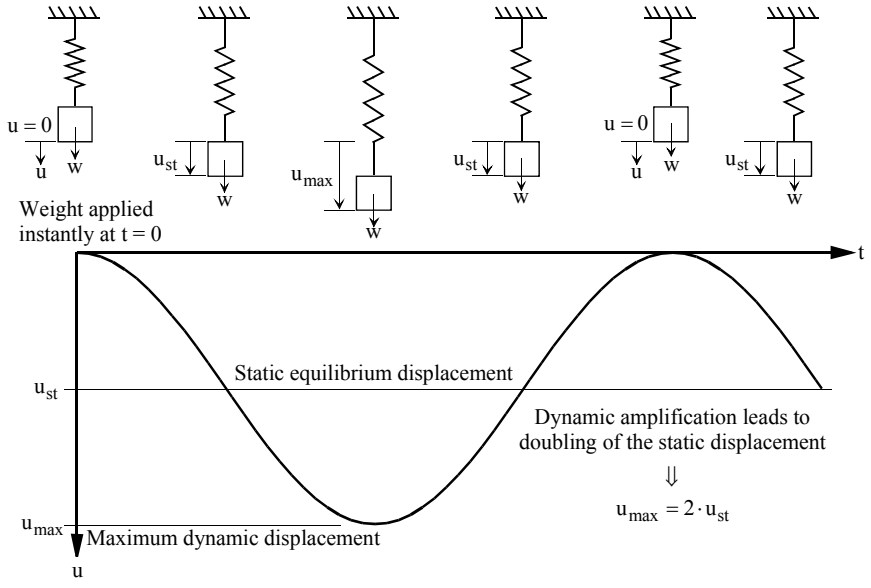

Figure 3.16 Dynamic amplification due to instantaneous application of gravity load to a single degree of freedom (SDOF) system

Under self-weight loading, the static vertical pile cap displacement was approximately 0.50 inches (Figure 3.20). However, when the gravity loading was applied instantaneously as part of a dynamic analysis, the bridge underwent significant oscillation. Abrupt gravity loading accelerated the bridge mass downward and induced significant inertial forces. Inertia was found to act as an additional source of loading, forcing the bridge far beyond the static displacement. In this case, the maximum dynamic gravity displacement (0.88 inches) exceeded the static gravity displacement (0.50 inches) by a factor of almost 1.8.

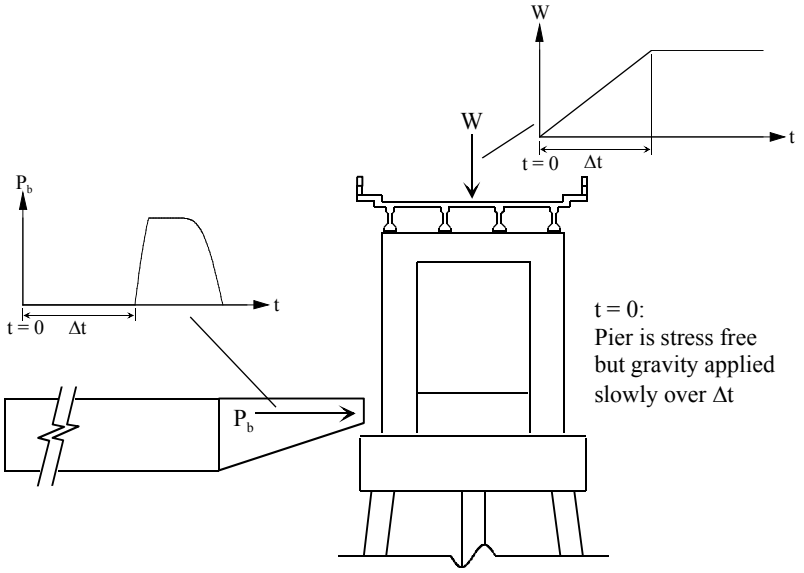

Figure 3.17 CVIA with gradual dynamic application of self-weight

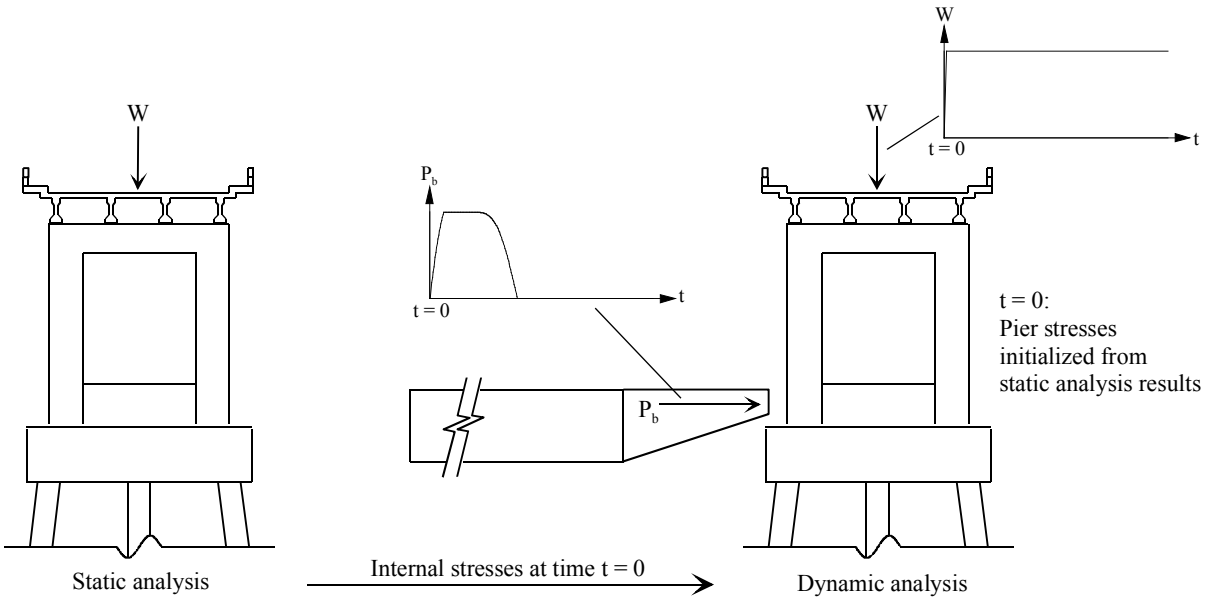

Figure 3.18 CVIA using static gravity analysis to initialize self-weight stresses

In contrast, no dynamic amplification was present when using a static gravity pre-analysis. While gravity forces were still applied abruptly in the dynamic analysis, the self-weight stresses were initialized prior to dynamic loading, resulting in an approximately instantaneous steady-state response. In fact, the dynamic displacement-history strays only nominally from the static displacement of 0.50 inches. It should be noted that the static gravity pre-analysis required less than 15 seconds of wall clock time to complete, increasing the overall analysis time by less than one percent. This example demonstrates that static preloading is a very efficient means of initializing long-term loads prior to conducting transient dynamic simulations such as vessel collision.

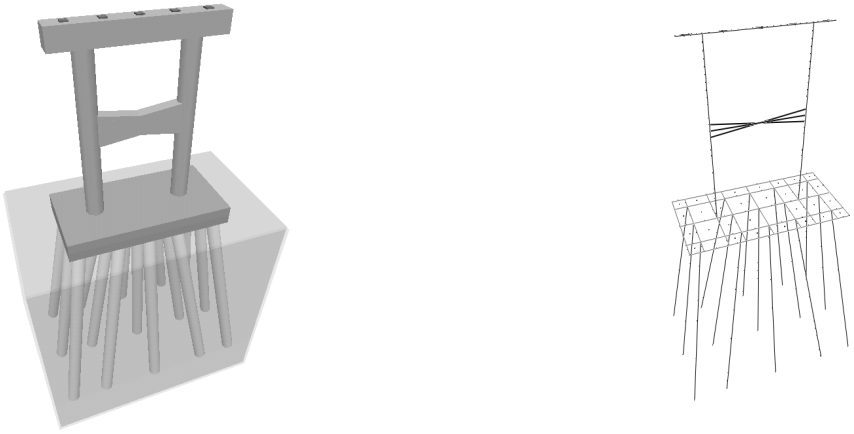

a) Three-dimensional rendering b) Finite element model

Figure 3.19 FB-MultiPier model of New St. George Island Causeway Bridge channel pier

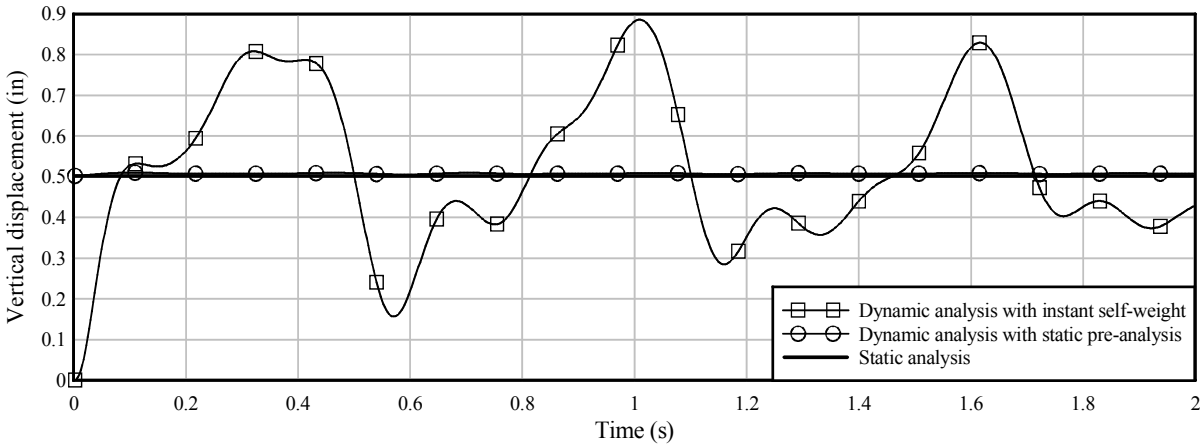

Figure 3.20 Comparison of vertical pile cap displacements under self-weight loading

CHAPTER 4
DYNAMIC AMPLIFICATION OF PIER COLUMN INTERNAL FORCES DUE TO BARGE-BRIDGE COLLISION

4.1 Introduction

In 2004, Consolazio et al. (2006) conducted full-scale barge impact experiments on various pier and partial-bridge configurations to quantify waterway vessel collision impact forces and corresponding pier responses. The impacted bridge structures were subsequently modeled using bridge analysis software and the models were, in turn, calibrated using experimentally measured impact forces and pier response-histories. Internal structural demands (e.g., shears, moments) obtained from dynamic barge impact analyses of the bridge models were then compared to demands obtained from corresponding static analyses. In comparison to the static analyses, larger pier column internal forces were predicted from dynamic analyses, indicating the presence of dynamic amplification in the tested bridge structures. It was discovered that the mass of the superstructure overlying an impacted pier can generate significant inertial forces during vessel collision events and that these inertial forces can amplify pier column demands.

The discovery of collision-induced dynamic amplifications was possible, in part, due to the availability of impact force-histories that were measured during the 2004 full-scale barge impact experiments. In 2005, the coupled vessel impact analysis (CVIA) was developed to enable calculation of impact force-history data given vessel mass, initial velocity, vessel force-deformation characteristics, and bridge and soil stiffnesses. In this chapter, the CVIA technique is used to investigate the extent to which bridges, with varying pier configurations and foundation types, exhibit dynamic amplifications during collision events. A parametric study is carried out to quantify dynamic amplifications by dynamically and statically analyzing models of numerous bridge-pier configurations subject to barge impact.

4.2 Parametric study

All analyses (static and dynamic) conducted in the parametric study account for nonlinear, inelastic deformations in the reinforced (or prestressed) concrete pier structures (pier columns and piles/shafts); in the steel barge; and, in the soil response. Inelastic pier deformations (e.g., plastic hinging) and inelastic crushing deformations of the barge bow constitute the primary sources of energy dissipation during head-on barge-bridge collisions. However, in this study, energy dissipation due to inelastic soil response and dissipation due to natural damping in the structural elements were also taken into account. Rayleigh damping was used to model natural damping in all structural members such that approximately 5% of critical damping was achieved over the first five natural modes of pier vibration. This is an acceptable scheme considering that levels of natural damping measured for hundreds of highway bridges range from 1.3% to 8.4% of critical damping for the fundamental vibration mode (Paultre et al. 1992).

For each bridge in the parametric study, dynamic amplification effects were quantified by conducting a dynamic analysis (using the CVIA procedure) and subsequently conducting a static analysis. If design forces predicted using dynamic analysis were larger

than those predicted by a corresponding static analysis, then dynamic amplification effects were present. In each dynamic case, time-histories of barge impact load and pier design forces was computed simultaneously (Figure 4.1a). A corresponding static analysis case was then generated by quantifying the maximum load from the CVIA impact load-history (P_b^{max}) and applying it to the bridge model as a static load (Figure 4.1b). Accordingly, maximum magnitude loads applied to the bridge in the dynamic and static analyses were identical (each being equal to P_b^{max}); any differences in computed pier response were therefore the result of mass-related dynamic effects (inertia, momentum).

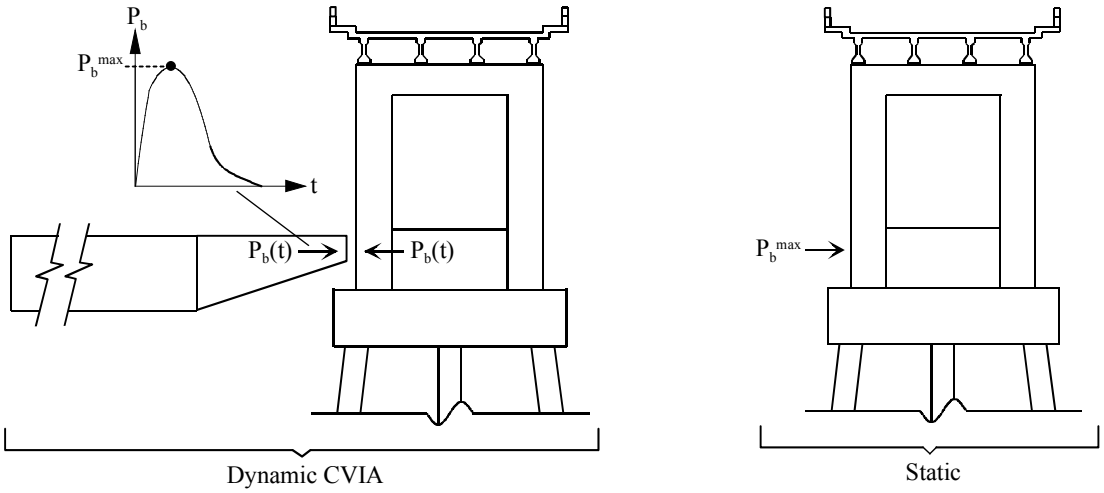

Figure 4.1 Analysis types: a) Dynamic CVIA; b) Static (using peak load, P_b^{max}, from CVIA)

4.2.1 Bridge inventory

Fifteen (15) models were developed for various piers and spans of 12 different bridges (Figure 4.2, Table 4.1) located in the state of Florida. For conciseness, and to simplify discussion, each bridge structure was assigned a three-letter identification code. Specific piers within each bridge were further delineated by proximity (with respect to the vessel transit path): the letters CHA appended to a bridge identification code indicate that the pier is a channel pier, whereas the letters OFF indicate an off-channel pier (a pier not directly adjacent to the channel). Bridges listed in Table 4.1—selected from a larger Florida Department of Transportation (FDOT) catalog of almost two-hundred bridges—constitute a representative cross-section of bridge types currently in service in Florida. The twelve (12) selected bridges also vary widely in age, with construction dates spanning from the late 1960s to 2004.

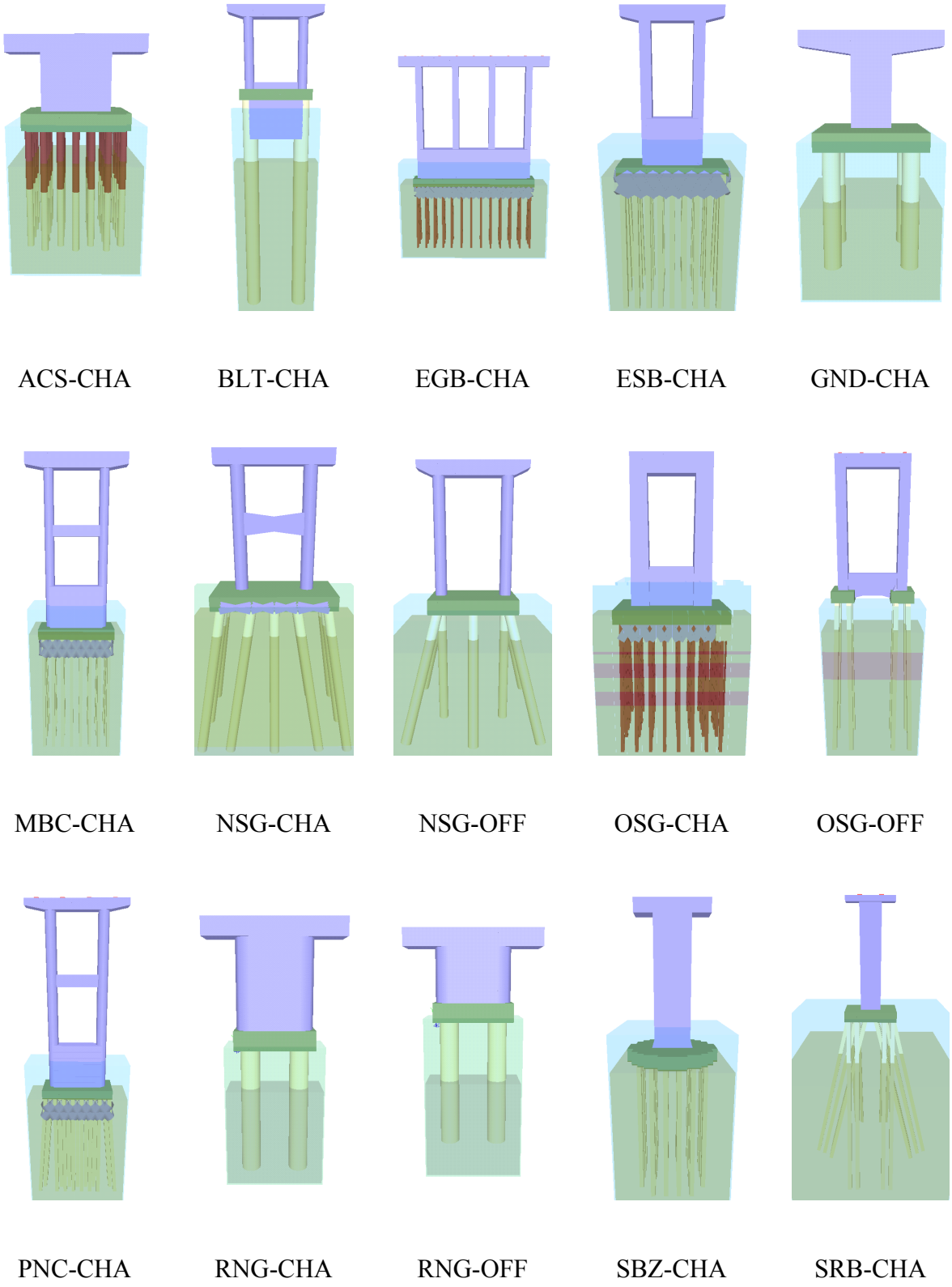

Figure 4.2 Bridge pier structural configurations (superstructure not shown).
(See for bridge pier abbreviations)

Table 4.1 Bridge pier configurations

Bridge ID	Bridge name	Cap[a,b] elevation	Impact surface shape	Impact surface width (ft)	Pier column data			Shaft/pile data			Superstructure type			Span lengths adjacent to pier (ft)	
					No.	Width (ft)	Height[c] (ft)	Type	No. shafts/ piles	Width (ft)	Box girder	Concrete slab on steel girders	Concrete slab on concrete girders	North or west	South or east
ACS-CHA	Acosta	Waterline	Flat	50	1	20	40	Drilled shaft	31	5.0	X			370	620
BLT-CHA	SR-20 at Blountstown	Waterline	Round	9.0	2	5.5	37	Drilled shaft	2	9.0			X	280	220
EGB-CHA	Eau Gallie	Mudline	Flat	4.0	4	4.0	69	Steel pile	39	1.2			X	150	150
ESB-CHA	I-10 Escambia Bay	Mudline	Flat	6.1	2	6.0	51	Concrete pile	27	2.0		X		169	120
GND-CHA	Gandy	Waterline	Flat	33	1	4.5	29	Drilled shaft	4	7.0			X	235	140
MBC-CHA	Melbourne	Mudline	Round	4.5	2	4.5	72	Concrete pile	32	1.5		X		145	110
NSG-CHA	New St. George Island	Waterline	Flat	28	2	6.0	52	Concrete pile	15	4.5			X	250	260
NSG-OFF	New St. George Island	Waterline	Flat	28	2	5.5	52	Concrete pile	9	4.5			X	140	140
OSG-CHA	Old St. George Island	Mudline	Flat	5.7	2	5.5	47	Steel pile	40	1.2		X		250	180
OSG-OFF	Old St. George Island	Waterline	Flat	3.5	2	3.5	40	Concrete pile	8	1.7			X	74	74
PNC-CHA	Pineda	Mudline	Round	4.5	2	4.5	73	Concrete pile	30	1.7			X	120	68
RNG-CHA	John Ringling	Waterline	Round	13	1	13	40	Drilled shaft	2	9.0	X			300	300
RNG-OFF	John Ringling	Waterline	Round	13	1	13	25	Drilled shaft	2	9.0	X			300	300
SBZ-CHA	Seabreeze	Mudline	Flat	8.0	1	8.0	58	Concrete pile	32	2.0	X			250	250
SRB-CHA	Santa Rosa Bay	Waterline	Flat	6.0	1	6.0	58	Concrete pile	22	1.7	X			230	140

[a] Waterline footing indicates a foundation top-surface elevation near the mean high water level.

[b] Mudline footing indicates a foundation top-surface elevation near the soil surface.

[c] Distance from top of foundation to bottom of pier cap.

Various past analytical studies have demonstrated that the geometry (shape and width) of the impacted portion of a bridge pier affects the magnitude of impact loads generated during collision (Consolazio et al. 2009, Consolazio and Cowan 2003, Yuan et al. 2008). Hence, in the parametric study, bridges were selected that vary in both pier column shape (flat-faced, round) and pier column width (ranging from 3.5 ft to 20 ft). Pier shape, foundation type (pile-and-cap or drilled shaft), and size data are summarized in Table 4.1.

The extent to which load applied to an impacted pier is transmitted to adjacent piers depends upon the type of superstructure that connects the piers together. Three common superstructure types are included in the parametric study (Table 4.1): slab on concrete girders; slab on steel girders; and, segmental concrete box girder. Superstructure span lengths included in this study are representative of common, moderate-span bridges that span U.S. inland waterways as opposed to less common, long-span bridges.

4.2.2 Barge impact conditions

Jumbo hopper barges are the most common type of vessel found in the U.S. barge fleet, and additionally, constitute the baseline design vessel for barge-bridge collision in the AASHTO provisions. For these reasons, a jumbo hopper barge was employed as the design vessel in the parametric study. Prescribed barge impact conditions for bridges in the parametric study were chosen to span the range of collision events that are conceivable for navigable Florida waterways. Vessel weight (flotilla weight) and collision velocity were varied to produce a representative range of impact energy cases: low, moderate, high, and severe (4.2). Based on waterway traffic characteristics, pier location (relative to the navigation channel), and pier strength, one or more suitable impact energy conditions were assigned to each pier in the study.

The AASHTO provisions require that all bridge components located in navigable water depths be designed for, at a minimum, impact from a single empty hopper barge (200 tons) drifting at a velocity equal to the mean water current for the waterway (AASHTO 1991). This low-energy drifting barge condition is meant to be representative of a barge that breaks loose during a storm and drifts into a pier. Such a condition is only relevant to the design of piers distant from the navigation channel (since near-channel piers must be designed for greater impact energies, which are associated with errant, tug-propelled barge flotillas). Therefore, the low-energy impact condition was only applied to off-channel piers (4.2). Using water-current data for several waterways in Florida, an approximate average current velocity of 1 knot was determined. Thus, the low-energy case is defined as a 200-ton barge drifting at a velocity of 1 knot.

The majority of impact cases considered in this study fall into the categories of either moderate or high energy (4.2). A moderate-energy impact condition is defined as one fully-loaded hopper barge (2030 tons with tug) traveling at 2.5 knots, and a high-energy impact condition is defined as a flotilla consisting of three fully-loaded hopper barges (5920 tons with tug) traveling at 5.0 knots. These conditions cover the majority of possible impact energies that would be generated by collisions from typical Florida barge traffic (Liu & Wang 2001). For two of the piers considered in this study (channel piers of the Acosta and New St. George bridges), barge traffic and waterway conditions warrant the definition of an additional severe-energy impact condition: a flotilla consisting of four fully-loaded hopper barges (7820 tons with tug) traveling at 7.5 knots.

Table 4.2 Analysis matrix of barge impact energy conditions

	Impact energy condition			
	Low	Moderate	High	Severe
	Impact condition characteristics			
Velocity (knot)	1.0	2.5	5.0	7.5
Weight (tons)	200	2030	5920	7820
ID and location	Cases analyzed			
ACS-CHA		X	X	X
BLT-CHA		X	X	
EGB-CHA		X		
ESB-CHA		X	X	
GND-CHA		X	X	
MBC-CHA		X		
NSG-CHA		X	X	X
NSG-OFF	X	X	X	
OSG-CHA		X		
OSG-OFF	X			
PNC-CHA		X		
RNG-CHA		X	X	
RNG-OFF	X	X		
SBZ-CHA		X	X	
SRB-CHA		X	X	

4.3 Results

A comparison of static and dynamic (CVIA) results obtained from the parametric study revealed that maximum dynamic internal forces almost universally exceed corresponding static forces. Insight into which bridge configurations are most susceptible to dynamic amplifications was gained by categorizing the parametric study results according to the dynamic response mode that is active when maximum internal pier column demands occur:

- Superstructure inertial restraint amplification;
- Superstructure momentum-driven sway mode amplification; or,
- Mixed inertial restraint and momentum-driven sway mode amplification.

In the first two categories, maximum values of pier column shear and moment occurred during the same stage of the impact event (i.e., early stage, before peak pier displacements occur, for inertial restraint amplification; later stage, at or beyond the time at which peak pier displacements occur, for momentum-driven sway amplification). Cases falling into the third category developed maximum pier column shear and moment during different response modes and different stages of the impact event. Each of the three response types are discussed in detail below.

4.3.1 Amplification due to superstructure inertial restraint

For the Blountstown Bridge—formally known as the New Trammell Bridge—moderate-energy case (BLT-CHA-M), barge impact occurs on the channel pier near the top of a 30.5 ft tall shear wall that connects two 9 ft diameter drilled shafts (Figure 4.3a). Two circular pier columns (5.5 ft diameter), which are axially collinear with each foundation shaft, span from the foundation elements to the top of the pier.

Statically (Figure 4.3b), relative portions of impact load that flow into the foundation—versus those portions that flow into the superstructure—are determined by satisfying static equilibrium between the applied load and displacement-dependent resistance forces from the impacted pier and superstructure. The pier columns are not sufficiently stiff to transfer significant forces to the superstructure, and furthermore, the foundation is stiff relative to the superstructure. Consequently, the superstructure provides little static resistance to the applied load, and displacements produced at the foundation level increase in proportion to pier column height, with little column curvature. Correspondingly, significant internal forces (shear and moment) are not generated in the pier columns. Due to the limited displacement-dependent (or stiffness-dependent) resistance of the superstructure, the entire pier exhibits rigid body pier rotation where the pier top displacement is greater than the impact point displacement in the direction of impact loading.

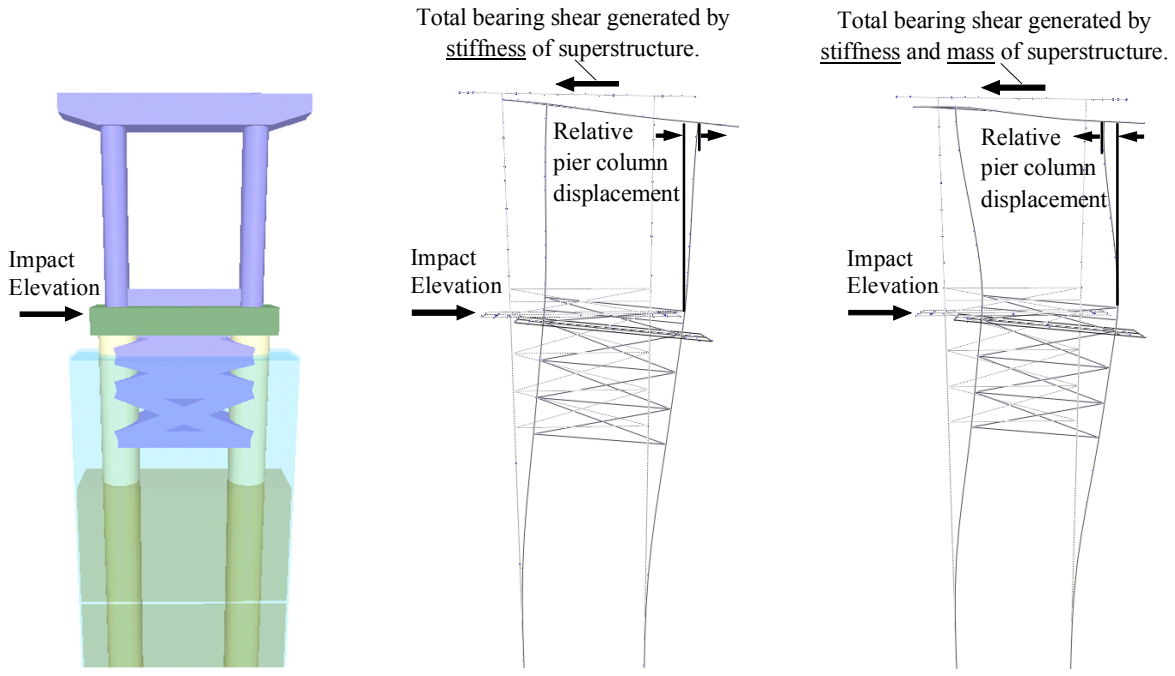

a) b) c)

Figure 4.3 Summary data for inertial restraint case BLT-CHA-M.
a) Pier configuration (superstructure not shown);
b) Static analysis case; c) Dynamic analysis case

Dynamically (Figure 4.3c), after the onset of impact, the pier motion causes pier top acceleration from the initial (at rest) state. Due to the mass of the superstructure, inertial forces develop at the superstructure level to resist this acceleration. Furthermore, the mass-dependent inertial forces atop the impacted pier act in unison with displacement-dependent stiffness forces to produce the total resistance of the superstructure. The combined effects of superstructure inertia and superstructure stiffness produce greater momentary (transient) restraint at the top of the pier (relative to the stiffness-based resistance alone). The presence of this phenomenon is evident in the predicted displacement-histories at the impact point and pier top locations (Figure 4.4b). Shortly after the onset of impact, the impact point displacement far exceeds the displacement at the pier column top, where inertial restraint inhibits the motion of the overlying superstructure. Peak dynamic internal forces occur almost simultaneously (0.13 sec and 0.14 sec for shear and moment, respectively) with a local peak in impact point displacement (at 0.15 sec); global peak pier displacements occur much later, near 0.50 sec. The transient increase in pier-top restraint (due to superstructure inertia) produces increased deformation within the pier columns, and therefore, elevated maximum pier column forces.

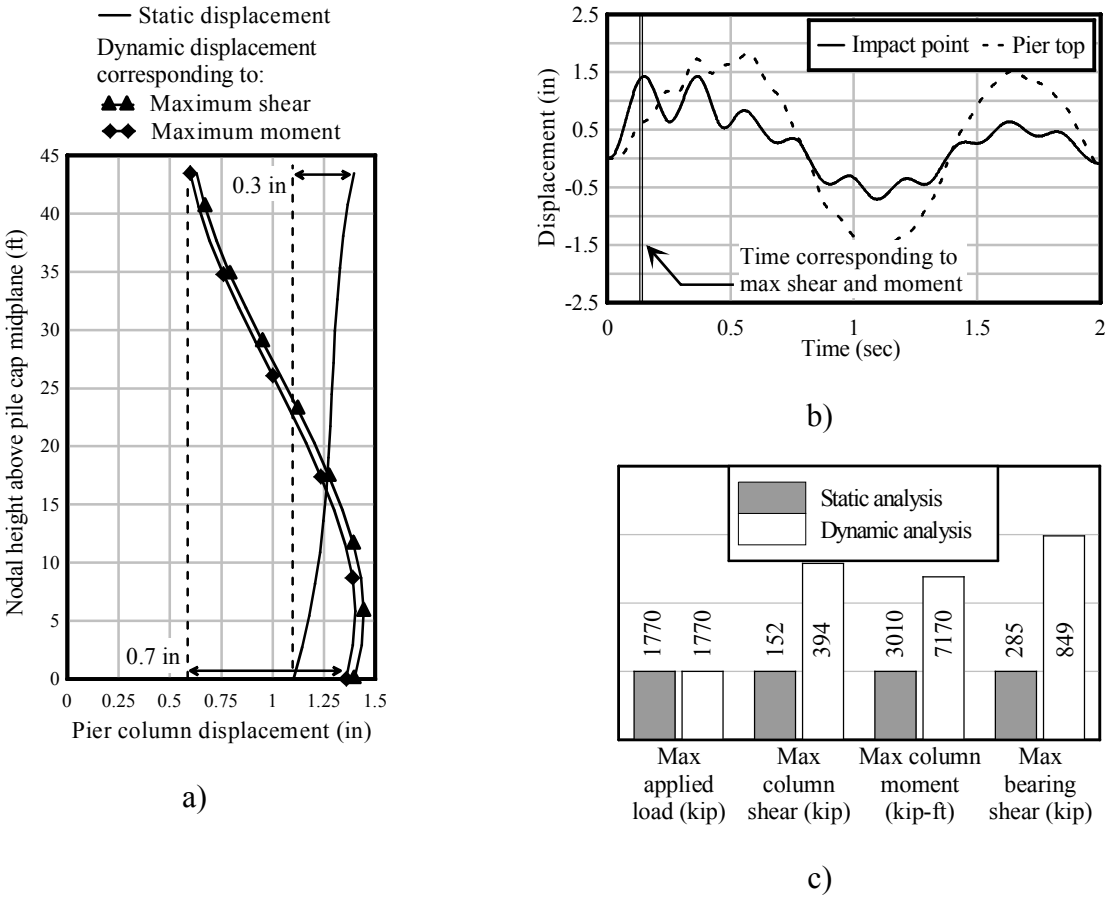

Figure 4.4 Summary data for inertial restraint case BLT-CHA-M.
a) Displacement profiles; b) Displacement time-histories; c) Maximum internal forces

To quantify the difference between static and dynamic predictions of pier column response, profiles of pier column displacement are presented (Figure 4.4a). [The dynamic displacement profiles correspond to times at which maximum pier column internal shear and moment occur.] Pier displacements of similar magnitude are predicted at the impact point (Figure 4.4a at a nodal height of 0 ft) in both cases. However, although 0.3 in. of relative displacement occurs above the impact point in the static case, a nearly linear pier column displacement profile is maintained. In contrast, for the dynamic case, approximately 0.7 in. of relative pier column displacement develops across the same elevation range, and furthermore, a substantial amount of curvature develops between nodal heights of 0 ft and 15 ft. The presence of relatively larger pier column displacements and curvatures (in the dynamic response) leads, in turn, to larger internal forces.

Dynamic and static predictions of maximum pier column internal forces and bearing forces for the BLT-CHA-M case are shown in Figure 4.4c. Although the peak loads applied in the dynamic and static analyses were of equal magnitude (1770 kips), dynamic predictions of maximum internal force were consistently and significantly larger than those predicted statically. Specifically, dynamic predictions of maximum pier column shear, moment, and bearing shear were each two to three times larger than the respective static predictions. The larger dynamic predictions of internal forces arise from the presence of additional superstructure resistance, which develops due to inertia of the superstructure mass. The disparity between static and dynamic response demonstrates that traditional static methods are incapable of predicting inertial restraint effects.

4.3.2 Amplification due to superstructure momentum

In the Pineda Causeway channel pier moderate-energy case (PNC-CHA-M), barge impact occurs near the top of a 20 ft tall shear wall that directly overlies a stiff, soil-embedded pile cap and tremie seal foundation (Figure 4.5a). The pier contains two circular columns (4.5 ft diameter) that extend approximately 53 ft from the top of the shear wall to the overlying pier cap; a 5 ft tall shear strut is provided (at mid-height) to brace the columns.

In static analysis, stiffness-related superstructure forces always act to resist pier motion. As shown in Figure 4.5b, the static superstructure resistance force acts from right to left as the pier top statically undergoes a positive displacement. In contrast, both stiffness-dependent and mass-dependent resistance forces are mobilized during dynamic analysis. Furthermore, in this case, maximum dynamic demands develop after the impact load phase, as the pier undergoes rebound motion. During this later stage of the impact event (after peak displacements have occurred and the superstructure has been accelerated by the impact load), the superstructure develops momentum, which becomes the primary driver of bridge response. Specifically, for the displaced shape shown in Figure 4.5c, the pier top displacement is negative, and hence, superstructure forces related to displacement (stiffness) act in opposition to the motion, from left to right. However, because the pier top is accelerating to the right at this time, inertial forces act from right to left (opposite to the direction of acceleration). Consequently, in the dynamic analysis (Figure 4.5c), the superstructure inertia force opposes the stiffness-based superstructure force (where the latter force always acts to resist pier displacement). The inertial force overcomes the stiffness-based resistance to amplify sway-mode bridge deformations and, consequently, internal member forces.

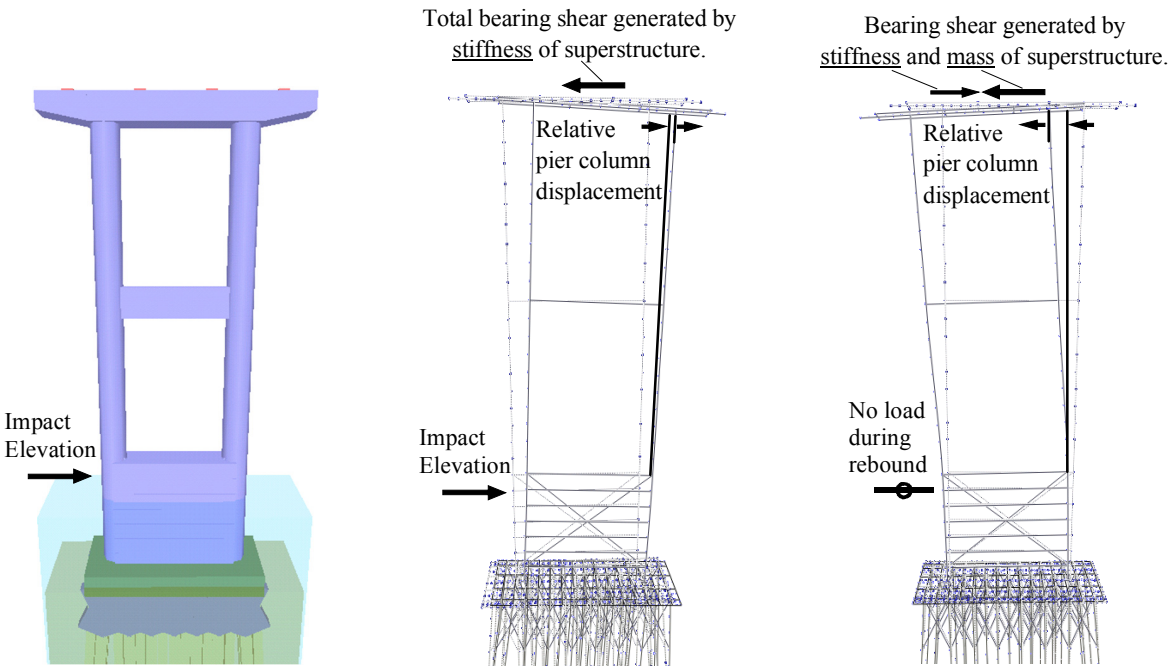

Figure 4.5 Summary data for superstructure momentum case PNC-CHA-M.
a) Pier configuration (superstructure not shown);
b) Static analysis case; c) Dynamic analysis case

The superstructure momentum-driven sway mode is also evident in the impact point and pier top displacement-histories (Figure 4.6b). Unlike the Blountstown Bridge case presented above, inertial restraint in the Pineda Causeway channel pier is minimal (occurring at approximately 0.13 sec). Instead, this tall and flexible pier is dominated by a sway mode response in which the pier top and impact point peaks of displacement occur at approximately the same point in time. From approximately 0.3 sec to 0.4 sec, the superstructure momentum is oriented in the same direction as the impact load, producing a peak pier top displacement at 0.41 sec.

While a global maximum of pier top displacement occurs at this time, maximum pier column forces develop later, during free vibration. [It should be noted, however, that pier column demands during this first oscillation are only approximately 10% smaller than subsequently developed maximum internal forces.] From approximately 0.4 sec to 0.8 sec, the superstructure motion reverses direction (rebounds), forcing the pier to sway in the opposite direction of impact and a second peak in pier top displacement occurs at 0.83 sec. Amplified sway-induced maximum internal forces develop in the pier columns at 0.79 sec (for column shear) and 0.86 sec (for column moment).

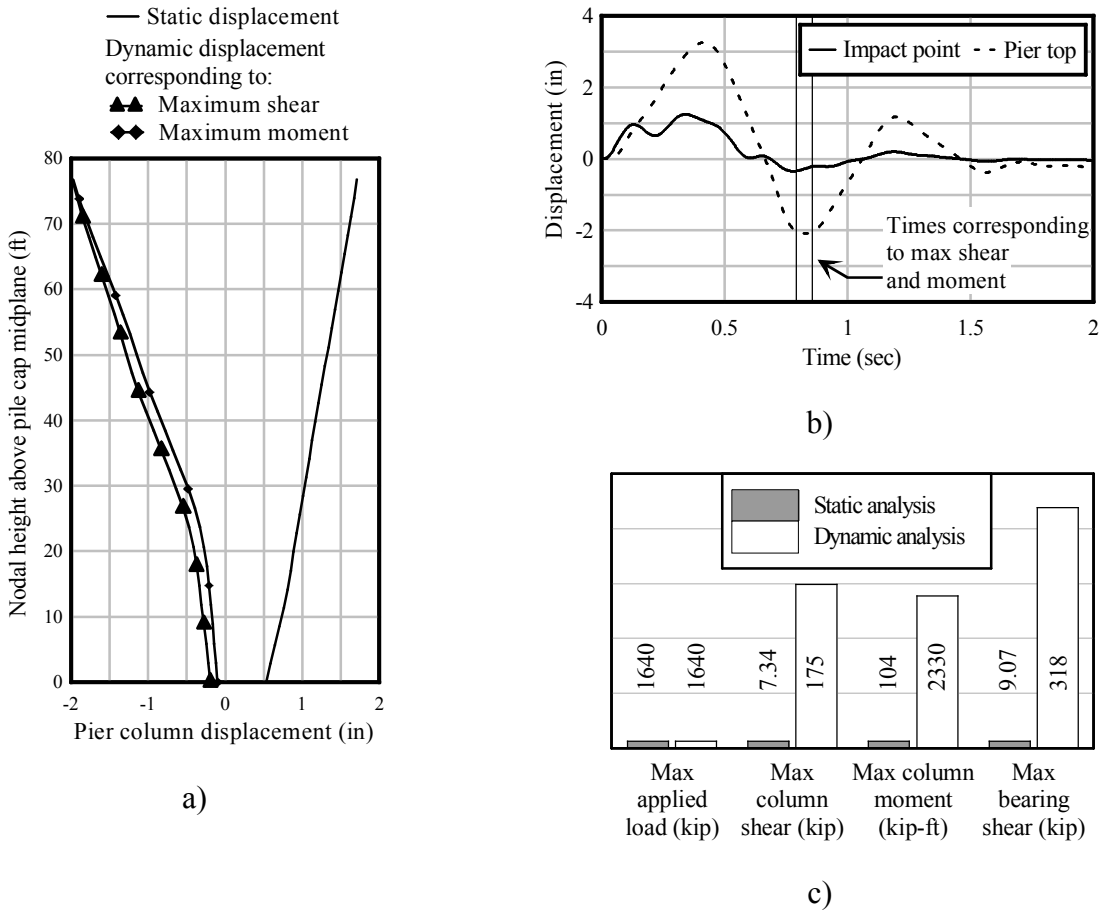

Figure 4.6 Summary data for inertial restraint case PNC-CHA-M.
a) Displacement profiles; b) Displacement time-histories; c) Maximum internal forces

Both the static and dynamic predictions of pier column displacement (Figure 4.6a) indicate a system-wide sway-type response; however, static and dynamic sway displacements occur in opposite directions. This disparity highlights a serious shortcoming of traditional static analytical methods in predicting pier displacements during collision events: traditional static methods cannot produce the (dynamic) displaced shape shown in Figure 4.6a. An additional source of discrepancy between the static and dynamic response predictions, in this case, is the fact that the superstructure possesses little static resistance. Consequently, the statically predicted pier column displacements produce only a nominal level of curvature. Relative displacement between the impact point and pier top stems primarily from rigid body pier rotation. In contrast, the dynamic sway-mode pier response exhibits substantial pier column flexural deformation (curvature), leading to dramatic amplification of internal column forces (Figure 4.6c) when compared to those of static analysis.

In Figure 4.6c, maximum pier column forces and total bearing shear forces (as computed by dynamic and static analyses) are compared for the PNC-CHA-M case. Even though the statically applied load is equal in magnitude to the maximum load generated during the dynamic analysis (1460 kips), extreme disparities exist in the predictions of pier column internal force and bearing shear. Dynamic demand predictions are an order of

magnitude (22 to 35 times) greater than those predicted statically. Among all cases included in the parametric study, the PNC-CHA-M results exhibit the most severe dynamic amplification. For this case, the significant flexibility of the superstructure (where such flexibility is due, in part, to the presence of an expansion joint atop each pier) leads to extreme levels of amplification in the pier. Such amplification exemplifies the limitations of employing static collision analysis methods that do not account for inertial forces: static analysis can vastly underpredict the internal forces that develop due to impact loading, especially when inertia forces are overtly dominant.

4.3.3 Mixed inertial restraint and superstructure momentum amplification

The Old St. George Island Bridge off-channel pier low-energy model (OSG-OFF-L) is shown in Figure 4.7a. In contrast to the two piers discussed in the previous sections, the displaced shapes shown in Figure 4.7b and Figure 4.7c for the OSG-OFF-L model are both dynamic shapes (the static displaced shape is not shown for this pier). In Figure 4.7b, the displaced shape corresponding to development of maximum dynamic pier column shear is shown; in Figure 4.7c, the shape corresponding to maximum dynamic pier column moment is shown. As these figures illustrate, the pier dynamically exhibits a combination of superstructure inertial restraint (Figure 4.7b) and momentum-driven sway (Figure 4.7c).

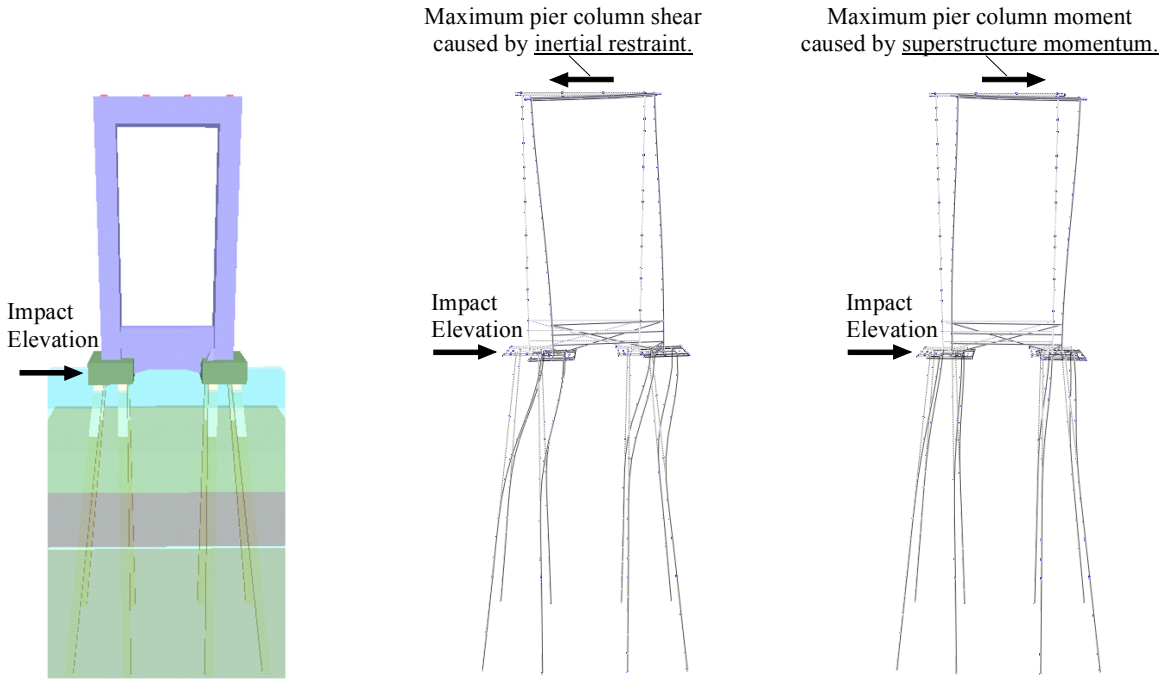

Figure 4.7 Summary data for mixed inertial restraint / superstructure momentum case OSG-OFF-L. a) Pier configuration (superstructure not shown); b) Dynamic displaced shape at time of max shear; c) Dynamic displaced shape at time of max moment

Even though maximum pier column shear force occurs due to dynamic inertial restraint at 0.10 sec (Figure 4.8b), the (subsequent) dynamic momentum-driven response induces maximum pier column moment at 0.22 sec. In the static analysis approach, only a single mode of pier response (displacements, forces) is predicted. In contrast, the maximum dynamic pier column internal forces are predicted to occur, respectively, in two distinct response modes (Figure 4.8a). Therefore, for bridges that are governed by a mixed dynamic response, static analysis is (at best) capable of accurately predicting only one of the two maximum dynamic internal forces of interest. In the OSG-OFF-L case, however, dynamic amplification effects are such that significant discrepancies exist between dynamic and static predictions for all pier column design forces of interest (Figure 4.8c). Specifically, the column shear and moment predicted by dynamic analysis each exceed the corresponding static demands by factors greater than 2. Also, the dynamic prediction of maximum bearing shear is nearly 4 times larger than the respective static prediction. This case demonstrates that amplification effects due to superstructure inertia can be significant, regardless of whether individual internal forces are driven by inertial restraint or superstructure momentum.

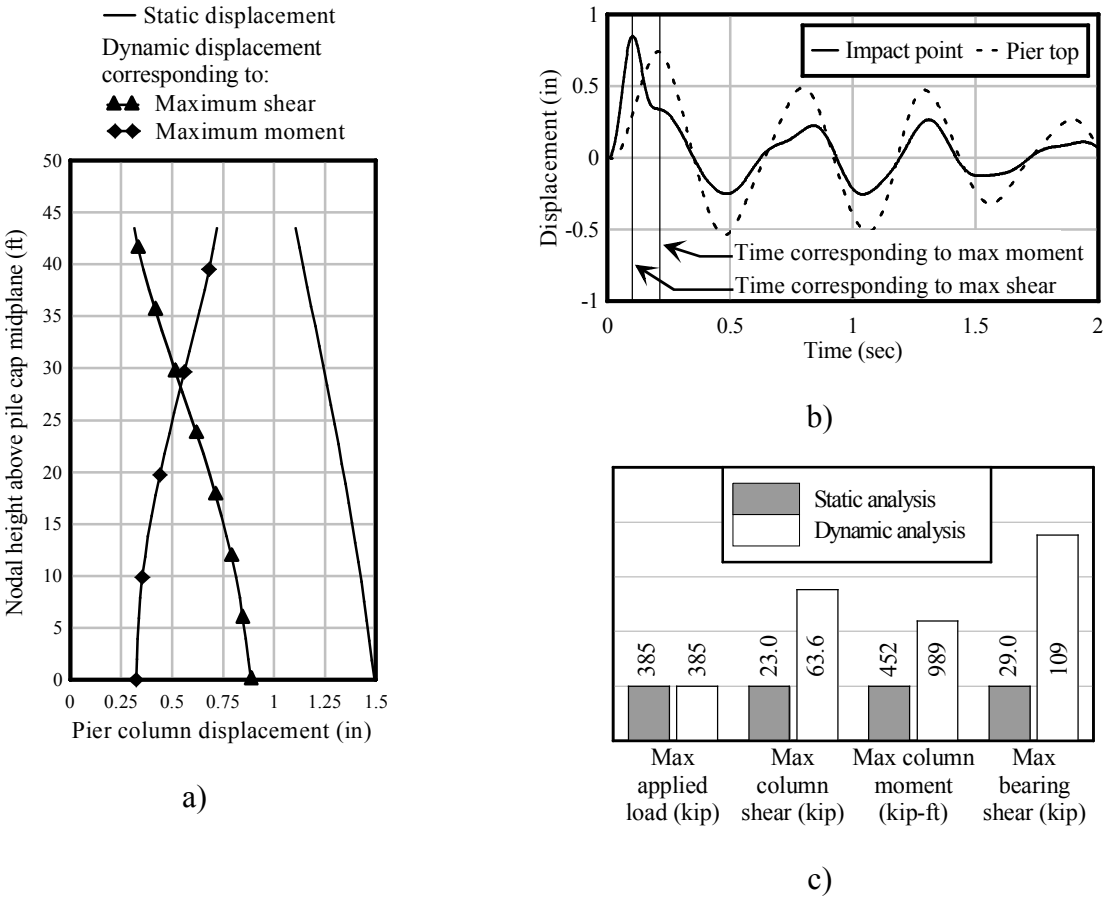

Figure 4.8 Summary data for inertial restraint case OSG-OFF-L.
a) Displacement profiles; b) Displacement time-histories; c) Maximum internal forces

4.3.4 Results summary

The cases presented above, sampled from the parametric study, are intended to illustrate specific modes of dynamic response and amplification. Overall, a total of 28 dynamic analyses and 28 corresponding static analyses were included in the parametric study. Static predictions of maximum pier column shear and moment, normalized by respective static analysis results, are presented in Figure 4.9. In this figure, a dynamic-to-static demand ratio greater than 1.0 indicates the occurrence of dynamic amplification. Data presented in Figure 4.9 are categorized primarily by response type and secondarily by applicable impact energy condition (increasing from left to right within each major grouping). Predicted ratios (dynamic relative to static) of maximum pier column shear are substantially greater than 1.0 for the vast majority of cases. Furthermore, a large number of ratios are substantially greater than 2.0, indicating that the dynamic predictions of demand are at least 100% larger than the static counterparts. Such ratios are found regardless of response type and impact energy; all three response types (restraint, sway, mixed) contain ratios greater than 2.0 and these values are observed for all four impact energy conditions. Also, magnitudes of demand ratios within a given response type vary widely. For example, the inertial restraint response type, which comprises the most common type among the dataset, contains a maximum value of more than 8.0 and a minimum value near 1.1. None of the demand ratios shown in Figure 4.9 are less than 1.0, clearly indicating that—for all cases studied here—the results from static analysis are unconservative in comparison to dynamic.

4.4 Conclusion

Using the results from dynamic and static barge impact analyses of numerous bridge structures, dynamic amplification phenomena in bridge pier columns have been quantified and categorized. Two principal dynamic barge-bridge collision response mechanisms have been identified: inertial restraint and momentum-driven sway. Importantly, both of these mechanisms are attributable to the mass of the superstructure overlying an impacted pier. In all cases, dynamic predictions of pier column demand (shear and moment) meet or exceed static predictions of demand, clearly indicating the occurrence of dynamic amplification.

Large variations in the amplification of maximum column forces demonstrates that dynamic influences, such as superstructure inertia, are inherently difficult to capture using existing static analysis procedures. Combinations of structural flexibility with either transient (momentary) restraint or superstructure momentum can produce dynamic member forces that substantially exceed the design forces predicted by static analysis. The results presented here demonstrate that the effects of both superstructure stiffness and mass (inertia) must be included in structural analyses performed for the purpose of establishing design forces for pier columns subjected to vessel impact loads. Failure to account for superstructure-generated inertial forces in the pier may result in the determination of unconservative design forces. In the following chapter, an equivalent static analysis procedure is proposed that empirically accounts for mass-related forces manifested during barge-bridge collision.

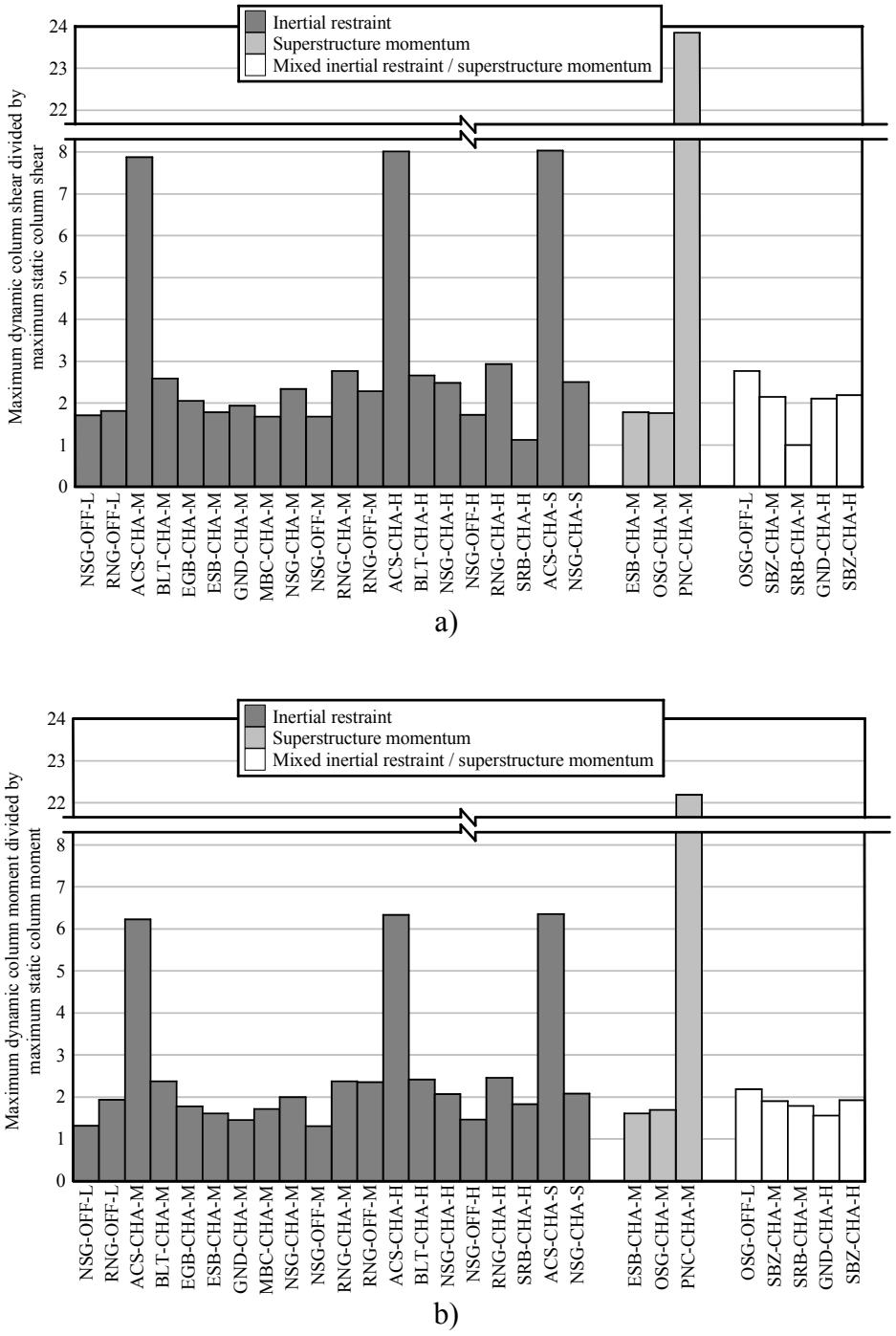

Figure 4.9 Maximum pier column dynamic demands relative to static demands
a) Shear; b) Moment

CHAPTER 5
STATIC BRACKETED IMPACT ANALYSIS (SBIA) METHOD

5.1 Introduction

As illustrated in previous chapters, current static analytical methods for barge-bridge collision do not account for dynamic amplification of pier member forces exhibited during impact events. Consequently, design forces obtained using traditional static procedures can be markedly unconservative. The ideal means by which to simulate inertial forces stemming from an impact event—and accurately predict member forces—is to use a fully dynamic time-history structural analysis procedure such as CVIA. However, such simulation procedures can be computationally expensive (relative to static analysis) and require a relatively detailed numerical description of the structure. These issues may be prohibitive in some design situations, particularly during preliminary bridge design when pertinent bridge details are subject to significant variation and frequent revision.

To address the accuracy limitations of static analysis and the computational requirements of dynamic time-history analysis while still accounting for inertial effects manifested during barge-bridge collision events, an equivalent static analysis method is developed, demonstrated, and validated in this chapter. The newly developed equivalent static analysis method is both simple to use and conservative (i.e., the proposed method accounts for dynamic amplification).

5.2 Conceptual overview

The primary limitation of existing static analysis methods for barge-bridge collision is the assumption that lateral pier resistance is provided only by soil and superstructure stiffness (Figure 5.1a). However, as was demonstrated in previous chapters, superstructure mass acceleration results in significant inertial restraint at the top of the pier immediately after impact (Figure 5.1b). In many cases, superstructure inertial resistance can equal or greatly exceed stiffness based resistance. Consequently, for most bridges, momentary maximum pier forces are manifested during this early stage of the impact event.

In addition to inertial restraint based dynamic amplification, a second mode of amplification was also identified in the previous chapter: superstructure momentum-driven sway. In this case, maximum pier forces occur later in time, perhaps after the barge is no longer in contact with the pier. Furthermore, oscillation of the superstructure mass can act as a source of loading, ultimately driving maximum pier forces. However, even in cases where superstructure momentum is the dominant dynamic amplification mode, a sudden, significant increase in member demands initially occurs as a result of inertial restraint (resistance) at the pier top. For the sway-controlled cases described in the previous chapter, the initial restraint based demands reached magnitudes that were 70-80% as large as the maximum demands observed later, during the superstructure sway response. As such, the superstructure inertial resistance phenomenon is present and significant for all structural configurations studied. In addition, no adequate means have been identified to predict which dynamic amplification mode will dominate the response of a given bridge. Therefore, focus is given to the development of analytical procedures that statically approximate superstructure inertial resistance, which can be scaled up to conservatively envelope the sway-driven values.

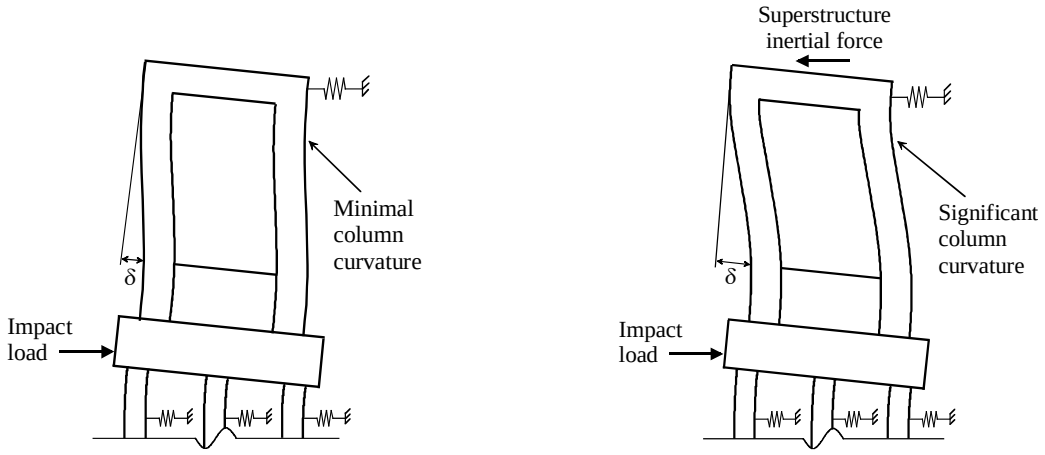

(a) (b)

Figure 5.1 Static barge impact analysis: a) Existing methods (AASHTO 1991), and b) Accounting for superstructure inertial resistance.

5.2.1 Superstructure modeling

Three primary superstructure stiffness modeling schemes were considered for use in this study:

- Full multiple-pier, multiple-span bridge model
- One-pier, two-span (OPTS) bridge model including impacted pier and adjacent spans
- One-pier model with a single lateral spring representing the superstructure stiffness

However, it has previously been demonstrated (Consolazio and Davidson 2008) that a one-pier, two-span (OPTS) bridge model provides an accurate approximation of both static and dynamic behavior of full multiple-pier multiple-span bridge models. As such, OPTS modeling will be employed in development of the equivalent static analysis method (i.e., the use of full bridge models is not necessary in this study).

To develop and validate the equivalent static analysis method for barge impact, both OPTS and spring-based superstructure models were considered (Figure 5.2). While the OPTS modeling technique is more accurate, the representation of superstructure stiffness with a single equivalent spring is common practice in bridge design, especially during preliminary design. As such, both approaches are considered in the suitability assessment of the proposed analytical method for use in design practice.

5.2.2 Static impact load determination

A critical step in any impact analysis is to quantify the maximum dynamic load imparted to the structure of interest. In the equivalent static method developed here, maximum magnitude dynamic loads are determined, in part, by using the principle of conservation of energy (Cowan 2007, Consolazio et al. 2008) as follows:

$$\Delta KE_{if} + \Delta DE_{if} = 0 \tag{5.1}$$

where ΔKE_{if} is the change in kinetic energy of the barge, and ΔDE_{if} is the change in total deformation energy (i.e., the sum of the elastic and plastic deformation energies), associated with the deformation of the barge bow, from the initial state (i) to the final state (f). Conservation of energy enables a relationship between the maximum impact load and the barge parameters to be defined.

Assuming that barge mass does not change during the collision, the change in barge kinetic energy can be expressed as:

$$\Delta KE_{if} = 1/2\, m_B \left(v_{Bf}^2 - v_{Bi}^2 \right) \tag{5.2}$$

where m_B is the constant (unchanging) mass of the barge and v_{Bf} and v_{Bi} are the magnitudes of the barge velocities at the initial and final states respectively.

In general, the deformation energy for the barge can be described as:

$$\Delta DE_{if} = \int_{a_{Bi}}^{a_{Bf}} P_B(a_B)\, da_B \tag{5.3}$$

where $P_B(a_B)$ is the impact force as a function of barge crush depth (a_B); a_{Bi} and a_{Bf} are the barge crush depths at the initial and final states respectively.

To estimate the maximum impact load acting on the pier, the following assumptions were made: 1.) the initial barge crush depth (a_{Bi}) is assumed to be zero, 2.) the barge bow force-deformation relationship is assumed to be elastic, perfectly-plastic (Figure 5.3), and 3) the pier is *initially* assumed to be rigid and fixed in space (note that this assumption is later removed, as described later).

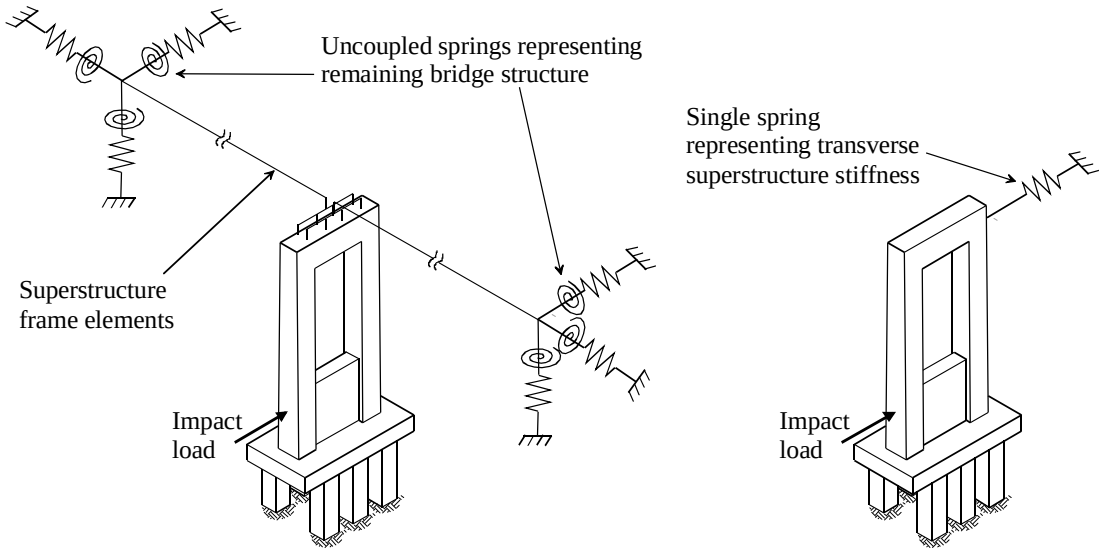

a) OPTS superstructure model b) Spring superstructure model

Figure 5.2 Superstructure modeling techniques considered

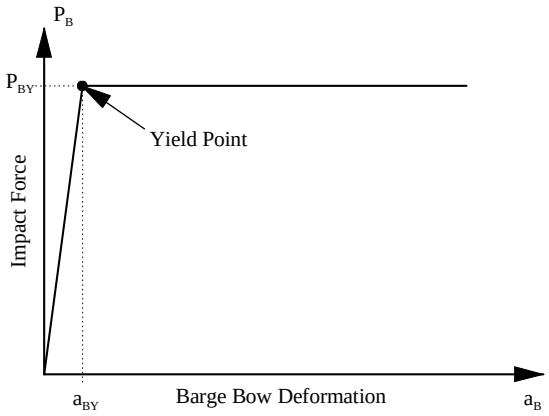

Figure 5.3 Barge bow force-deformation relationship

The rigid pier assumption implies that the initial kinetic energy of the barge is fully converted into deformation energy of the barge bow during loading of the barge (Figure 5.4a). Thus, once all of the barge initial kinetic energy has been converted into deformation of the barge bow (i.e., the barge velocity becomes zero) the barge bow crush depth has reached a maximum value. Additionally, when the barge bow recovers the elastic portion of its deformation energy through unloading, this energy is then converted back into rebound motion of the barge (Figure 5.4b). The final barge kinetic energy can then be determined from the recovered deformation energy.

If the barge bow remains linear-elastic, the conservation of energy up to the point of maximum barge bow deformation can be represented by the following equation:

$$\Delta KE_{im} + \Delta DE_{im} = -1/2 \cdot m_B \cdot v_{Bi}^2 + 1/2 \cdot P_B \cdot a_{Bm} = 0 \tag{5.4}$$

where P_B is the maximum impact force observed during the impact, and a_{Bm} is the maximum barge bow deformation. The maximum impact force and barge bow deformation, however, remain undetermined up this point, and thus, an additional equation is required.

If the barge bow remains elastic, the maximum bow deformation can be defined as follows:

$$a_{Bm} = \frac{P_B}{k_B} = \frac{P_B}{\left(P_{BY}/a_{BY}\right)} \tag{5.5}$$

where a_{BY} and P_{BY} are the barge bow deformation and force at yield, respectively, and k_B is the initial elastic stiffness of the barge bow. Combining Eqns. 5.4 and 5.5, and solving for the maximum load produces the following equation:

$$P_B = v_{Bi}\sqrt{\frac{P_{BY}}{a_{BY}} m_B} = v_{Bi}\sqrt{k_B m_B} \le P_{BY} \tag{5.6}$$

Due to the elastic, perfectly-plastic assumption for the barge bow force-deformation relationship, the maximum barge impact force is limited to the yield load of the barge bow.

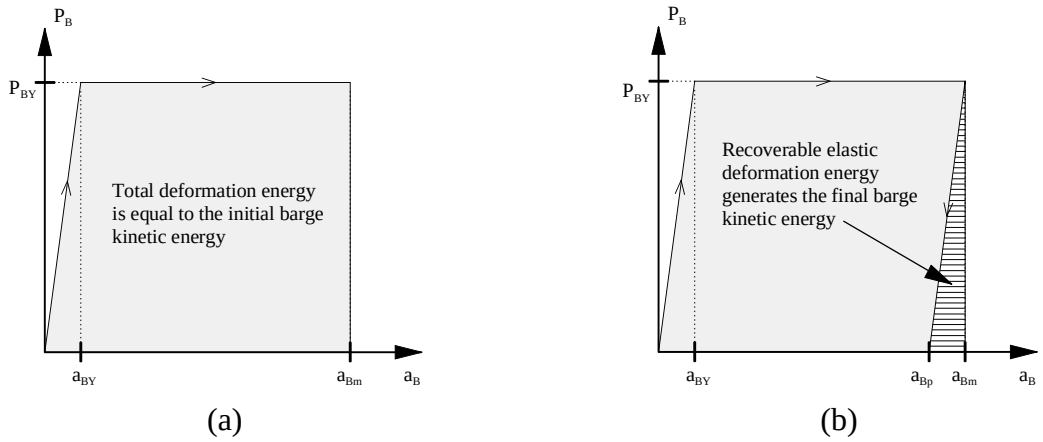

Figure 5.4 Inelastic barge bow deformation energy: a) Loading, and b) Unloading

Validation attempts, using the analytical model in Eqn. 5.6, revealed that the rigid pier assumption is overly conservative in cases where the barge deformation remains elastic (Cowan 2007, Consolazio et al. 2008). This finding necessitates inclusion of the finite stiffness of the impacted pier-soil system into the formulation. The stiffness of the barge and pier-soil system are then combined to form a series stiffness (k_S).

$$k_S = \left(\frac{1}{k_B} + \frac{1}{k_P} \right)^{-1} = \left(\frac{a_{BY}}{P_{BY}} + \frac{1}{k_P} \right)^{-1} \tag{5.7}$$

where k_P is the linear stiffness pier-soil system. Replacing the initial elastic barge stiffness (k_B) in Eqn. 5.6 with the effective barge-pier-soil series spring stiffness (k_S) (Eqn. 5.7) produces the following equation:

$$P_B = v_{Bi}\sqrt{k_S m_B} = v_{Bi} \cdot c_{BP} \le P_{BY} \tag{5.8}$$

where c_{BP} is the barge-pier pseudo-damping coefficient, defined as follows:

$$c_{BP} = \sqrt{k_S m_B} \tag{5.9}$$

By incorporating the series stiffness (k_S) in place of the barge stiffness (k_B), the accuracy of the load prediction model is greatly enhanced, providing a reliable means of estimating the peak vessel impact load. Note that two of the three initial assumptions: the initial barge crush depth (a_{Bi}) is assumed to be zero; and, the barge bow force-deformation relationship is assumed to be elastic, perfectly-plastic (recall Figure 5.3) are still employed in the maximum impact force calculation. See Cowan (2007) or Consolazio et al. (2008) for additional details and validation of the procedure.

5.3 Potential static approximations of superstructure inertial resistance

In previous chapters, superstructure inertial resistance was identified as the dominant source of dynamic pier force amplification during vessel impact events. Current static analytical methods (e.g., those given in the AASHTO provisions) do not account for such

dynamic effects. To address this important shortcoming, three analytical schemes were assessed to statically approximate the additional source of superstructure resistance that is attributable to inertia:

- Restrain the pier top with an infinitely stiff lateral boundary condition (Figure 5.5a)
- Amplify the lateral superstructure stiffness (Figure 5.5b)
- Directly apply an inertial load at the superstructure level (Figure 5.5c)

Each of these approaches incorporated one of three components common to all static analyses: boundary conditions, stiffness, and loads.

Approximating superstructure inertial resistance by means of boundary conditions (i.e., fixing the pier-top elevation) generally proved overly conservative; static predictions of pier demands greatly exceeded those quantified by dynamic simulations. In addition, the level of conservatism varied greatly between various structural configurations. This result is, in part, predictable, as a fixed boundary condition allows no lateral deflection at the pier-top elevation. Dynamic simulations consistently show positive, non-zero displacements (in the direction of impact) at this elevation during times at which maximum structural demands occur. As such, a fixed pier-top boundary condition provides an unreasonable level of restraint.

Given these findings, use of a finite-stiffness boundary condition at the pier-top elevation was then considered. As noted in previous chapters, static superstructure stiffness alone does not provide sufficient resistance to adequately predict dynamic amplification effects. Thus, the lateral superstructure stiffness was amplified to account for both static superstructure resistance and superstructure inertial resistance. This approach proved reasonably effective in producing displaced pier shapes and member demand predictions that were consistent with dynamic analysis. However, a large degree of variability in the stiffness magnification factors was observed across a range of structural configurations. Furthermore, no correlation was observed between these magnification factors and corresponding bridge parameters. Consequently, amplifying superstructure stiffness was deemed an impractical means of approximating superstructure inertial resistance.

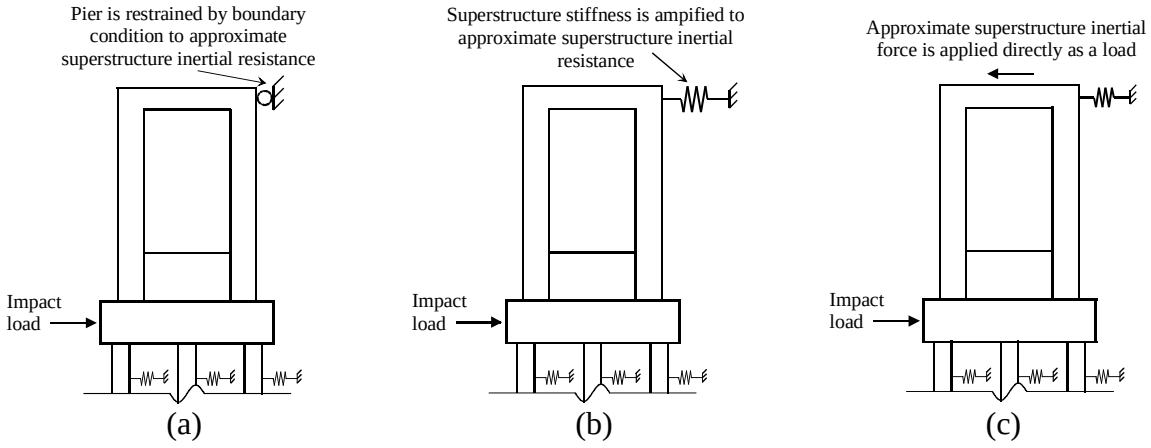

Figure 5.5 Static approximation of superstructure inertial resistance:
a) Pier top restraint with boundary conditions; b) Amplified superstructure stiffness; and c) Directly applied inertial load

Given the significant level of conservatism and variability associated with boundary condition and stiffness-based approximations of inertial resistance, a third major static approach was considered—approximating the superstructure inertial resisting force and applying it as a static load (Figure 5.5c). As was the case with magnified superstructure stiffnesses, static inertial forces varied substantially among differing structural configurations. However, correlations were identified between the static inertial loads and corresponding bridge parameters, thus providing an accurate static approximation of dynamic pier behavior.

5.4 Static approximation of inertial resistance by direct load application

An empirical approach was employed to develop equivalent static loading conditions that provide accurate predictions of both maximum dynamic member forces and dynamic pier displacements. Ideal static loading conditions were determined for eleven (11) Florida bridge piers, incorporating a wide range of common pier styles. In addition, one or more representative impact energy conditions were considered for each bridge, resulting in twenty (20) pier/energy cases. Load prediction equations were then developed that correlate static inertial loads to readily available bridge parameters.

5.4.1 Factored impact load

Static superstructure inertial forces were found to be strongly sensitive to the choice of impact load. For any given impact-point load (within a reasonable range), a corresponding pier-top load can be identified that will provide an adequate prediction of dynamic member forces (shears and moments). However, if the impact-point load is too small, unrealistic pier displacements result. Specifically, if the maximum dynamic impact load is applied as calculated from Eqn. 5.8, the corresponding pier-top loads must be very large to obtain member forces similar to those predicted dynamically. In many cases, the large pier-top load causes the pier to deflect laterally into the negative range (opposite of the impact direction). Negative lateral displacements were not observed from dynamic analysis, thus this static response is undesirable.

To counteract this tendency, a factored impact load was employed. Use of an amplified impact load causes piers, as a whole, to deflect in the impact direction, avoiding possibly unrealistic negative lateral pier displacements. Through an iterative process, an impact load factor of 1.45 (Figure 5.6) was found to be optimal in terms of producing realistic displaced shapes, while still providing accurate estimations of dynamic member forces.

5.4.2 Determination of ideal pier-top loads

Having factored the peak impact load (P_B) by 1.45, ideal static pier-top inertial loads (P_I) were determined by iteration. An ideal pier-top load is defined as the load that generates a static pier demand equal to the respective maximum dynamic pier demand (e.g., that pertaining to pier column moment, as shown in Figure 5.7). For each of the twenty (20) pier/energy cases studied, ideal pier-top loads were determined utilizing both OPTS and spring-based superstructure models (recall Figure 5.2). Ideal pier-top inertial loads were normalized by corresponding impact loads (P_B) to form ideal inertial resistance factors

(IRF_{ideal}). In total, three sets of ideal inertial resistance factors (IRF) were developed, one for each of: pier column moment, pier column shear, and total bearing shear.

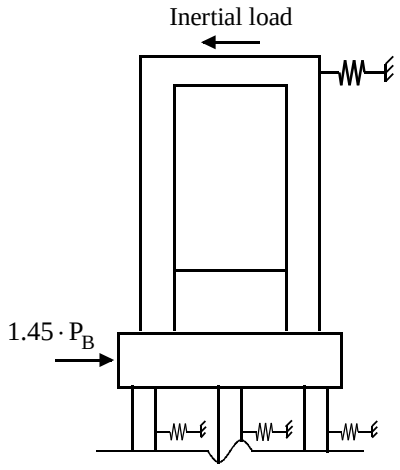

Figure 5.6 Impact load magnified by a factor of 1.45

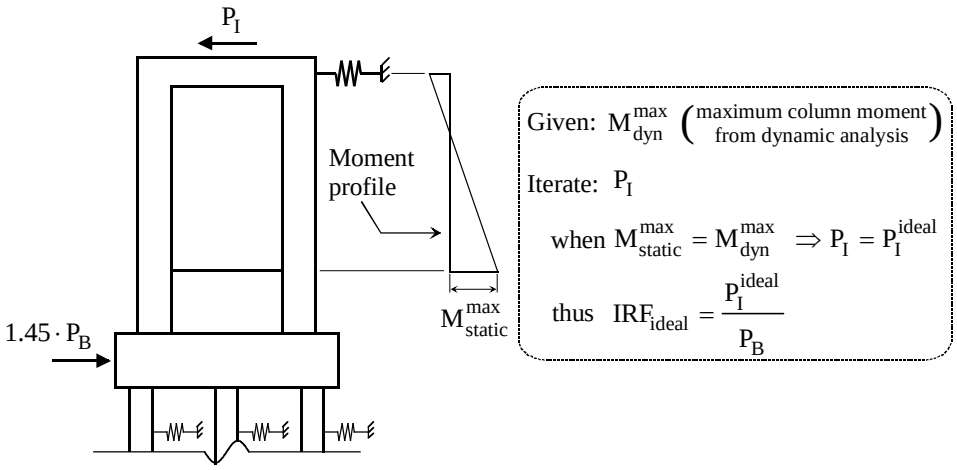

Figure 5.7 Determination of ideal pier-top load and IRF for a given bridge pier (calibrated to column moment)

5.4.3 Correlation of pier-top inertial resistance (IR) factors to bridge parameters

In the interest of developing a universal loading condition for all bridge configurations, one possible approach is to use the maximum observed IR value for all bridges types. However, significant variation in ideal IRF magnitudes was observed between differing structural configurations—IRF values ranged from a minimum of 0.02 to a maximum of 1.17. Thus, applying an equivalent inertial load equal to $1.17 \cdot P_B$ to a bridge for which the ideal IRF is 0.02 is unreasonably conservative. To mitigate excessive conservatism, ideal IRF values were correlated to key structural parameters, to form empirical IRF prediction equations. These equations allow for computation of bridge-specific IRFs, providing a more accurate result than simply utilizing a uniform load factor for all

bridges. Additionally, IRF prediction equations were calibrated separately to each major pier demand type—column moment, column shear, and total bearing shear—so that conservatism was minimized.

Several bridge parameters were considered for possible correlation to inertial resistance. Quantities such as natural frequency or superstructure acceleration generally control dynamic pier behavior. However, quantities of this nature are not readily determined without first conducting a dynamic analysis. Furthermore, during the early portions of the bridge design process, sufficient information may simply not be available to estimate such dynamic properties. Instead, ideal IRF values were correlated to parameters that can be easily quantified or estimated at any practical stage of design. Parameters were considered that involve geometry, mass distribution, and stiffness of the various bridge components—all of which influence dynamic pier behavior. The following quantities were considered:

- Pier height (h_p)
- Span length (L_s)
- Superstructure weight (W_{sup})
- Superstructure stiffness (k_{sup})
- Pier weight (W_p)
- Pier stiffness (k_p)

Since these parameters were identified as likely predictors of inertial bridge response, it was expected that a combination of these parameters would correlate well with computed ideal IRF values. To assess this expectation, an algorithm was developed that systematically evaluated each of several thousand possible combinations of the six bridge parameters listed above ($p_1 \ldots p_6$), subject to the following functional form:

$$\gamma = \left(p_1^{\alpha_1}\right) \cdot \left(p_2^{\alpha_2}\right) \cdot \left(p_3^{\alpha_3}\right) \cdot \left(p_4^{\alpha_4}\right) \cdot \left(p_5^{\alpha_6}\right) \cdot \left(p_6^{\alpha_6}\right) \tag{5.10}$$

where, $\alpha_1 \ldots \alpha_6 = +1, -1, +\frac{1}{2}, -\frac{1}{2}, +\frac{1}{4}, -\frac{1}{4}$.

For each possible combination, the product of bridge parameters (γ) was computed for each bridge considered in the study. Linear regression was used to correlate γ values to observed ideal IRF factors for each pier/energy condition. To quantify the level of dependency between γ and IRF, correlation coefficients (r) were computed for each of the several thousand trial correlations. This combinatorial analysis yielded viable relationships between the six bridge parameters and IRF. Specifically, the following parameter combination was most meaningfully correlated with IRF:

$$\gamma = \frac{1}{h_p} \sqrt{\frac{k_{sup}}{\sqrt{W_p}}} \tag{5.11}$$

By correlating each of the three sets of ideal IRF values to γ (as computed in Eqn. 5.11), the following linear regression equations result (Figure 5.8):

$$IRF_m^{ideal} = 0.12 + 3.4 \cdot \gamma = 0.12 + \frac{3.4}{h_p} \sqrt{\frac{k_{sup}}{\sqrt{W_p}}} \tag{5.12}$$

$$IRF_v^{ideal} = 0.24 + 1.6 \cdot \gamma = 0.24 + \frac{1.6}{h_p}\sqrt{\frac{k_{sup}}{\sqrt{W_p}}} \tag{5.13}$$

$$IRF_b^{ideal} = 0.20 + 5.1 \cdot \gamma = 0.20 + \frac{5.1}{h_p}\sqrt{\frac{k_{sup}}{\sqrt{W_p}}} \tag{5.14}$$

where IRF_m^{ideal} (Figure 5.8a), IRF_v^{ideal} (Figure 5.8b), and IRF_b^{ideal} (Figure 5.8c) are ideal IRF factors calibrated to pier moment, pier shear, and total bearing shear, respectively.

Correlation coefficients (r) were computed for the correlations defined by Eqns. 5.12, 5.13, and 5.14 (0.88, 0.59, and 0.85 respectively). Each of the correlation coefficients exceed the Pearson's critical r value of 0.561 (Pearson and Hartley 1958)—for a sample size of 20 and 0.01 significance—implying that the correlations are statistically meaningful.

Note that Eqns. 5.12, 5.13, and 5.14 do not constitute a static analytical method that is conservative when compared to dynamic analysis. These regression equations predict conservative values of IRF (and corresponding pier-top forces) for only 50% of conceivable cases. Consequently, an upper bound envelope was needed that had a greatly increased likelihood of conservatism. Thus, envelopes were developed for each correlation, corresponding to a 99% confidence level (using the Student's t-distribution)—implying that the resulting static pier demands will equal or exceed the corresponding dynamic demands 99 out of 100 times. Envelopes of this form for each demand type are described by the following equations (Figure 5.8):

$$IRF_m = 0.22 + \frac{4.5}{h_p}\sqrt{\frac{k_{sup}}{\sqrt{W_p}}} \tag{5.15}$$

$$IRF_v = 0.36 + \frac{3.0}{h_p}\sqrt{\frac{k_{sup}}{\sqrt{W_p}}} \tag{5.16}$$

$$IRF_b = 0.37 + \frac{7.0}{h_p}\sqrt{\frac{k_{sup}}{\sqrt{W_p}}} \tag{5.17}$$

Thus, dynamic column moment, column shear, and total bearing shear demands may be conservatively estimated by statically analyzing the impacted pier under the load conditions illustrated in Figure 5.9. Note that three distinct static analyses must be conducted, where the results from each analysis are used to predict the maximum demand corresponding to the chosen IRF. For example, when the structure is analyzed using the IRF corresponding to moment (IRF_m), the column shears and bearing shears predicted by this analysis are not utilized.

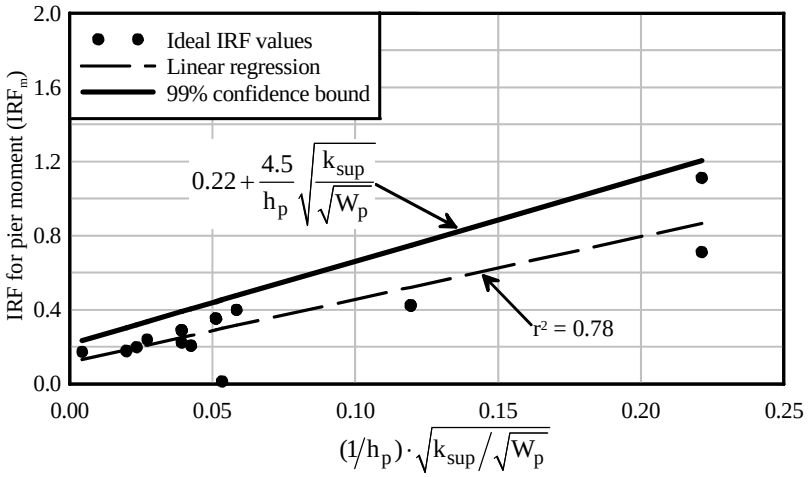

(a) Calibrated to pier moment

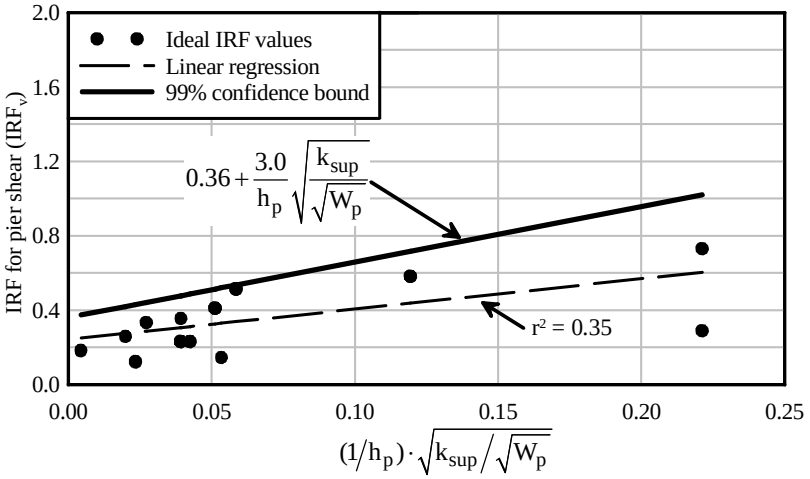

(b) Calibrated to pier shear

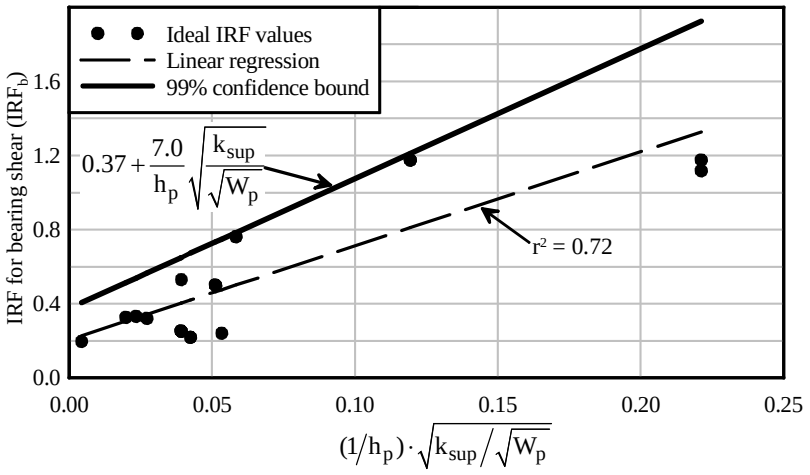

(c) Calibrated to total bearing shear

Figure 5.8 Correlation between inertial resistance factor (IRF) and bridge parameters

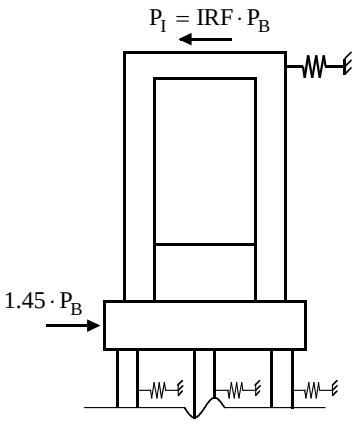

To obtain pier moments:

$$IRF_m = 0.22 + \frac{4.5}{h_p}\sqrt{\frac{k_{sup}}{\sqrt{W_p}}}$$

To obtain pier shears:

$$IRF_v = 0.36 + \frac{3.0}{h_p}\sqrt{\frac{k_{sup}}{\sqrt{W_p}}}$$

To obtain bearing shears:

$$IRF_b = 0.37 + \frac{7.0}{h_p}\sqrt{\frac{k_{sup}}{\sqrt{W_p}}}$$

Figure 5.9 Static loading to approximate superstructure dynamic amplification

The static loading scheme illustrated in Figure 5.9 constitutes a (minimally) conservative static analysis procedure for predicting both direct load effects of barge impact and indirect dynamic amplifications caused by superstructure inertial resistance. Prediction equations for pier-top inertial resistance factors (Eqns. 5.15, 5.16, and 5.17) include structural parameters that are important to dynamic amplification, and are simultaneously quantifiable during design. Furthermore, the level of conservatism—relative to dynamic analysis—is minimized by separately analyzing for pier moment, pier shear, and total bearing shear.

5.5 Substructure considerations

While the static loading conditions shown in Figure 5.9 provide adequate predictions of pier column and bearing shear demands, dynamic substructure forces (pile/shaft moments and shears) are consistently underestimated by this procedure. Since static inertial load ($IRF \cdot P_B$) opposes amplified impact load ($1.45 \cdot P_B$), forces transmitted through the foundation to the soil are relieved. Thus, foundation demands must be considered separately, excluding a pier-top inertial load. An empirical static loading condition was developed for predicting pile/shaft design forces, where a methodology similar to that described above was implemented.

5.5.1 Determination of ideal impact-point loads

To develop a load model for predicting dynamic pile/shaft demands, ideal impact-point loads were developed for each of the twenty (20) pier/impact energies considered. As illustrated in Figure 5.10, the ideal amplified impact load (P_{Bamp}^{ideal}) is defined as the load for which the static pile/shaft moment (M_{static}^{max}) equals the maximum moment predicted by dynamic analysis (M_{dyn}^{max}). For each case, ideal amplified impact loads were normalized by corresponding approximate impact loads (P_B) to form ideal impact-point dynamic magnification factors (DMF_{ideal}).

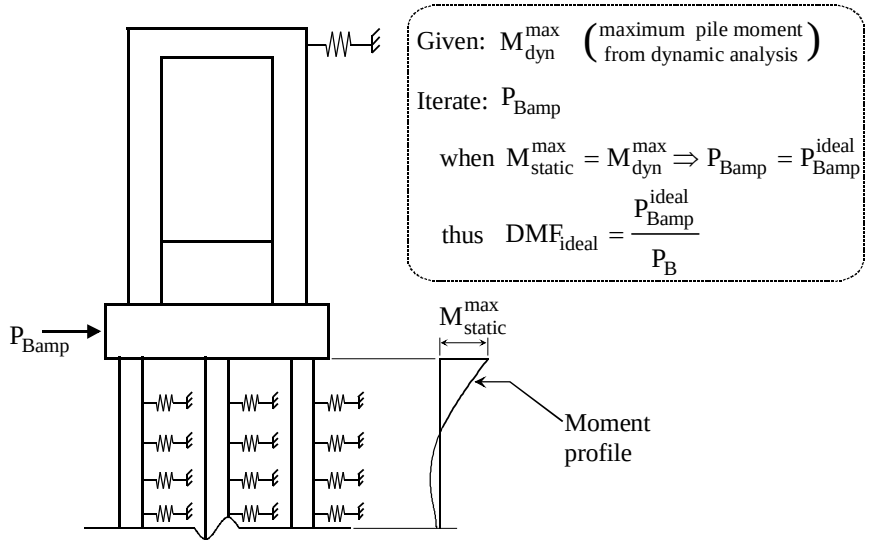

Figure 5.10 Determination of ideal amplified impact load and DMF for a bridge pier (calibrated to pile moment)

5.5.2 Correlation of impact-point DMF to bridge parameters

Ideal impact-point DMF values for the cases considered ranged from 0.93 to 1.6—implying that the impact force (P_B, calculated from Eqn. 5.8) is too small to provide conservative estimates of dynamic pile/shaft demands, in most cases. Thus, a dynamic magnification factor must be considered for impact loads.

A combinatorial study was conducted using the methodology described previously to identify correlations between bridge structural parameters and impact-point DMF. As before, several-thousand trial correlations were computed and assessed by means of correlation coefficients (r). In contrast to the previous investigation, no statistically meaningful correlations were observed between bridge parameters and impact-point DMF. Consequently, the impact-point DMF was treated as uniform across all structural configurations and impact conditions. Among the twenty (20) cases studied, the mean DMF was 1.34. However, an upper bound envelope was desired to greatly increase the probability of conservatism. Thus, a uniform envelope of 1.85 was established (Figure 5.11)—corresponding to a 99% confidence upper bound—using the Student's t-distribution. Thus, by amplifying the barge impact load (P_B) by a factor of 1.85, conservative estimates of foundation design forces are produced.

5.6 Static bracketed impact analysis (SBIA) method

The static bracketed impact analysis (SBIA) method consists of bracketing (or enveloping) member design forces using the two static loading conditions described above. In this manner, pier column, bearing shear, and foundation design forces are conservatively quantified with regard to dynamic amplifications. The SBIA method is summarized and demonstrated in this section.

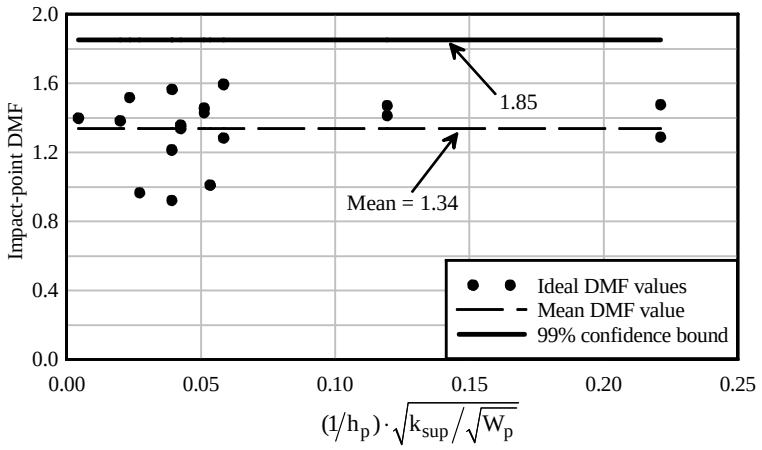

Figure 5.11 Mean value and envelope of impact-point DMF

5.6.1 SBIA overview

The proposed SBIA procedure (Figure 5.12) consists of two primary load cases. Load Case 1 involves statically applying both an amplified impact load equal to $1.45 \cdot P_B$ and a statically equivalent superstructure inertial load equal to $IRF \cdot P_B$. The magnitude of IRF depends on both bridge structural parameters (h_p, k_{sup}, and W_p) and the desired pier demand type (pier moment, pier shear, or total bearing shear). Typically, Load Case 1 controls the design of pier columns and bearing connections to resist vessel collision forces. Load Case 2 consists of a single amplified impact load equal to $1.85 \cdot P_B$. Load Case 2 typically controls the design of foundation elements such as piles or drilled shafts.

It should be noted, however, that feasible structural configurations and impact conditions exist for which the typical controlling load case does not control for a given member type. Consequently, maximum pier demands obtained between both load cases should be considered for design (i.e. the results must be bracketed by both load cases). This bracketing approach is consistent with widely accepted structural design practice concerning multiple loading conditions. Figure 5.12 provides a summary of the entire SBIA procedure as well as specific definitions for the quantities h_p, k_{sup}, and W_p, where these quantities are required for calculation of IRF values.

5.6.2 SBIA Demonstration

In this section, the SBIA method is demonstrated in detail for one of the twenty (20) pier/energy cases considered in this study—the Blountstown Bridge channel-pier high-energy case (BLT-CHA-H). The bridge is analyzed using both OPTS and spring superstructure models (recall Figure 5.2). Refer to Table 4.1 and Table 4.2, in the previous chapter, for additional details of the structural configuration for this bridge and for a definition of the impact condition. For the Blountstown Bridge—formally known as the New Trammell Bridge—high-energy case (BLT-CHA-H), barge impact occurs on the channel pier near the top of a 30.5 ft tall shear wall that connects two 9 ft diameter drilled shafts (Figure 5.13). Two circular pier columns (5.5 ft diameter), which are axially collinear with each foundation shaft, span from the foundation elements to the top of the pier.

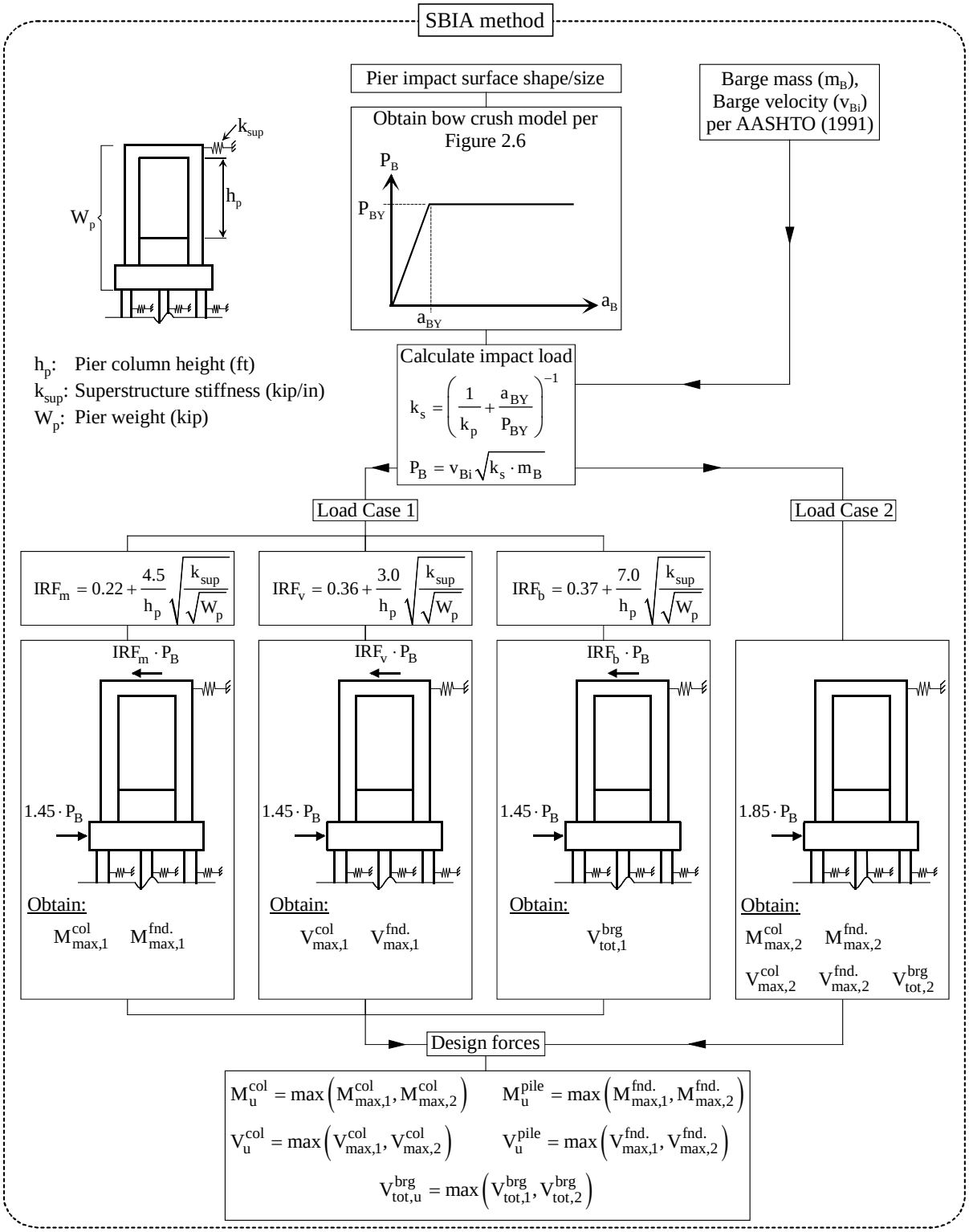

Figure 5.12 Static bracketed impact analysis (SBIA) method

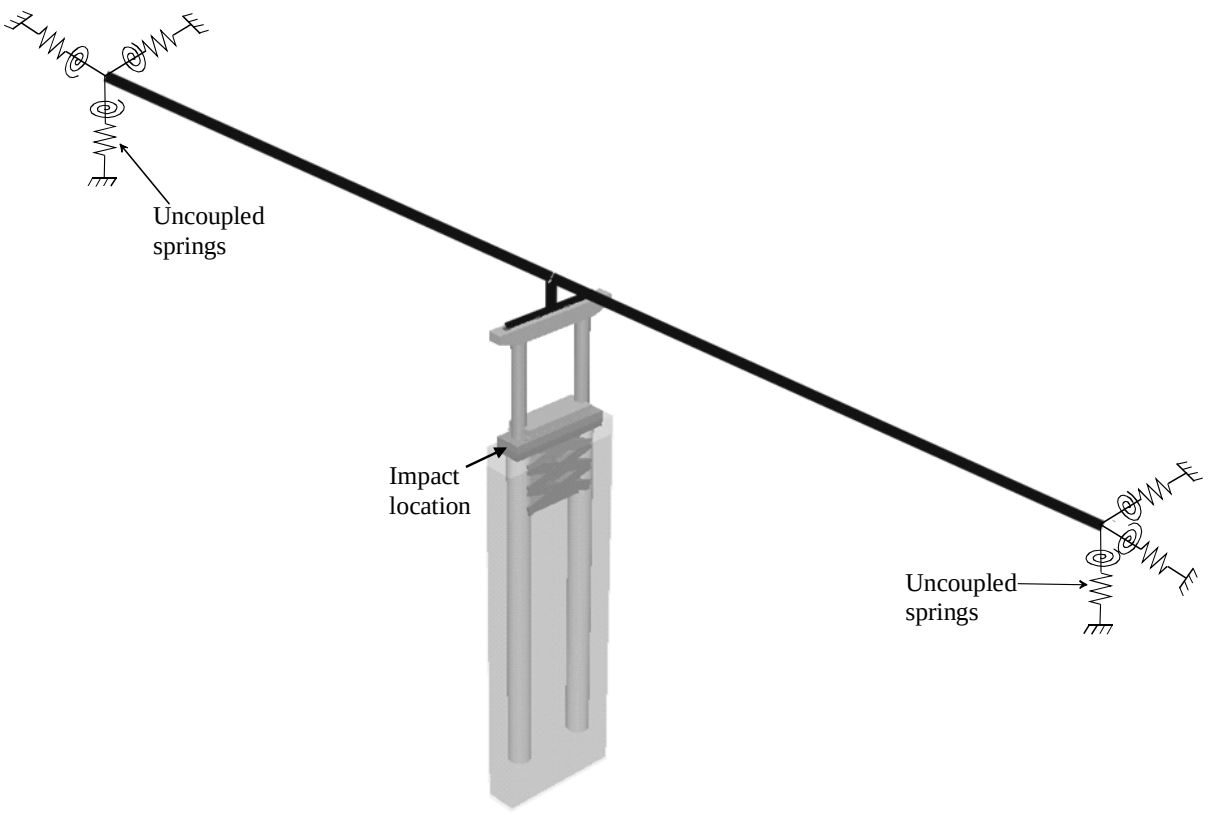

Figure 5.13 Structural configuration for Blountstown Bridge channel pier (BLT-CHA)

Prior to constructing the SBIA load cases, the barge impact force must be computed. For this bridge, impact occurs near the top of the shear wall, which has a 9-ft diameter round impact surface ($w_p = 9\,\text{ft}$). Thus, the barge yield force is calculated per Figure 2.6 in Chapter 2:

$$P_{BY} = 1500 + 30 \cdot w_p = 1500 + 30 \cdot (9) = 1770\,\text{kips} \tag{5.18}$$

The yield force occurs (conservatively) at a barge crush depth (a_{BY}) of 2 in (Consolazio et al. 2009).

With the yield force quantified, the impact force corresponding to the high-energy barge collision (5920-ton flotilla, traveling at 5.0 knots) is computed. First, the series stiffness of the barge and pier/soil system (k_S) is calculated per Eqn. 5.7. Note that the stiffness of the pier/soil system for this bridge (k_p) is 963 kip/in.

$$k_S = \left(\frac{a_{BY}}{P_{BY}} + \frac{1}{k_P} \right)^{-1} = \left(\frac{2}{1770} + \frac{1}{963} \right)^{-1} = 461\,\text{kip/in.} \tag{5.19}$$

Thus, the high-energy crush force is computed given the barge tow velocity (v_{Bi}) of 5.0 knots (101 in/s) and mass (m_B) of 5920 tons (30.7 kip/in/s^2):

$$P_B = v_{Bi} \cdot \sqrt{k_S \cdot m_B} = (101) \cdot \sqrt{(461) \cdot (30.7)} = 12,015 \text{ kips}$$
$$12,015 \text{ kips} > P_{BY} \tag{5.20}$$
$$\therefore P_B = P_{BY} = 1,770 \text{ kips}$$

This calculation illustrates that the initial kinetic energy of the barge tow is more than sufficient to yield the barge bow, generating the maximum crush force for this pier (1770 kips).

With the barge impact load (P_B) quantified, the two SBIA load cases are constructed. For Load Case 1, the amplified static impact load is computed:

$$1.45 \cdot P_B = 1.45 \cdot (1770) = 2567 \text{ kips} \tag{5.21}$$

This amplified impact load is used for each part of Load Case 1, regardless of the demand type of interest. However, unique pier-top loads are computed, corresponding to pier column moment, pier column shear, and total bearing shear (recall Figure 5.12). To quantify these loads, corresponding IRFs are computed, based on bridge structural parameters. For this bridge, the height of the pier (h_p) is 37 ft, the lateral superstructure stiffness (k_{sup}) is 199 kip/in, and the total weight of the pier (W_p) is 1815 kips. Thus,

$$IRF_m = 0.22 + \frac{4.5}{h_p}\sqrt{\frac{k_{sup}}{\sqrt{W_p}}} = 0.22 + \frac{4.5}{(37)}\sqrt{\frac{(199)}{\sqrt{(1815)}}} = 0.48 \tag{5.22}$$

$$IRF_v = 0.36 + \frac{3.0}{h_p}\sqrt{\frac{k_{sup}}{\sqrt{W_p}}} = 0.36 + \frac{3.0}{(37)}\sqrt{\frac{(199)}{\sqrt{(1815)}}} = 0.54 \tag{5.23}$$

$$IRF_b = 0.37 + \frac{7.0}{h_p}\sqrt{\frac{k_{sup}}{\sqrt{W_p}}} = 0.37 + \frac{7.0}{(37)}\sqrt{\frac{(199)}{\sqrt{(1815)}}} = 0.78 \tag{5.24}$$

Lastly, the amplified impact load for Load Case 2 (Figure 5.12) is calculated as:

$$1.85 \cdot P_B = 1.85 \cdot (1770) = 3275 \text{ kips} \tag{5.25}$$

With SBIA inertial resistance factor expressions formed, two approaches to statically analyzing bridge response to barge impact loading are now considered.

5.6.2.1 SBIA demonstration with OPTS superstructure model

The SBIA method is first demonstrated using a one-pier, two-span (OPTS) bridge model (recall Figure 5.13). Load Case 1 is analyzed by conducting three separate static analyses (Figure 5.14). The amplified impact load (as computed in Eqn. 5.21) is applied at the impact location for all three analyses. For each of the three analyses, the corresponding IRF (as calculated in Eqns. 5.22, 5.23, and 5.24) is multiplied by the impact force (P_B), and applied at the superstructure center of gravity, in the opposite direction of impact (Figure 5.14).

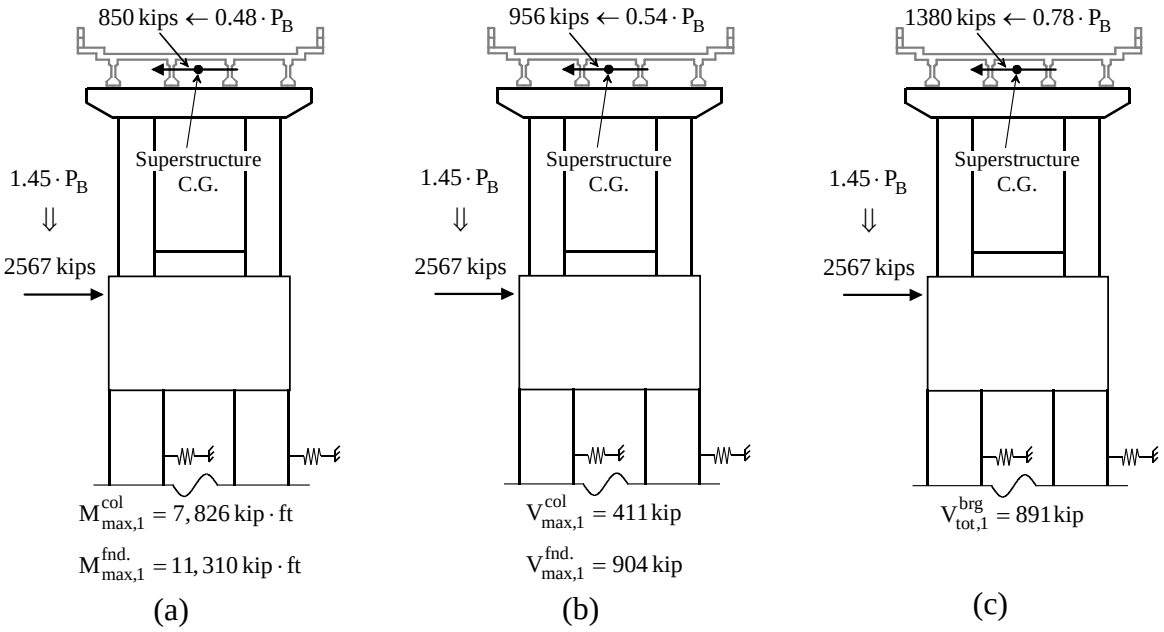

Figure 5.14 Loading conditions and maximum demand predictions for Load Case 1 with OPTS superstructure model

Having formed the complete loading condition for Load Case 1, the structure is statically analyzed. Predictions of pier member (column and foundation) moment, pier member (column and foundation) shear, and total bearing shear demands are quantified using the respective analyses (shown in Figure 5.14). Note that beam-column axial forces are obtained from the Load Case 1 moment analysis (Figure 5.14a), for use in load-moment interaction calculations. SBIA Load Case 2 is also analyzed as shown in Figure 5.15. From this analysis, all pertinent member forces are quantified—pier member (column and foundation) moments, pier member (column and foundation) shears, and total bearing shear.

Design forces predicted by Load Cases 1 and 2 are summarized in Table 5.1. For each demand type, the maximum is selected for design. In this example, Load Case 1 controlled pier column and bearing design forces, while Load Case 2 controlled foundation design forces. This pattern is typical of the SBIA procedure; however, it is possible, given specific pier configurations and loading conditions, for either load case to dominate a given demand. Thus, the maximum demand predicted between both load cases must be considered for design.

The SBIA results for the Blountstown Bridge are additionally compared to dynamic predictions of design forces. Specifically, a corresponding dynamic analysis was conducted using the coupled vessel impact analysis (CVIA) method. The bridge was analyzed considering identical impact conditions—a 5920-ton barge tow, impacting the pier at 5.0 knots. Design forces obtained from CVIA are compared to SBIA predictions in Table 5.2. The SBIA method conservatively predicts all relevant design forces, when compared to CVIA. For this example, SBIA predictions of pier column and bearing shear forces are within 2 to 8% of corresponding dynamic forces. The disparity is larger for foundation

forces, at 27 to 35%. However, this level of conservatism is deemed acceptable, given the relative simplicity of the analysis procedure.

5.6.2.2 SBIA demonstration with spring superstructure model

In addition to demonstrating the SBIA method using an OPTS bridge model, the procedure and results are assessed using a more simplistic spring superstructure model. Specifically, the superstructure is removed and replaced by an equivalent 199 kip/in lateral spring. This modeling approach is common in bridge design practice; thus, compatibility is assessed between SBIA and spring-based superstructure modeling.

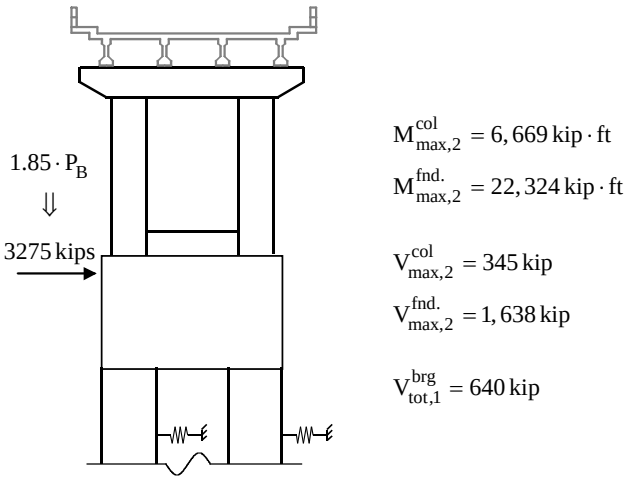

Figure 5.15 Loading conditions and maximum demand predictions for Load Case 2 with OPTS superstructure model

Table 5.1 SBIA demand prediction summary (OPTS superstructure)

	Load Case 1			Load Case 2	Maximum
	Calibrated to pier moment	Calibrated to pier shear	Calibrated to bearing shear		
Column moment (kip-ft)	7,826	--	--	5,559	7,826
Column shear (kips)	--	411	--	345	411
Foundation moment (kip-ft)	11,310	--	--	22,324	22,324
Foundation shear (kips)	--	904	--	1,638	1,638
Total bearing shear (kips)	--	--	891	640	891

Table 5.2 Comparison of demand predictions—CVIA vs. SBIA (OPTS superstructure)

	Dynamic (CVIA)	Equiv. static (SBIA)	Percent difference
Column moment (kip-ft)	7,281	7,826	7.5%
Column shear (kips)	404	411	1.7%
Foundation moment (kip-ft)	17,569	22,324	27.1%
Foundation shear (kips)	1,216	1,638	34.7%
Total bearing shear (kips)	883	891	0.9%

As before, SBIA loads are calculated per Eqns. 5.21, 5.22, 5.23, and 5.24. While load magnitudes are identical to those applied to the OPTS model, placement of the pier-top load differs. Using an OPTS model, this load is applied at the superstructure center of gravity. However, without adding additional connecting elements and increasing model complexity, this location is not available in the simplified numerical model. Instead, the pier-top load is applied at the pier cap beam center of gravity (Figure 5.16). Load Case 2 involves only replacing the OPTS superstructure with an equivalent spring. The amplified barge load is then applied at the impact location (Figure 5.17).

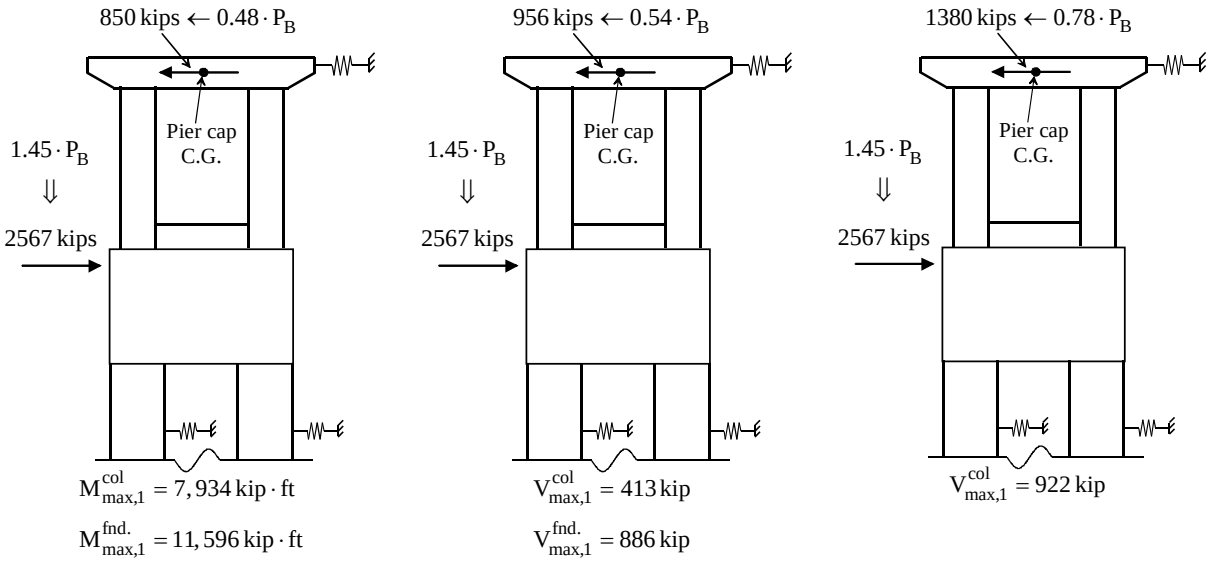

Figure 5.16 Loading conditions and maximum demand predictions for Load Case 1 with spring superstructure model

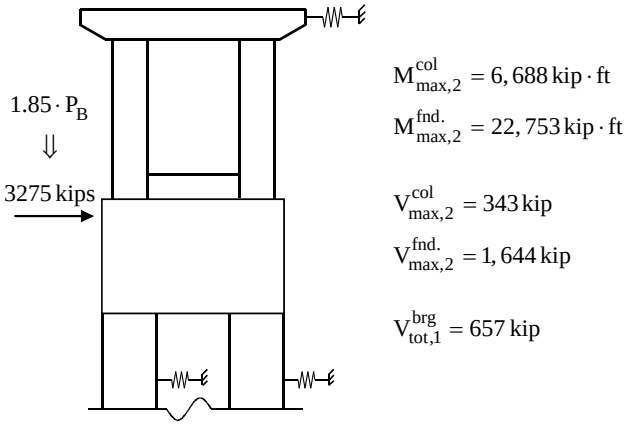

Figure 5.17 Loading conditions and maximum demand predictions for Load Case 2 with spring superstructure model

As before, maximum demands obtained between the two load cases are selected as design forces (Table 5.3). Again, Load Case 1 controlled pier and bearing demands, while Load Case 2 controlled foundation demands.

Static (SBIA) and dynamic (CVIA) demand predictions are compared in Table 5.4. Using an equivalent spring superstructure model, SBIA column and bearing forces differ from CVIA by 2 to 9%, while foundation forces differ by 30 to 35%.

5.6.2.3 Comparison of SBIA using OPTS vs. spring superstructure model

Predictions of static (SBIA) design forces are compared in Table 5.5 for both OPTS and spring superstructure models. Observed discrepancies are small—less than 4%—across all demand types. Additionally, forces predicted by the spring superstructure model were always conservative relative to the OPTS model, though this finding is specific to the demonstration case. In the next section, it will be shown that it is possible for spring superstructure models to produce lower force predictions than OPTS models. In general, the small relative difference between OPTS and spring-based design forces confirms the compatibility of either superstructure modeling technique for use with the SBIA procedure.

Table 5.3 SBIA demand prediction summary (spring superstructure)

	Load Case 1			Load Case 2	Maximum
	Calibrated to pier moment	Calibrated to pier shear	Calibrated to bearing shear		
Column moment (kip-ft)	7,934	--	--	6,688	7,934
Column shear (kips)	--	413	--	343	413
Foundation moment (kip-ft)	11,596	--	--	22,753	22,753
Foundation shear (kips)	--	886	--	1,644	1,644
Total bearing shear (kips)	--	--	922	657	922

Table 5.4 Comparison of demand predictions—CVIA vs. SBIA (spring superstructure)

	Dynamic (CVIA)	Equiv. static (SBIA)	Percent difference
Column moment (kip-ft)	7,281	7,934	9.0%
Column shear (kips)	404	413	2.2%
Foundation moment (kip-ft)	17,569	22,753	29.5%
Foundation shear (kips)	1,216	1,644	35.2%
Total bearing shear (kips)	883	922	4.4%

Table 5.5 Comparison of SBIA demand predictions—OPTS vs. spring superstructure

	SBIA (OPTS)	SBIA (spring)	Percent difference
Column moment (kip-ft)	7,826	7,934	1.4%
Column shear (kips)	411	413	0.5%
Foundation moment (kip-ft)	22,324	22,753	1.9%
Foundation shear (kips)	1,638	1,644	0.4%
Total bearing shear (kips)	891	922	3.5%

In addition to quantifying maximum forces, deflected pier shapes and structural demand profiles (shear and moment) are compared in Figure 5.18. Displacement and force profiles are shown for CVIA (dynamic analysis), SBIA using an OPTS model, and SBIA using a spring superstructure model. Note that the SBIA displacement profiles shown in Figure 5.18 were obtained from the Load Case 1 analysis, which was calibrated to pier moment (recall Figure 5.14 and Figure 5.16).

The displacement profile for the Blountstown Bridge is representative of many of the cases studied in that the overall shape of the profile matches well with CVIA, but the pier displacements are smaller in magnitude, and sometimes negative. Negative pier displacements indicate that the net static loading pushed portions of the structure in the opposite direction of impact (typically near the pier-top). Negative displacements are not indicative of dynamic inertial restraint behavior, and are primarily a consequence of the conservative nature of SBIA. As discussed in Section 5.4.1, this tendency is somewhat mitigated by scaling the impact load by 1.45. Using a scaled impact load, the ideal inertial resistance static loading conditions (recall Section 5.4.2) did *not* produce negative pier displacements. However, when using the conservative 99% upper bound inertial resistance loading conditions (recall Figure 5.8), negative pier displacements occur in ten of the twenty pier/energy cases considered (see Appendix A for displacement profiles for all cases). Given that barge impact loading conditions are used in ultimate strength limit checks, but not in serviceability limit state checks, the potential for negative pier-top displacements of little practical consequence.

With regard to pier forces, SBIA profiles match well with CVIA (Figure 5.18). In this case, the overall shape of the profiles is consistent with CVIA, though SBIA generally predicts larger magnitudes—as is desired. Furthermore, in this case, all maximum SBIA pier demands occur in the same physical locations as predicted dynamically. However, this is not universal for all bridges (see Appendix A) therefore it is recommended that the maximum SBIA force predictions be used to design an entire member (column or foundation) as opposed to using the detailed shear or moment profile.

5.7 Parametric study results

In addition to the demonstration case described in the previous section, the SBIA method was assessed for a broad range of structural configurations and barge impact conditions by means of a parametric study. Specifically, the SBIA procedure was used to quantify pier design forces—pier column moments and shears, foundation moments and shears, and total bearing shear forces—for twenty (20) pier/impact energy conditions. As discussed previously, SBIA was additionally assessed using both OPTS and spring superstructure models.

In the results summary plots (Figure 5.19 through Figure 5.23), recall that each pier/energy case is denoted by a three-part identifier. The first portion is an abbreviation of the bridge name (e.g., ACS refers to the Acosta Bridge). The second portion refers to the impacted pier location—CHA for a channel pier, and OFF for a pier located away from the navigation channel. The third portion refers to the impact energy condition—L, M, H, and S for low, moderate, high, and severe impact energy, respectively. See Chapter 4 for additional details regarding the bridges and energy conditions considered.

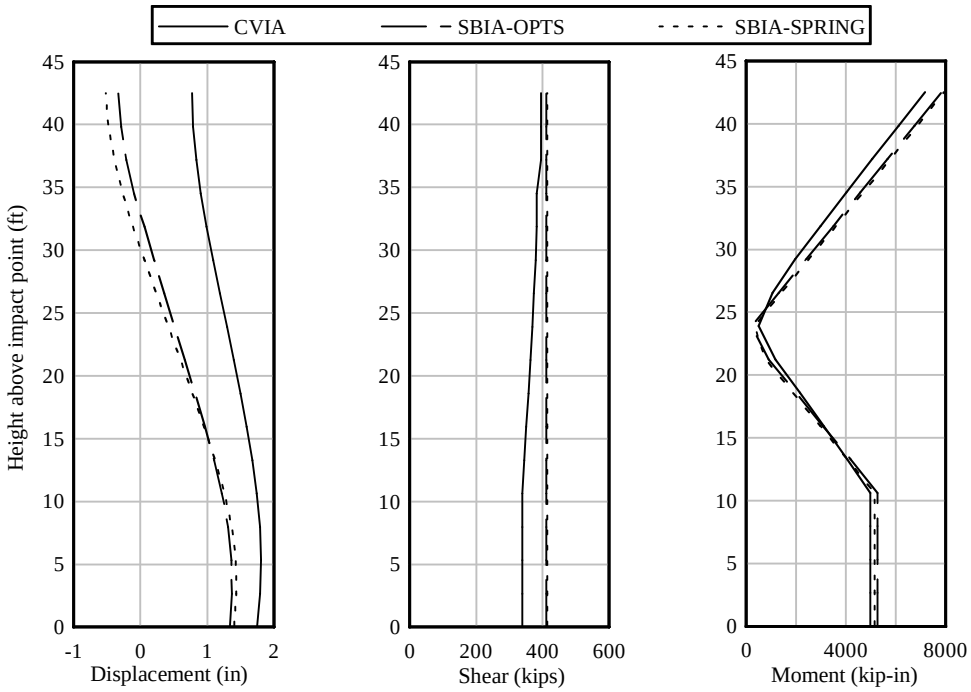

(a) Column profiles

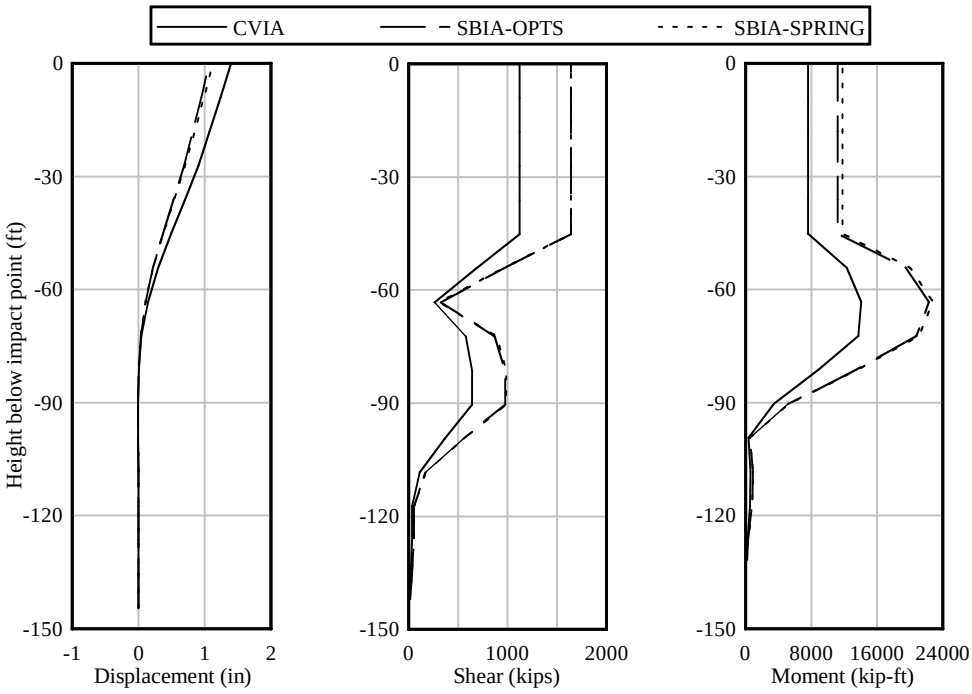

(b) Foundation profiles

Figure 5.18 Comparison of CVIA and SBIA bridge responses for New Trammel Bridge at Blountstown (BLT-CHA)

For comparison, corresponding fully dynamic simulations were conducted using the CVIA method, from which dynamic design force predictions were developed. To assess the suitability of SBIA for conservatively estimating dynamic design forces, SBIA demands are normalized by corresponding CVIA demands to form demand ratios. If a given demand ratio is equal to 1.0, this indicates that the SBIA demand exactly matches that obtained from CVIA. Ratios greater than 1.0 indicate that SBIA is conservative compared to CVIA, and ratios less than 1.0 indicate that SBIA is unconservative.

Based on the data presented Figure 5.19 through Figure 5.23, it is observed that SBIA is always conservative relative to CVIA for the cases studied. This is a natural consequence of utilizing upper bound envelopes (99% confidence) for the two SBIA load cases. Not only is SBIA conservative relative to CVIA, the overall level of conservatism is reasonable—with mean values ranging from 1.3 to 1.6, depending on the demand type. Furthermore, nearly every relative demand is less than 2.0. Lastly, Figure 5.19 through Figure 5.23 illustrate that using a spring-based superstructure model is compatible with SBIA. Specifically, observed discrepancies between OPTS and spring demands are typically small—ranging from 0.01% to 36%, with an average of 7.0%. In general, the SBIA method provides adequate estimates of dynamic design forces across a wide spectrum of bridge configurations and impact conditions.

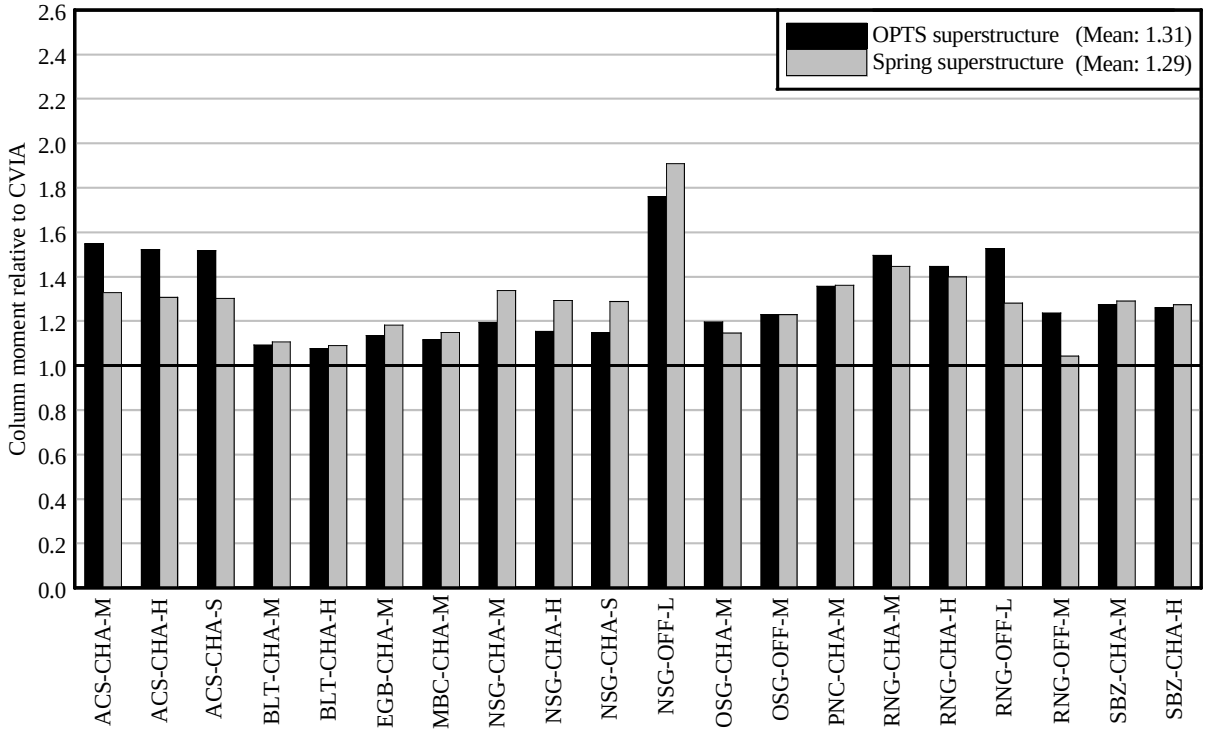

Figure 5.19 SBIA pier column moment demands relative to CVIA

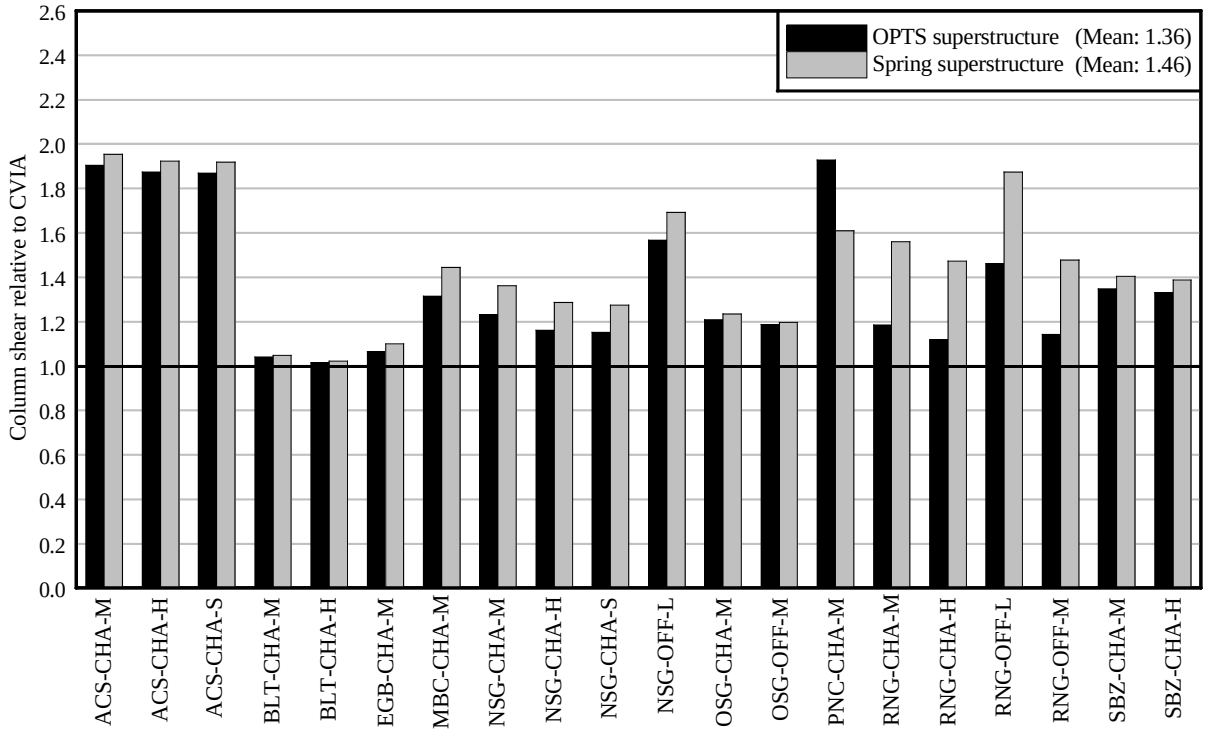

Figure 5.20 SBIA pier column shear demands relative to CVIA

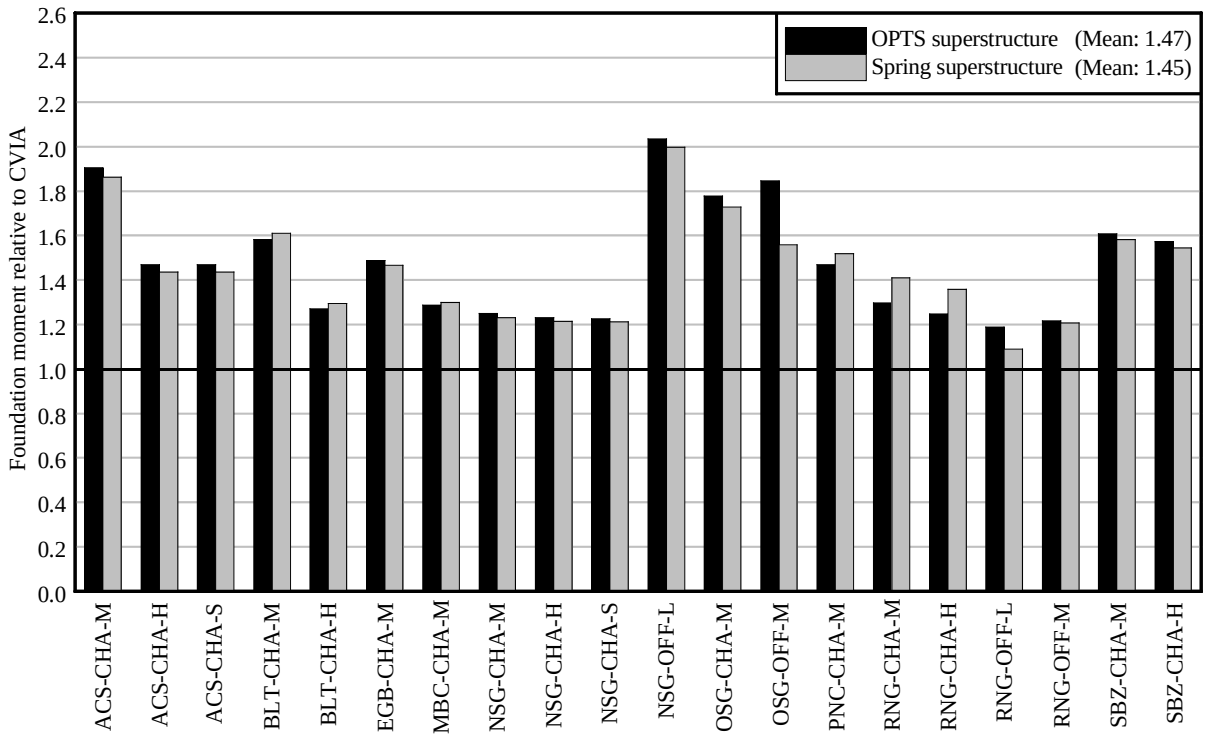

Figure 5.21 SBIA foundation moment demands relative to CVIA

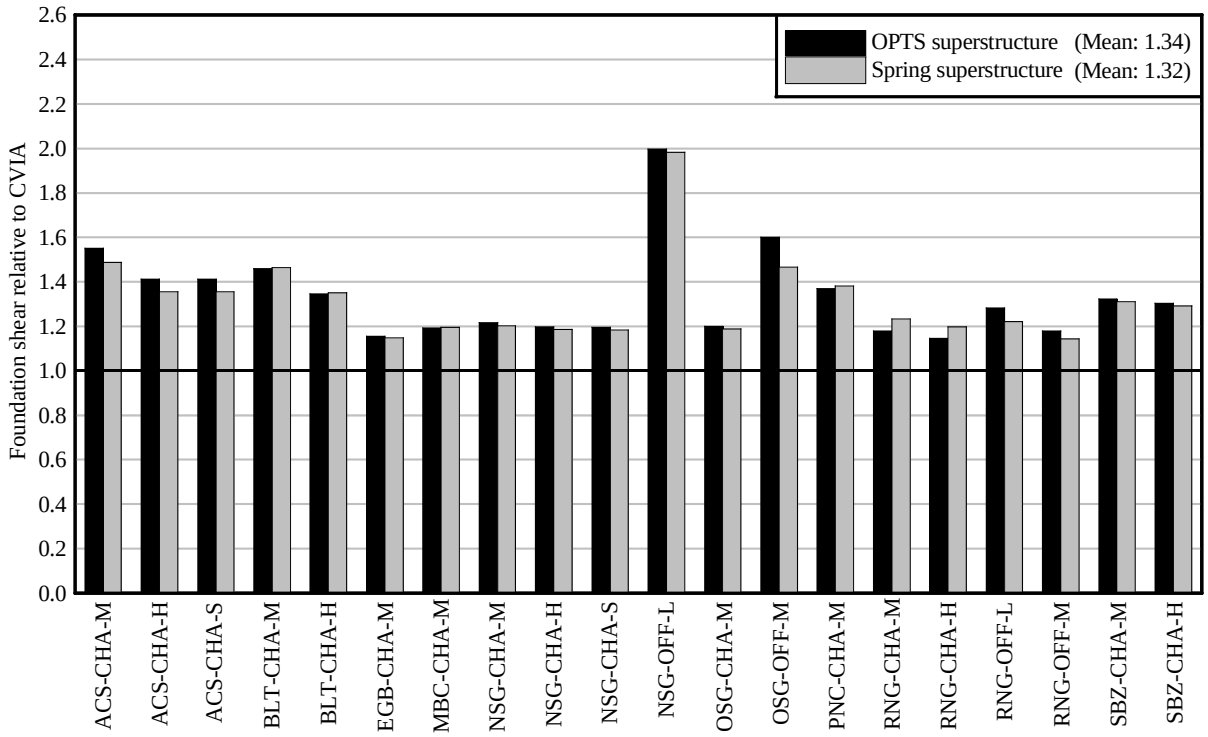

Figure 5.22 SBIA foundation shear demands relative to CVIA

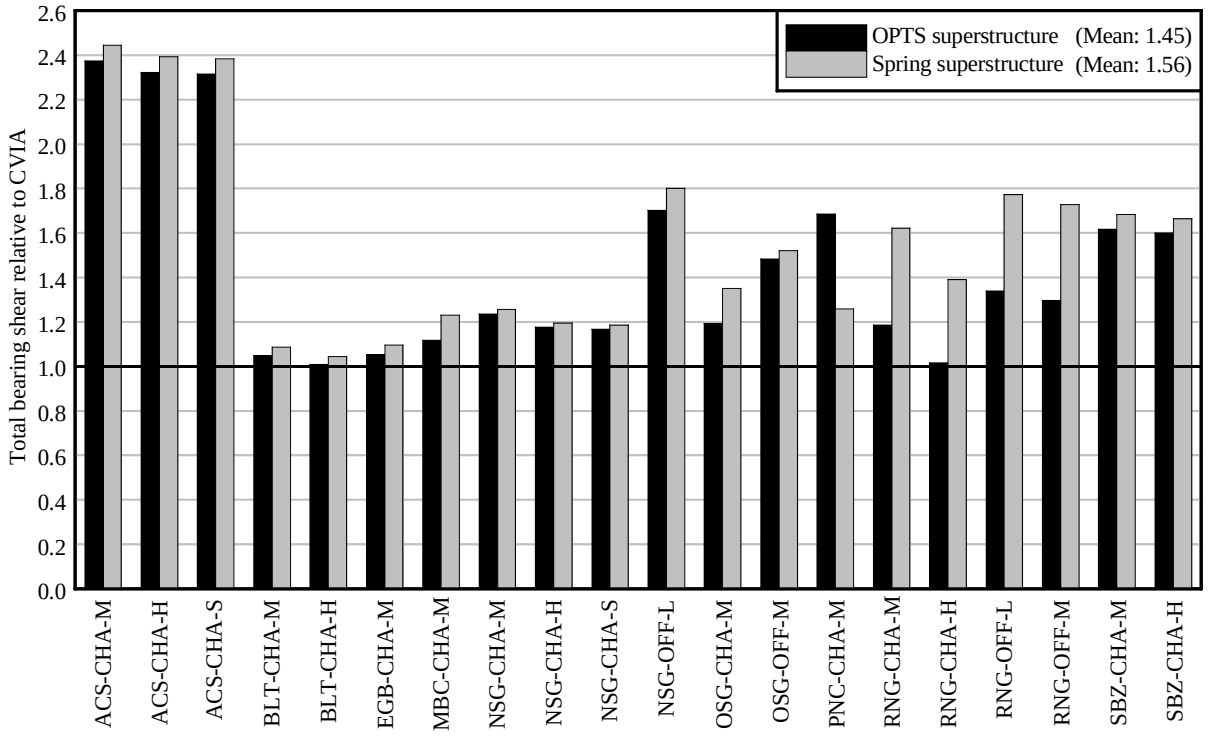

Figure 5.23 SBIA total bearing shear demands relative to CVIA

CHAPTER 6
CONCLUSIONS AND RECOMMENDATIONS

6.1 Summary and conclusions

Previously conducted experimental and analytical research has highlighted the importance of dynamic effects that are present during barge-bridge collision events. Specifically, these studies identified superstructure inertia as a critical component of dynamic bridge pier behavior. Furthermore, current static analysis methods do not account for dynamic amplification of pier forces generated by inertial effects. Thus, dynamic analytical methods were developed, as part of prior research, which directly consider the effects of bridge mass distribution and bridge motions developed during barge impact.

While time-domain dynamic analysis procedures—notably the coupled vessel impact analysis (CVIA) procedure—provide accurate predictions of bridge response to barge collision loads, the computational requirements of such methods can be prohibitive in some design situations. In addition, the structural characteristics of a bridge in preliminary design may not be sufficiently well-defined to permit a refined dynamic analysis. Thus, a need was identified to develop an equivalent static analysis procedure that simply and conservatively accounts for dynamic amplifications present during barge impact events. The research presented in this report has been carried out to address this need.

The first major component of this study involved analytically identifying sources of dynamic amplification and quantifying to what degree these effects increase design forces. Inertial phenomena were studied across a broad range of bridge structural configurations and impact conditions. This work uncovered two primary sources of dynamic amplification of pier forces—superstructure inertial restraint and superstructure momentum-driven sway. While superstructure sway is an important mode of dynamic amplification, the inertial resistance mode was significantly more common in the impact cases studied. Furthermore, significant inertial resistance was identified even in cases where superstructure sway caused maximum pier forces. Regardless of which dynamic response mode dominates, these phenomena, in most cases, greatly increase pier forces relative to those predicted by typical static analytical procedures.

With an improved understanding of dynamic amplification effects, an equivalent static analysis procedure was developed that statically emulates superstructure inertial restraint. The proposed static bracketed impact analysis (SBIA) method consists of two static load cases. The first load case addresses inertial resistance by means of a static inertial load applied at the superstructure elevation, in addition to the barge impact load. This inertial load is quantified using empirical expressions that relate inertial force to readily available structural parameters. The second load case excludes the inertial load, and provides a reliable means of quantifying maximum foundation forces. By bracketing pier forces between both load cases, reasonably conservative estimates of pier demands are assessed, including dynamic amplifications.

6.2 Recommendations

- Consideration of superstructure inertial effects: It is recommended that superstructure inertia be considered as part of the bridge design process for barge collision. As demonstrated in this report, superstructure inertia can greatly amplify pier forces, and

such amplifications are not considered in existing static analysis procedures. Dynamically amplified design forces should be quantified using either the time-domain CVIA method or the newly developed equivalent static SBIA method.

- Use of static bracketed impact analysis (SBIA) procedure: For preliminary design, or in cases where time-domain dynamic analysis is not warranted, the SBIA procedure is recommended to statically approximate dynamic amplification effects. This empirical method provides a conservative but simple static approach to impact-resistant bridge design. This report demonstrates that SBIA predicts minimally conservative estimates of dynamic pier forces for a wide range of structural configurations and impact conditions.
- Use of maximum member design forces from SBIA: To maximize the simplicity of the SBIA method, certain limitations in terms of accuracy had to be imposed. While the static load cases employed by SBIA are able to conservatively bracket maximum design forces arising in major structural bridge components (pier columns, piles, drilled shafts), the detailed vertical profiles of structural demand (moment, shear) produced by the SBIA load cases are not necessarily conservative at every elevation. Hence, it is recommended that each major bridge component be designed with uniform capacity along its entire length such that every section of the component possesses sufficient capacity to resist the maximum forces predicted by the SBIA method.
- Use of modeling techniques consistent with those used to develop the SBIA method: In this study, it has been demonstrated that the SBIA method produces design forces that are minimally conservative in comparison to dynamically predicted design forces when the bridge structure and soil are modeled as described earlier in this report (e.g., the use of nonlinear structure and soil models). It is not known whether the SBIA method will also produce conservative results if less refined structure or soil modeling techniques are employed (e.g., the use of linear structure or soil models). Hence, it is recommended that nonlinear structure and soil modeling techniques be used when employing the SBIA method for the prediction of bridge design forces.

REFERENCES

AASHTO, *Guide Specification and Commentary for Vessel Collision Design of Highway Bridges*, 2nd Edition, AASHTO, Washington D.C., 2009.

AASHTO, *Guide Specification and Commentary for Vessel Collision Design of Highway Bridges*, AASHTO, Washington D.C., 1991.

AASHTO, *LRFD Bridge Design Specifications*, 4th Edition, AASHTO, Washington D.C., 2008.

Cameron, J., Nadeau, J., and LoSciuto, J. "Ultimate Strength Analysis of Inland Tank Barges," United States Coast Guard Marine Safety Center, 1997.

Consolazio, G.R., Cook, R.A., McVay, M.C., Cowan, D.R., Biggs, A.E., and Bui, L., *Barge Impact Testing of the St. George Island Causeway Bridge - Phase III: Physical Testing and Data Interpretation*, University of Florida Engineering and Industrial Experiment Station, University of Florida, Gainesville, Florida, Structures Research Report No. 26868, 2006.

Consolazio, G.R., Cowan, D.R., "Numerically Efficient Dynamic Analysis of Barge Collisions with Bridge Piers," *ASCE Journal of Structural Engineering*, Vol 131, No 8, pp. 1256-1266, 2005.

Consolazio, G.R., Cowan, D.R., "Nonlinear Analysis of Barge Crush Behavior and its Relationship to Impact Resistant Bridge Design," *Computers and Structures*, Vol 81, No 8-11, pp. 547-557, 2003.

Consolazio, G.R., Davidson, M.T., "Simplified Dynamic Barge Collision Analysis for Bridge Design," *Journal of the Transportation Research Board*. No 2050, pp. 13-25, 2008.

Consolazio, G.R., Davidson, M.T., Cowan, D.R. "Barge Bow Force-Deformation Relationships for Barge-Bridge Collision Analysis," *Journal of the Transportation Research Board*, (In press), 2009.

Consolazio, G.R., McVay, M.C., Cowan D.R., Davidson, M.T., and Getter, G.J., *Development of Improved Bridge Design Provisions for Barge Impact Loading.* Structures Research Report No. 2008/51117, Engineering and Industrial Experiment Station, University of Florida, Gainesville, Florida, 2008.

Cowan, D.R., *Development of Time-History and Response Spectrum Analysis Procedures for Determining Bridge Response to Barge Impact Loading*, Doctoral Dissertation, University of Florida, Gainesville, FL, 2007.

FB-MultiPier, *FB-MultiPier User's Manual*. Florida Bridge Software Institute, University of Florida, Gainesville, Florida, 2009.

FB-MultiPier, *FB-MultiPier User's Manual*. Florida Bridge Software Institute, University of Florida, Gainesville, Florida, 2007.

Liu, C. and T.L. Wang. "Statewide Vessel Collision Design for Bridges," *ASCE Journal of Bridge Engineering*, ASCE, Vol. 6, No. 3, 2001, pp. 213-219.

LSTC, *LS-DYNA Keyword User's Manual: Version 971*, Livermore Software Technology Corporation, Livermore, CA, 2008.

Meier-Dörnberg, K.E., *Ship Collisions, Safety Zones, and Loading Assumptions for Structures in Inland Waterways*, Verein Deutscher Ingenieure (Association of German Engineers) Report No. 496, pp. 1-9, 1983.

Paultre, P., O. Chaallal, and J. Proulx. "Bridge Dynamics and Dynamic Amplification Factors – a Review of Analytical and Experimental Findings," *Canadian Journal of Civil Engineering*, Canadian Society of Civil Engineering, Vol. 19, No. 2, 1992, pp. 260-278.

Pearson, E.S., Hartley, H.O., *Biometrika Tables for Statisticians Vol. 1*, 2nd Ed., Cambridge, New York, NY, 1958.

Precast/Prestressed Concrete Institute (PCI), PCI *Design Handbook (5th Edition)*, PCI, Chicago, IL, 2004.

Tedesco, J.W., McDougal, W.G., and Ross, C.A., *Structural Dynamics: Theory and Applications*, Addison Wesley Longman, Inc., Menlo Park, CA, 1999.

Yuan, P., Harik, I.E., and Davidson, M.T., *Multi-Barge Flotilla Impact Forces on Bridges, Kentucky Transportation Center*, University of Kentucky, Lexington, Kentucky, Research Report No. KTC-05 /SPR261-03-1F, 2008.

APPENDIX A
COMPARISON OF SBIA AND CVIA RESULTS

In this appendix, SBIA (equivalent static) analysis results are compared to corresponding CVIA (dynamic) simulation results. For each bridge in the parametric study, three analyses were conducted: 1) Fully dynamic CVIA, 2) SBIA using one-pier, two-span (OPTS) models, and 3) SBIA using spring-based superstructure models. The data presented in this appendix form the basis for the relative demand ratios presented in Figures 5.19 through 5.23.

Figures presented in this appendix show the maximum magnitudes of displacement, shear force, and moment at each vertical elevation, for all three analyses. Elevation data have been adjusted such that the elevation datum (0 ft.) corresponds to the midplane elevation of the pile cap. In each figure, a gray rectangle is used to represent the pile cap vertical thickness. Each figure represents one impact energy condition applied to a respective bridge-pier configuration.

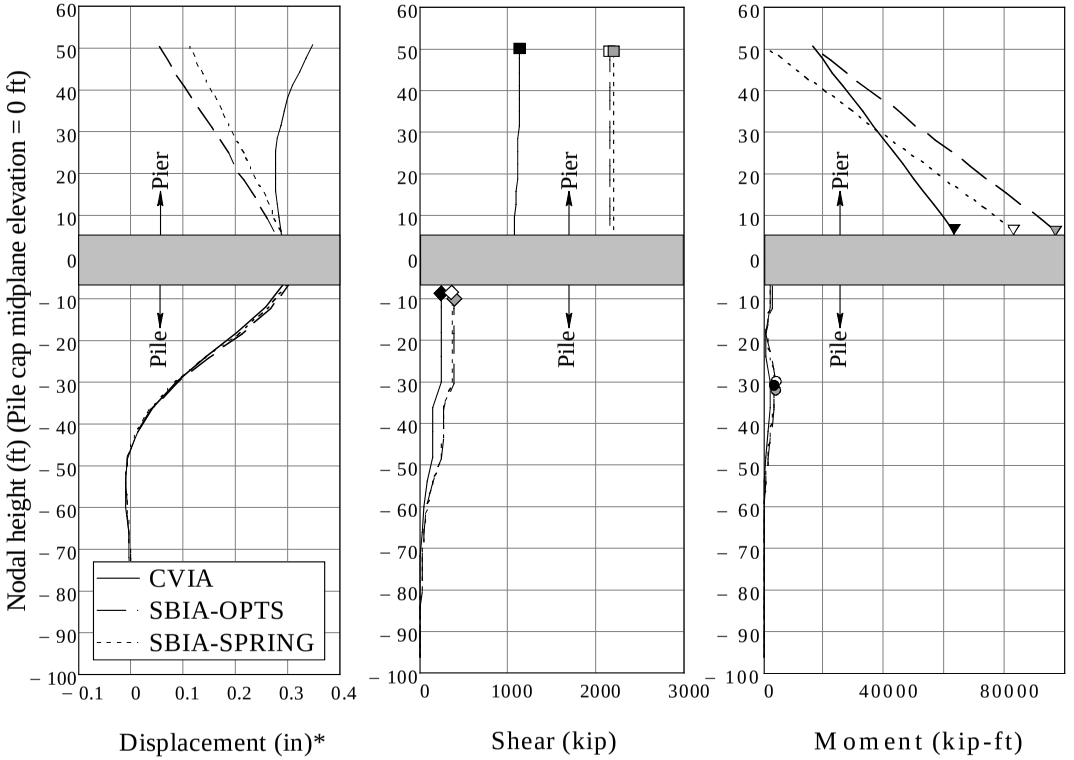

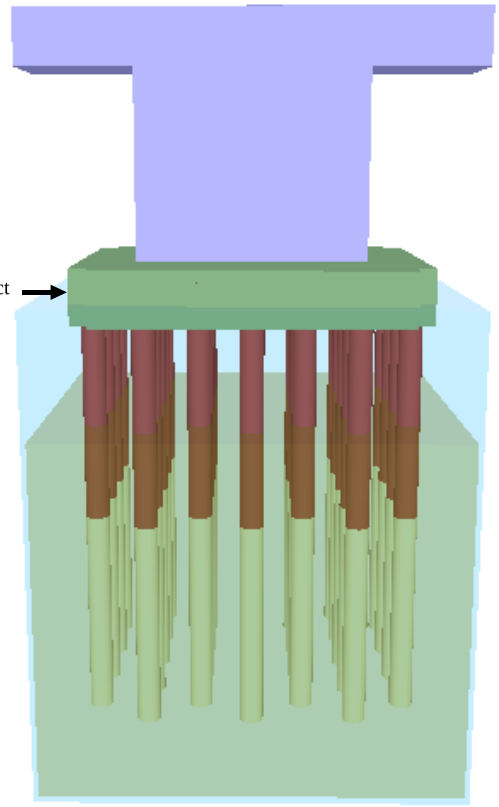

Peak Pier Demands	CVIA		SBIA OPTS		SBIA SPRING	
Column moment:	▼ 62823	kip-ft	▽ 97201	kip-ft	▽ 83425	kip-ft
Column shear:	■ 1127	kips	□ 2146	kips	▣ 2202	kips
Pile Moment:	● 2157	kip-ft	○ 4110	kip-ft	◍ 4018	kip-ft
Pile Shear:	◆ 248	kips	◇ 385	kips	◈ 369	kips
Total Bearing Shear:	1196	kips	2841	kips	2925	kips

* SBIA displacement profiles shown were obtained using SBIA Load Case 1 with the moment IRF equation (Equation 5.15)

Figure A.1 Comparison of CVIA, SBIA-OPTS, and SBIA-spring results
Bridge: Acosta Bridge (ACS) channel pier; Impact condition: 2030 tons at 2.5 knots

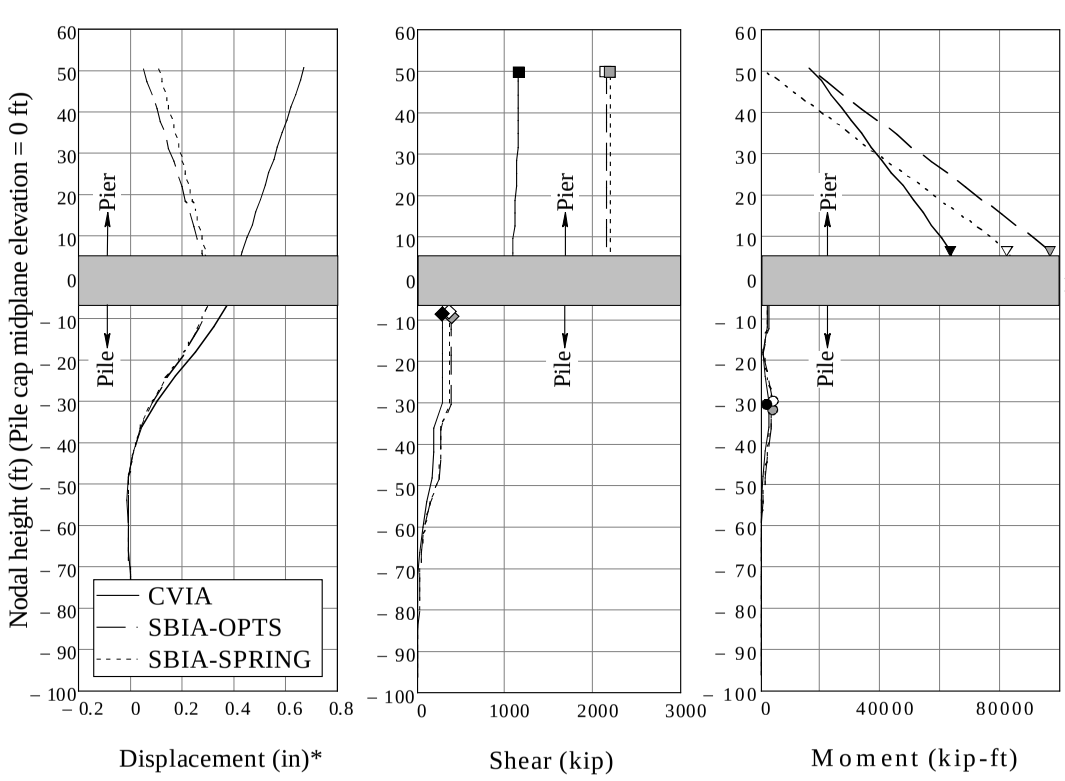

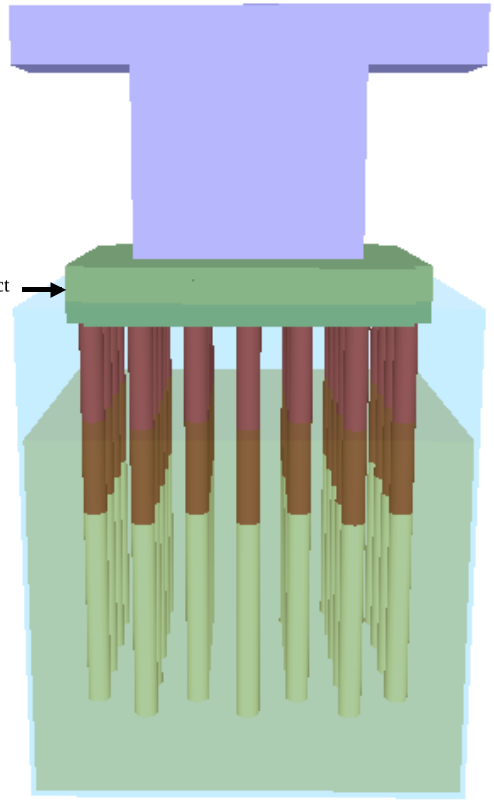

Peak Pier Demands	CVIA		SBIA OPTS		SBIA SPRING	
Column moment:	▼ 63873	kip-ft	▽ 97201	kip-ft	▽ 83425	kip-ft
Column shear:	■ 1145	kips	□ 2146	kips	■ 2202	kips
Pile Moment:	● 2797	kip-ft	○ 4110	kip-ft	● 4018	kip-ft
Pile Shear:	◆ 272	kips	◇ 385	kips	◆ 369	kips
Total Bearing Shear:	1223	kips	2841	kips	2925	kips

* SBIA displacement profiles shown were obtained using SBIA Load Case 1 with the moment IRF equation (Equation 5.15)

Figure A.2 Comparison of CVIA, SBIA-OPTS, and SBIA-spring results
Bridge: Acosta Bridge (ACS) channel pier; Impact condition: 5920 tons at 5.0 knots

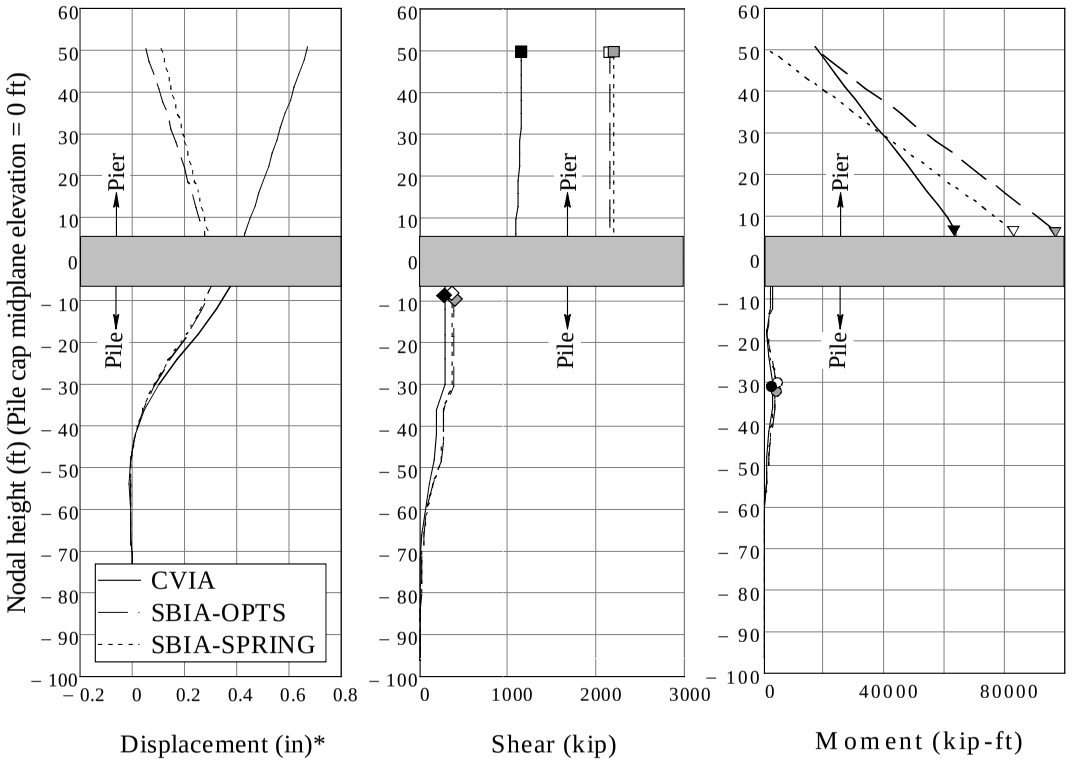

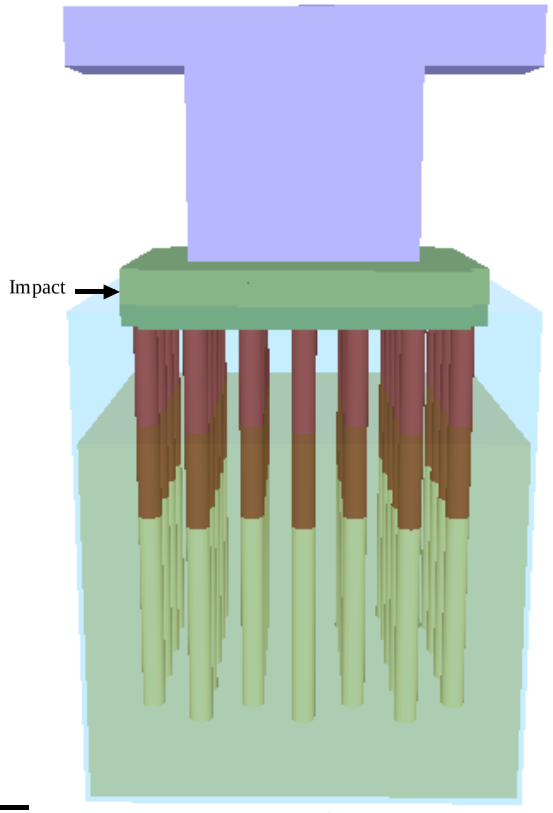

Peak Pier Demands	CVIA		SBIA OPTS		SBIA SPRING	
Column moment:	▼ 64036	kip-ft	▽ 97201	kip-ft	▽ 83425	kip-ft
Column shear:	■ 1148	kips	□ 2146	kips	■ 2202	kips
Pile Moment:	● 2798	kip-ft	○ 4110	kip-ft	● 4018	kip-ft
Pile Shear:	◆ 272	kips	◇ 385	kips	◆ 369	kips
Total Bearing Shear:	1227	kips	2842	kips	2925	kips

* SBIA displacement profiles shown were obtained using SBIA Load Case 1 with the moment IRF equation (Equation 5.15)

Figure A.3 Comparison of CVIA, SBIA-OPTS, and SBIA-spring results
Bridge: Acosta Bridge (ACS) channel pier; Impact condition: 7820 tons at 5.0 knots

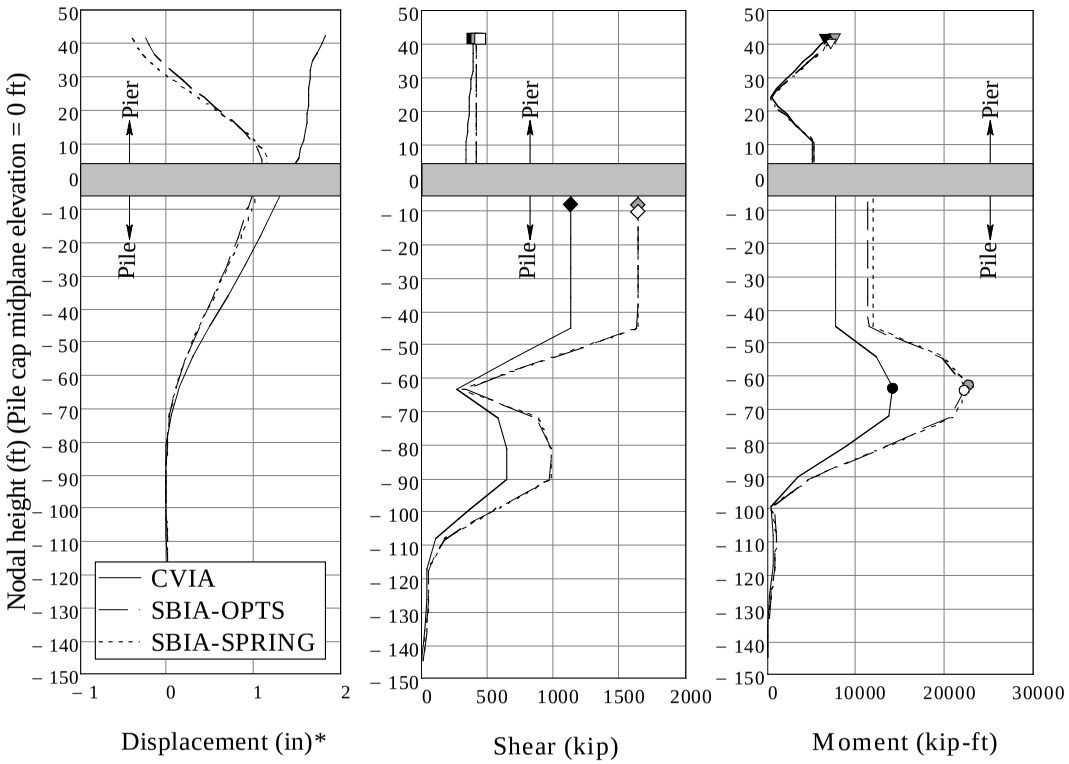

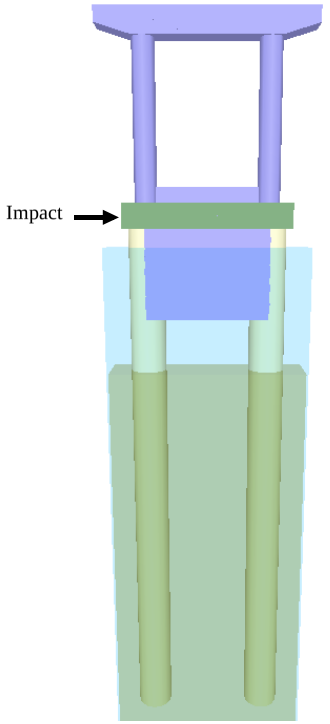

Peak Pier Demands	CVIA		SBIA OPTS		SBIA SPRING	
Column moment:	7165	kip-ft	7826	kip-ft	7934	kip-ft
Column shear:	394	kips	411	kips	413	kips
Pile Moment:	14124	kip-ft	22324	kip-ft	22753	kip-ft
Pile Shear:	1123	kips	1638	kips	1644	kips
Total Bearing Shear:	849	kips	891	kips	922	kips

* SBIA displacement profiles shown were obtained using SBIA Load Case 1 with the moment IRF equation (Equation 5.15)

Figure A.4 Comparison of CVIA, SBIA-OPTS, and SBIA-spring results
Bridge: SR-20 at Blountstown (BLT) channel pier; Impact condition: 2030 tons at 2.5 knots

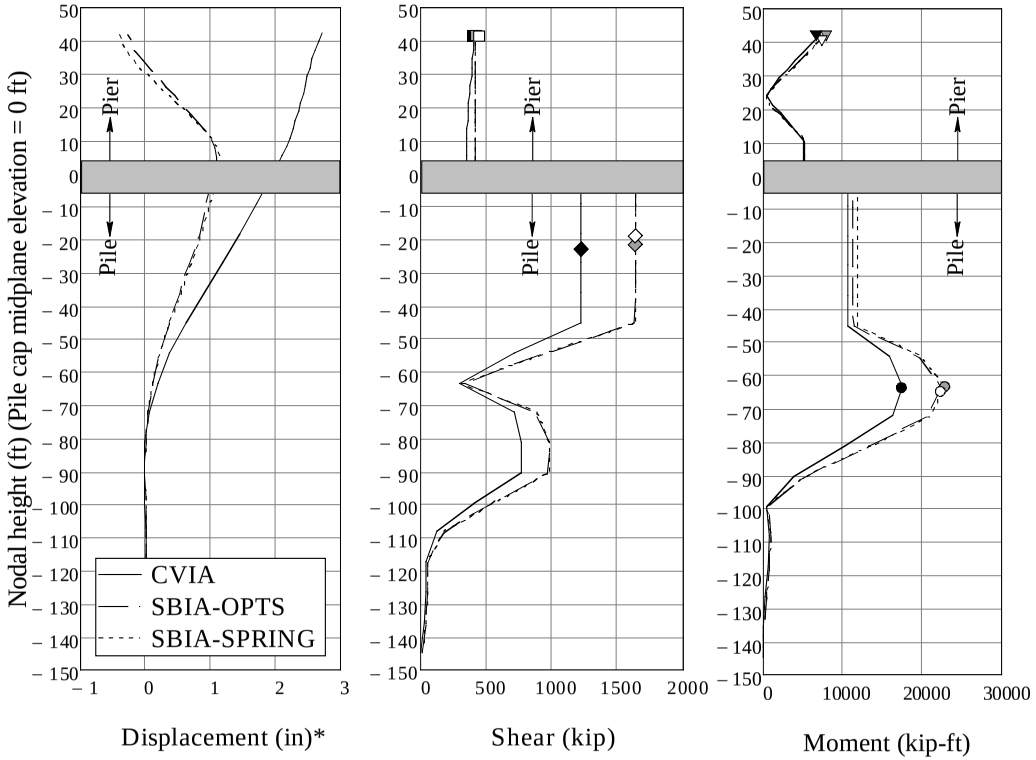

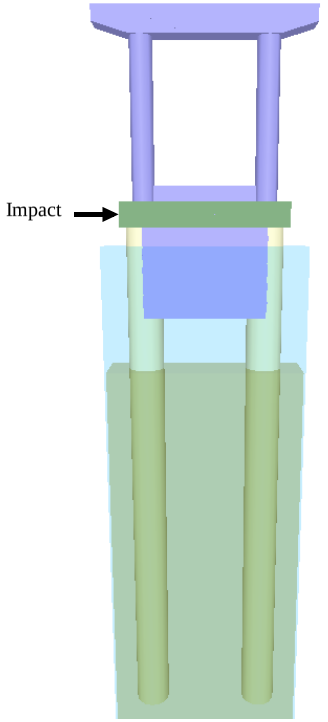

Peak Pier Demands	CVIA		SBIA OPTS		SBIA SPRING	
Column moment:	7281	kip-ft	7826	kip-ft	7934	kip-ft
Column shear:	404	kips	411	kips	413	kips
Pile Moment:	17569	kip-ft	22324	kip-ft	22753	kip-ft
Pile Shear:	1216	kips	1638	kips	1644	kips
Total Bearing Shear:	883	kips	892	kips	922	kips

* SBIA displacement profiles shown were obtained using SBIA Load Case 1 with the moment IRF equation (Equation 5.15)

Figure A.5 Comparison of CVIA, SBIA-OPTS, and SBIA-spring results
Bridge: SR-20 at Blountstown (BLT) channel pier; Impact condition: 5920 tons at 5.0 knots

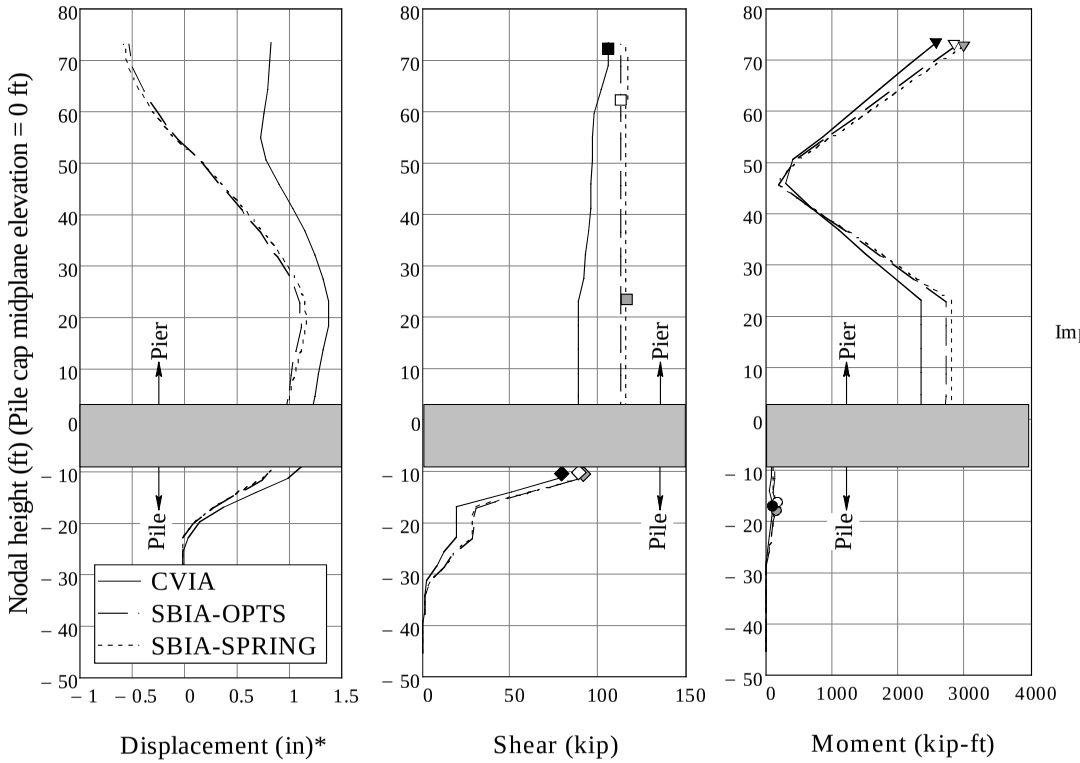

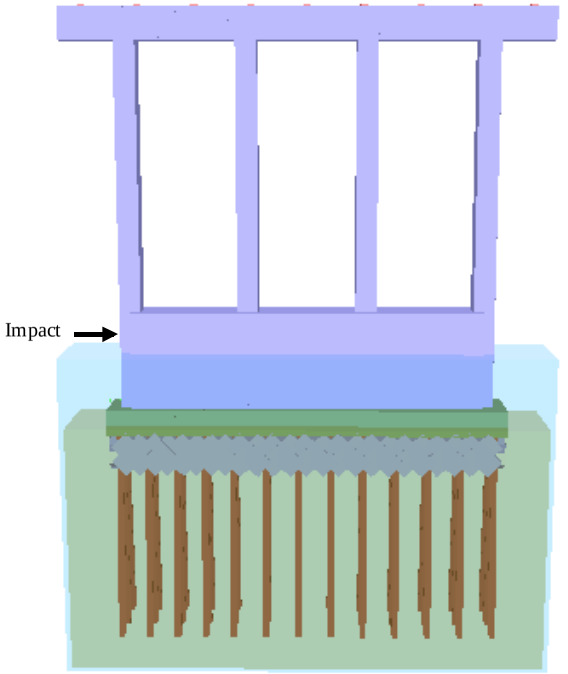

Peak Pier Demands	CVIA			SBIA OPTS			SBIA SPRING		
Column moment:	▼	2589	kip-ft	▽	2940	kip-ft	▽	3057	kip-ft
Column shear:	■	106	kips	□	113	kips	■	117	kips
Pile Moment:	●	106	kip-ft	○	158	kip-ft	●	156	kip-ft
Pile Shear:	◆	79	kips	◇	91	kips	◆	90	kips
Total Bearing Shear:		438	kips		461	kips		480	kips

* SBIA displacement profiles shown were obtained using SBIA Load Case 1 with the moment IRF equation (Equation 5.15)

Figure A.6 Comparison of CVIA, SBIA-OPTS, and SBIA-spring results
Bridge: Eau Gallie Bridge (EGB) channel pier; Impact condition: 2030 tons at 2.5 knots

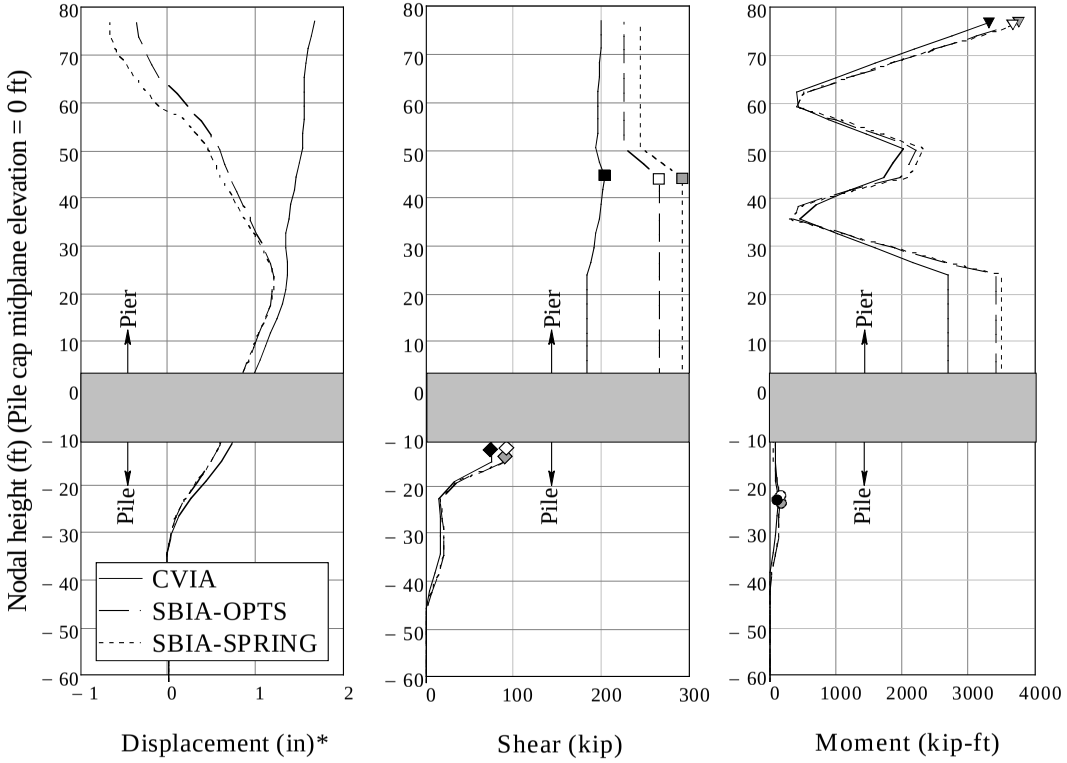

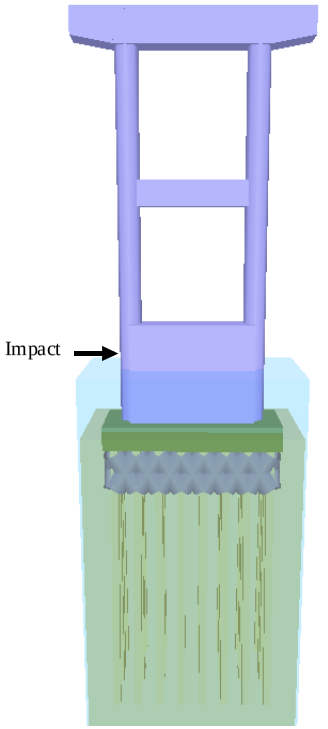

Peak Pier Demands	CVIA			SBIA OPTS			SBIA SPRING		
Column moment:	▼	3331	kip-ft	▽	3722	kip-ft	▽	3825	kip-ft
Column shear:	■	203	kips	□	266	kips	■	293	kips
Pile Moment:	●	123	kip-ft	○	158	kip-ft	●	159	kip-ft
Pile Shear:	◆	75	kips	◇	90	kips	◆	90	kips
Total Bearing Shear:		410	kips		459	kips		505	kips

* SBIA displacement profiles shown were obtained using SBIA Load Case 1 with the moment IRF equation (Equation 5.15)

Figure A.7 Comparison of CVIA, SBIA-OPTS, and SBIA-spring results
Bridge: Melbourne Causeway (MBC) channel pier; Impact condition: 2030 tons at 2.5 knots

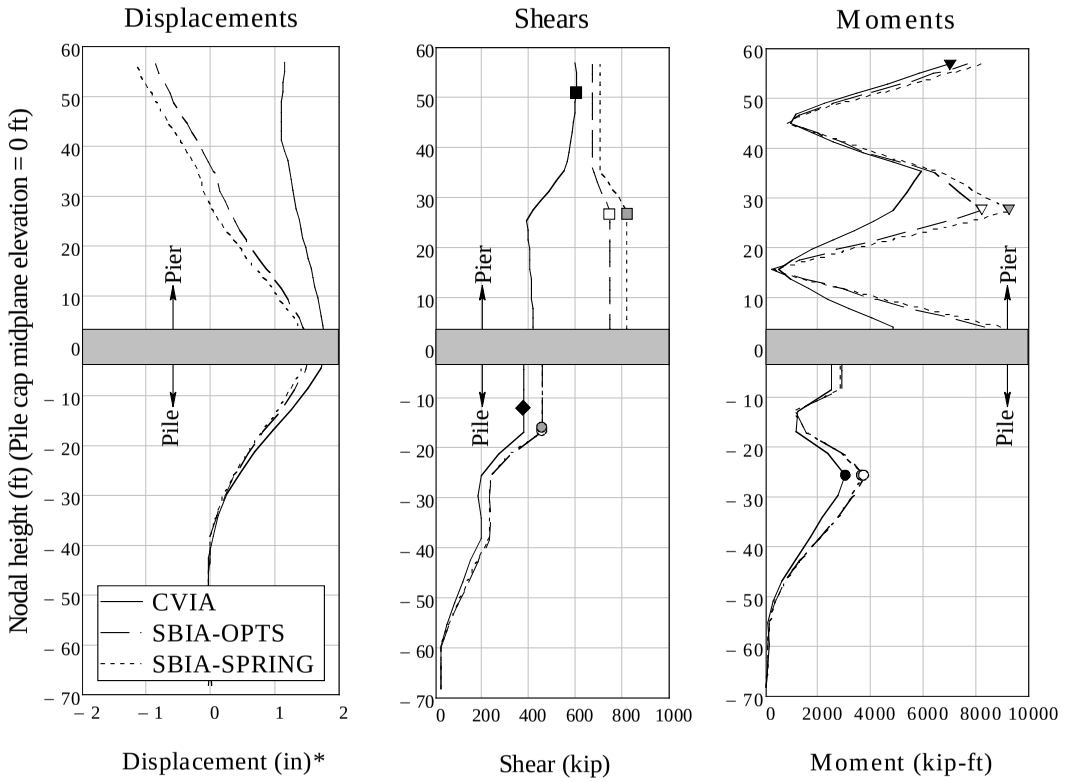

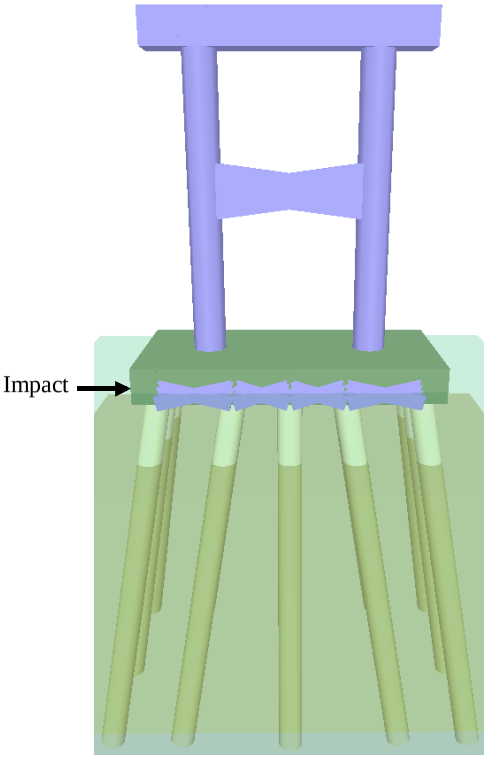

Peak Pier Demands		CVIA			SBIA OPTS			SBIA SPRING	
Column moment:	▼	6954	kip-ft	▽	8312	kip-ft	▽	9308	kip-ft
Column shear:	■	603	kips	□	742	kips	■	821	kips
Pile Moment:	●	3023	kip-ft	○	3775	kip-ft	●	3724	kip-ft
Pile Shear:	◆	377	kips	◇	459	kips	◆	454	kips
Total Bearing Shear:		1114	kips		1376	kips		1400	kips

* SBIA displacement profiles shown were obtained using SBIA Load Case 1 with the moment IRF equation (Equation 5.15)

Figure A.8 Comparison of CVIA, SBIA-OPTS, and SBIA-spring results
Bridge: new St. George Island (NSG) channel pier; Impact condition: 2030 tons at 2.5 knots

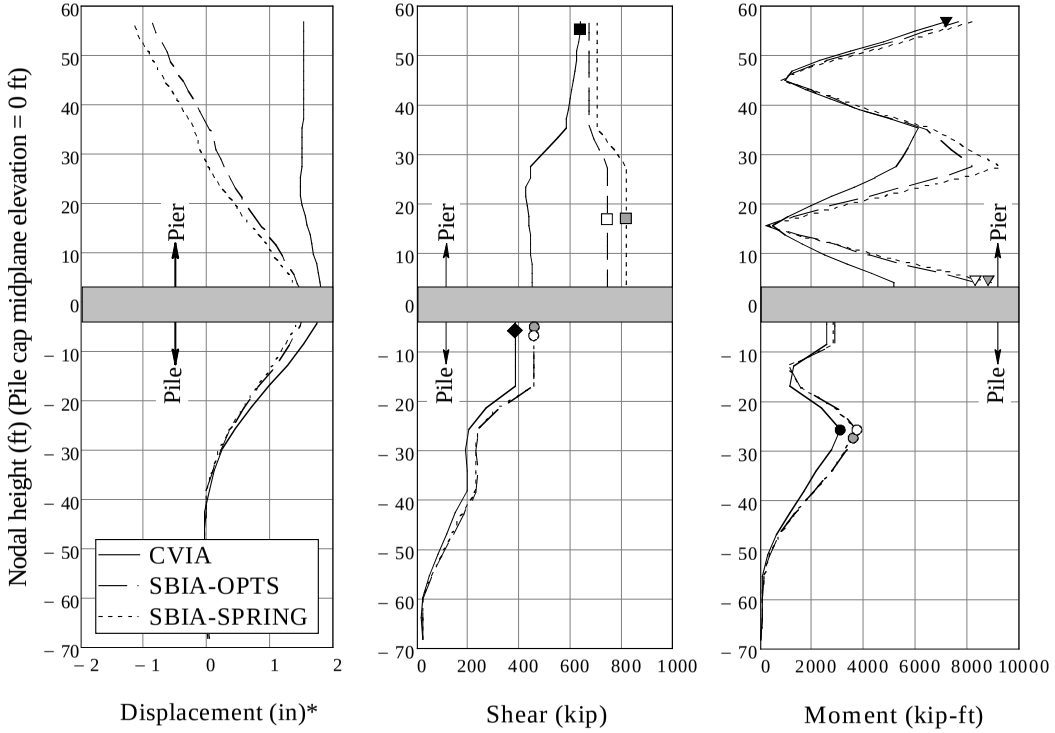

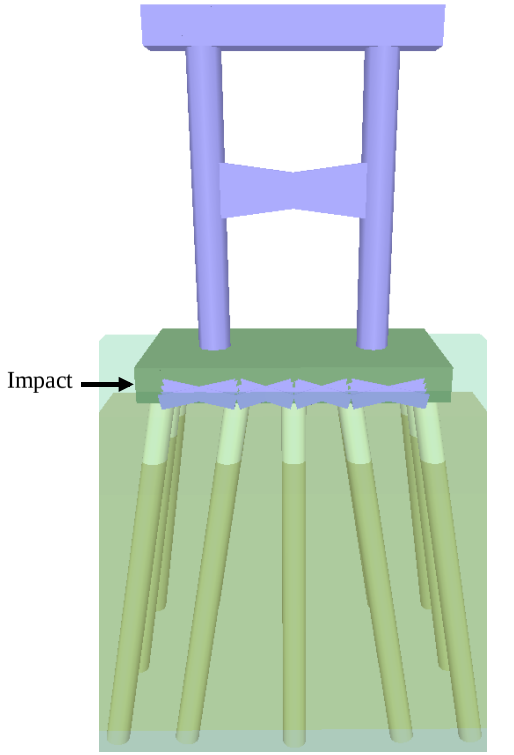

Peak Pier Demands	CVIA		SBIA OPTS		SBIA SPRING	
Column moment:	7194	kip-ft	8312	kip-ft	9308	kip-ft
Column shear:	638	kips	742	kips	821	kips
Pile Moment:	3070	kip-ft	3775	kip-ft	3724	kip-ft
Pile Shear:	383	kips	459	kips	454	kips
Total Bearing Shear:	1171	kips	1376	kips	1400	kips

* SBIA displacement profiles shown were obtained using SBIA Load Case 1 with the moment IRF equation (Equation 5.15)

Figure A.9 Comparison of CVIA, SBIA-OPTS, and SBIA-spring results
Bridge: new St. George Island (NSG) channel pier; Impact condition: 5920 tons at 5.0 knots

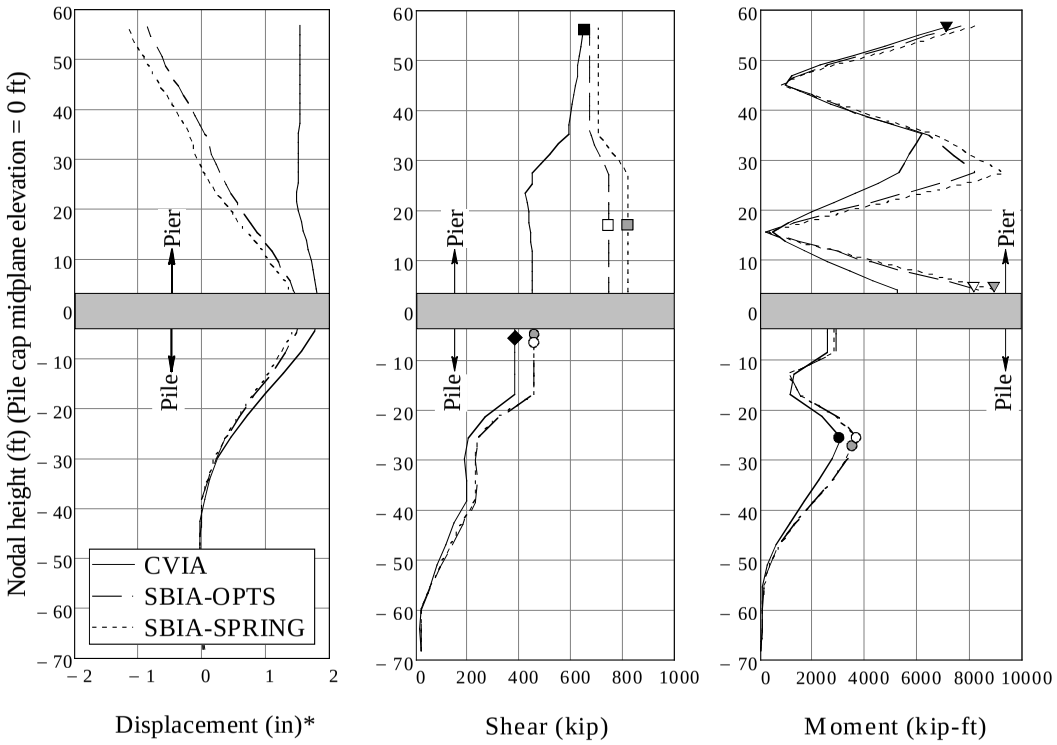

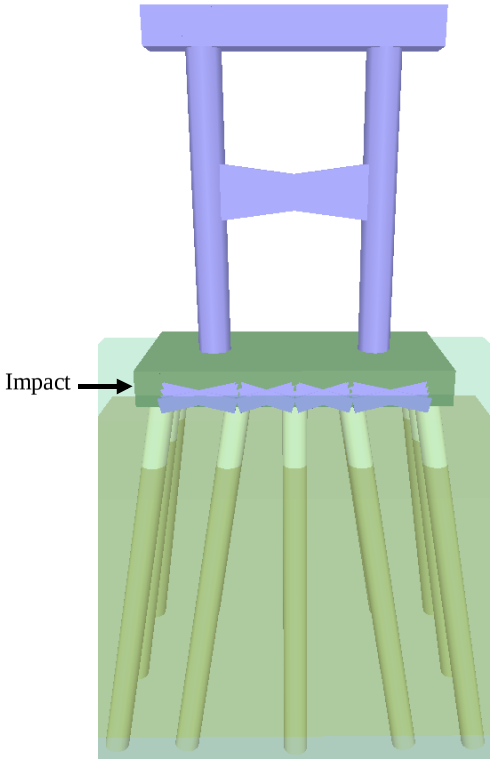

Peak Pier Demands	CVIA		SBIA OPTS		SBIA SPRING	
Column moment:	7233	kip-ft	8312	kip-ft	9308	kip-ft
Column shear:	644	kips	742	kips	821	kips
Pile Moment:	3076	kip-ft	3775	kip-ft	3724	kip-ft
Pile Shear:	384	kips	459	kips	454	kips
Total Bearing Shear:	1180	kips	1376	kips	1400	kips

* SBIA displacement profiles shown were obtained using SBIA Load Case 1 with the moment IRF equation (Equation 5.15)

Figure A.10 Comparison of CVIA, SBIA-OPTS, and SBIA-spring results
Bridge: new St. George Island (NSG) channel pier; Impact condition: 7820 tons at 7.5 knots

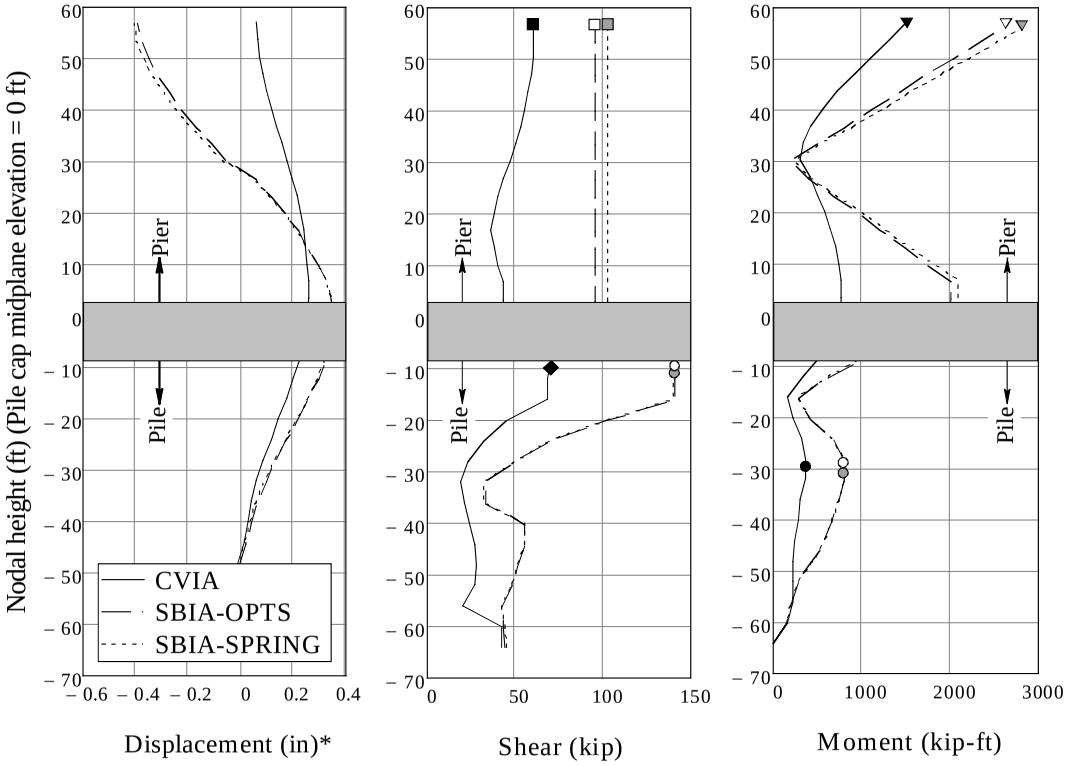

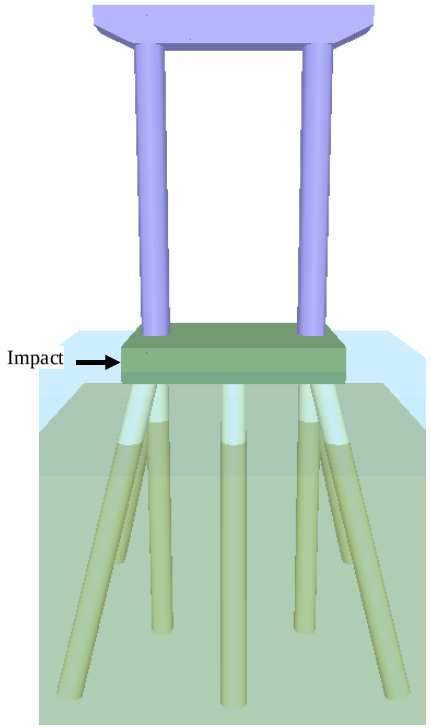

Peak Pier Demands	CVIA		SBIA OPTS		SBIA SPRING	
Column moment:	1518	kip-ft	2671	kip-ft	2898	kip-ft
Column shear:	61	kips	95	kips	103	kips
Pile Moment:	521	kip-ft	1060	kip-ft	1039	kip-ft
Pile Shear:	71	kips	141	kips	140	kips
Total Bearing Shear:	128	kips	218	kips	231	kips

* SBIA displacement profiles shown were obtained using SBIA Load Case 1 with the moment IRF equation (Equation 5.15)

Figure A.11 Comparison of CVIA, SBIA-OPTS, and SBIA-spring results
Bridge: new St. George Island (NSG) off-channel pier; Impact condition: 200 tons at 1.0 knots

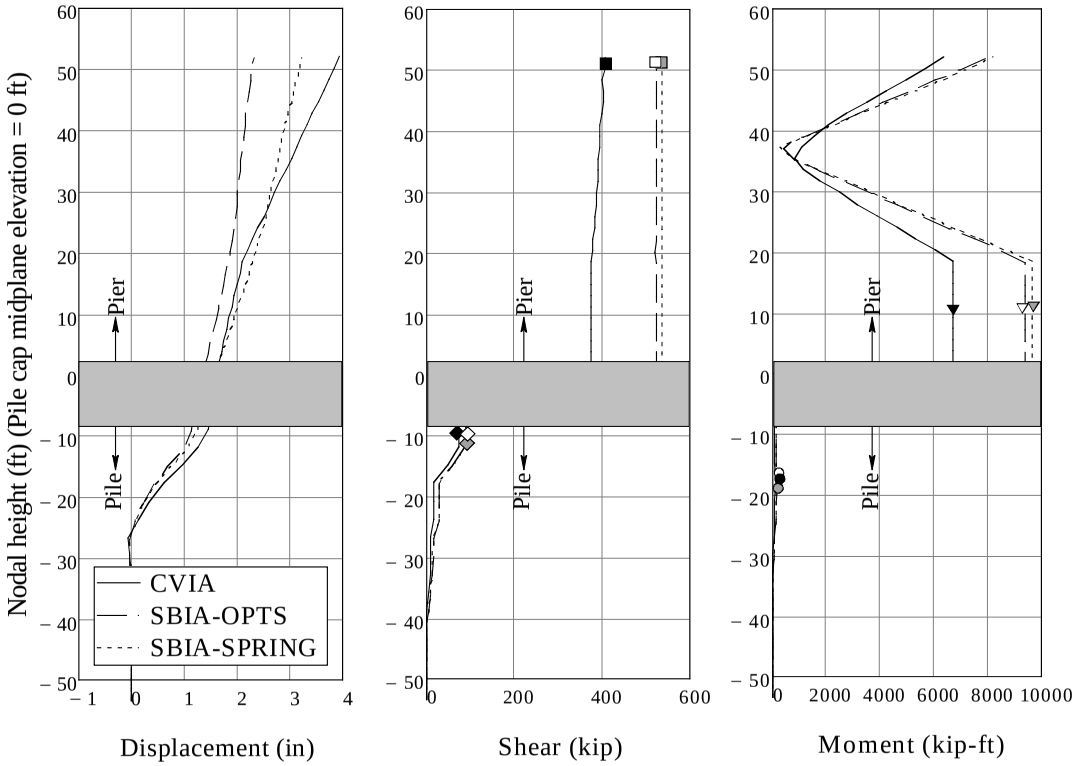

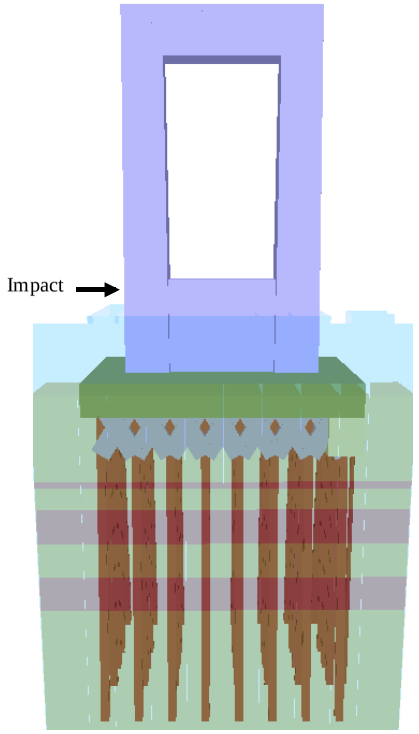

Peak Pier Demands	CVIA		SBIA OPTS		SBIA SPRING	
Column moment:	▼ 6710	kip-ft	▽ 8025	kip-ft	▽ 7689	kip-ft
Column shear:	■ 405	kips	□ 490	kips	■ 500	kips
Pile Moment:	● 107	kip-ft	○ 189	kip-ft	● 184	kip-ft
Pile Shear:	◆ 73	kips	◇ 88	kips	◆ 87	kips
Total Bearing Shear:	721	kips	860	kips	973	kips

* SBIA displacement profiles shown were obtained using SBIA Load Case 1 with the moment IRF equation (Equation 5.15)

Figure A.12 Comparison of CVIA, SBIA-OPTS, and SBIA-spring results
Bridge: old St. George Island (OSG) channel pier; Impact condition: 2030 tons at 2.5 knots

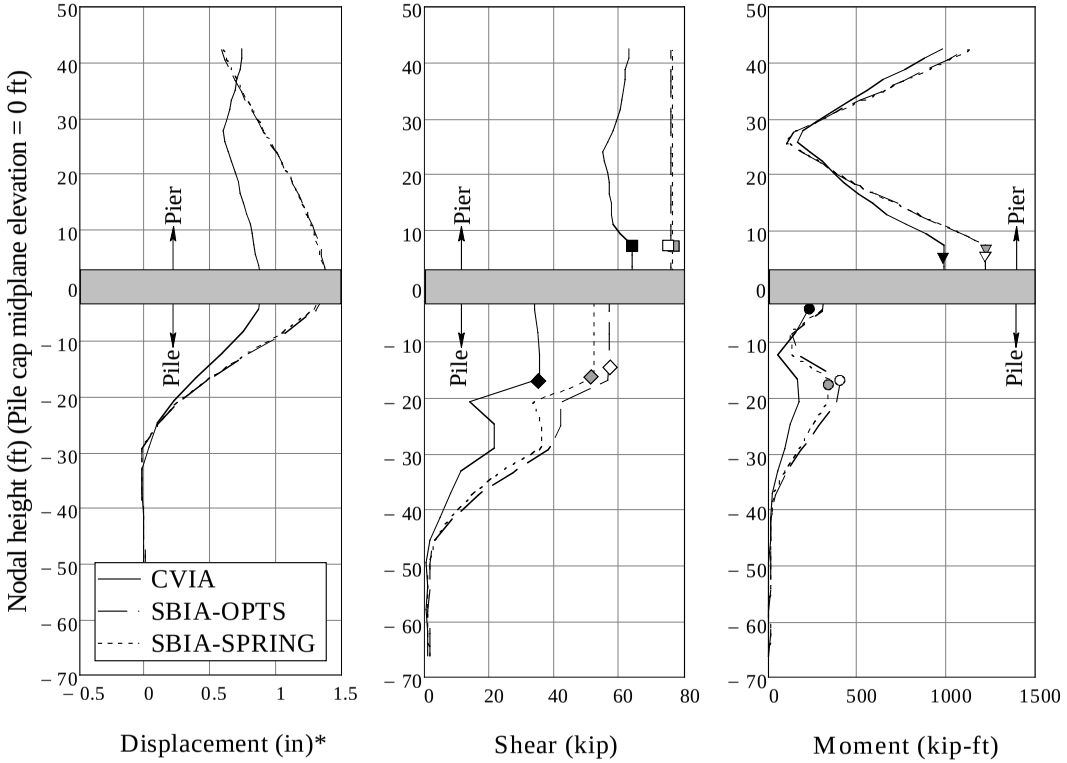

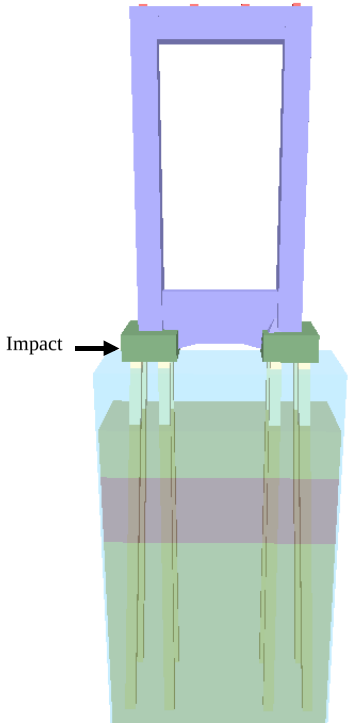

Peak Pier Demands	CVIA			SBIA OPTS			SBIA SPRING		
Column moment:	▼	989	kip-ft	▽	1217	kip-ft	▽	1217	kip-ft
Column shear:	■	64	kips	□	76	kips	■	76	kips
Pile Moment:	●	220	kip-ft	○	406	kip-ft	●	343	kip-ft
Pile Shear:	◆	36	kips	◇	57	kips	◆	52	kips
Total Bearing Shear:		109	kips		161	kips		165	kips

* SBIA displacement profiles shown were obtained using SBIA Load Case 1 with the moment IRF equation (Equation 5.15)

Figure A.13 Comparison of CVIA, SBIA-OPTS, and SBIA-spring results
Bridge: old St. George Island (OSG) off-channel pier; Impact condition: 200 tons at 1.0 knots

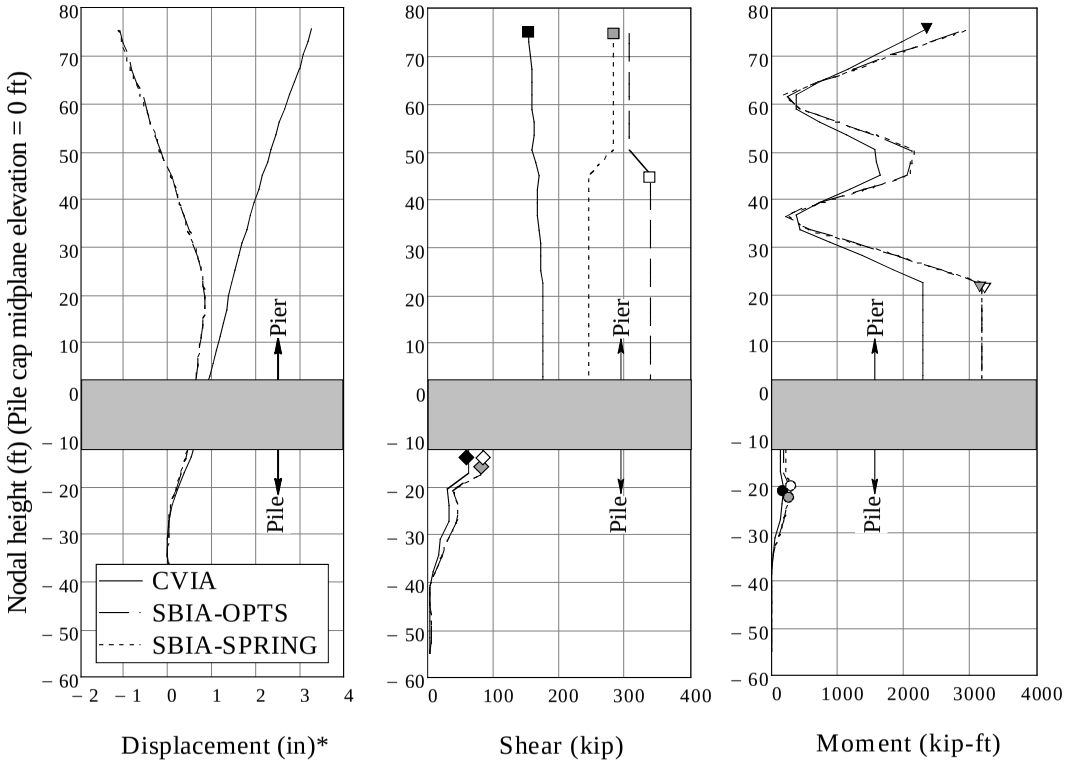

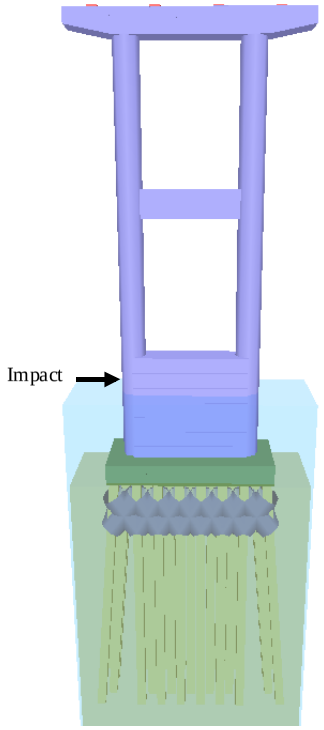

Peak Pier Demands	CVIA		SBIA OPTS		SBIA SPRING	
Column moment:	2334	kip-ft	3165	kip-ft	3177	kip-ft
Column shear:	175	kips	338	kips	282	kips
Pile Moment:	201	kip-ft	295	kip-ft	305	kip-ft
Pile Shear:	61	kips	84	kips	84	kips
Total Bearing Shear:	318	kips	537	kips	400	kips

* SBIA displacement profiles shown were obtained using SBIA Load Case 1 with the moment IRF equation (Equation 5.15)

Figure A.14 Comparison of CVIA, SBIA-OPTS, and SBIA-spring results
Bridge: Pineda Causeway (PNC) channel pier; Impact condition: 2030 tons at 2.5 knots

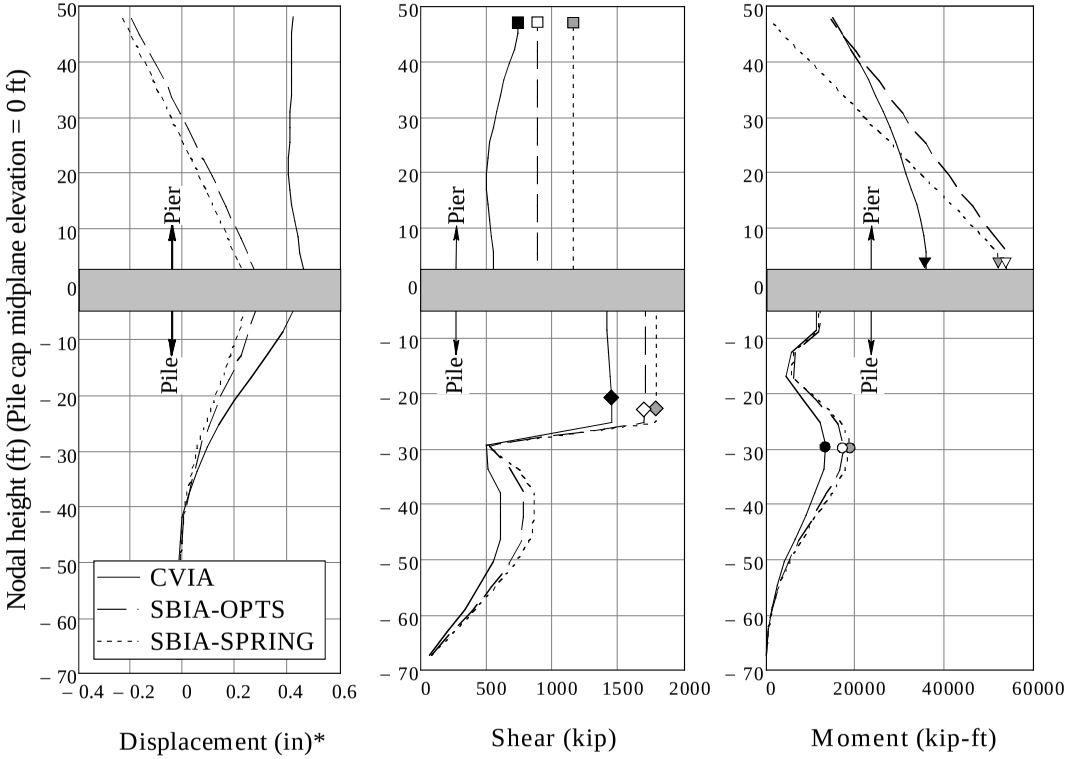

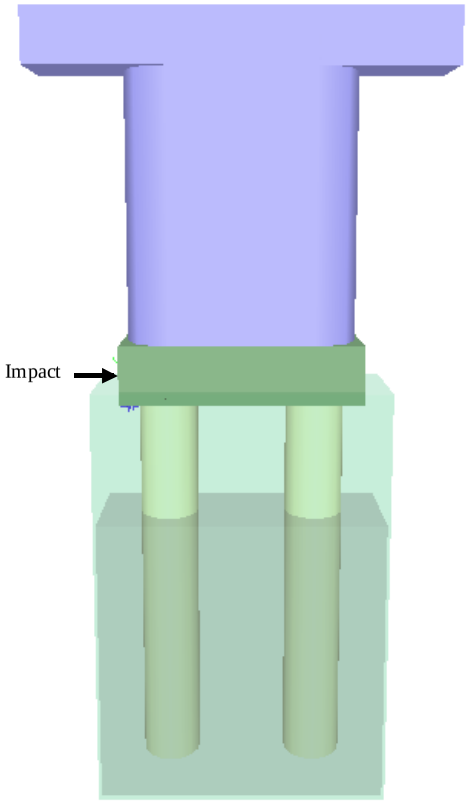

Peak Pier Demands	CVIA	SBIA OPTS	SBIA SPRING
Column moment:	35960 kip-ft	53783 kip-ft	51966 kip-ft
Column shear:	743 kips	881 kips	1160 kips
Pile Moment:	13291 kip-ft	17229 kip-ft	18760 kip-ft
Pile Shear:	1451 kips	1710 kips	1789 kips
Total Bearing Shear:	1028 kips	1219 kips	1667 kips

* SBIA displacement profiles shown were obtained using SBIA Load Case 1 with the moment IRF equation (Equation 5.15)

Figure A.15 Comparison of CVIA, SBIA-OPTS, and SBIA-spring results
Bridge: Ringling (RNG) channel pier; Impact condition: 2030 tons at 2.5 knots

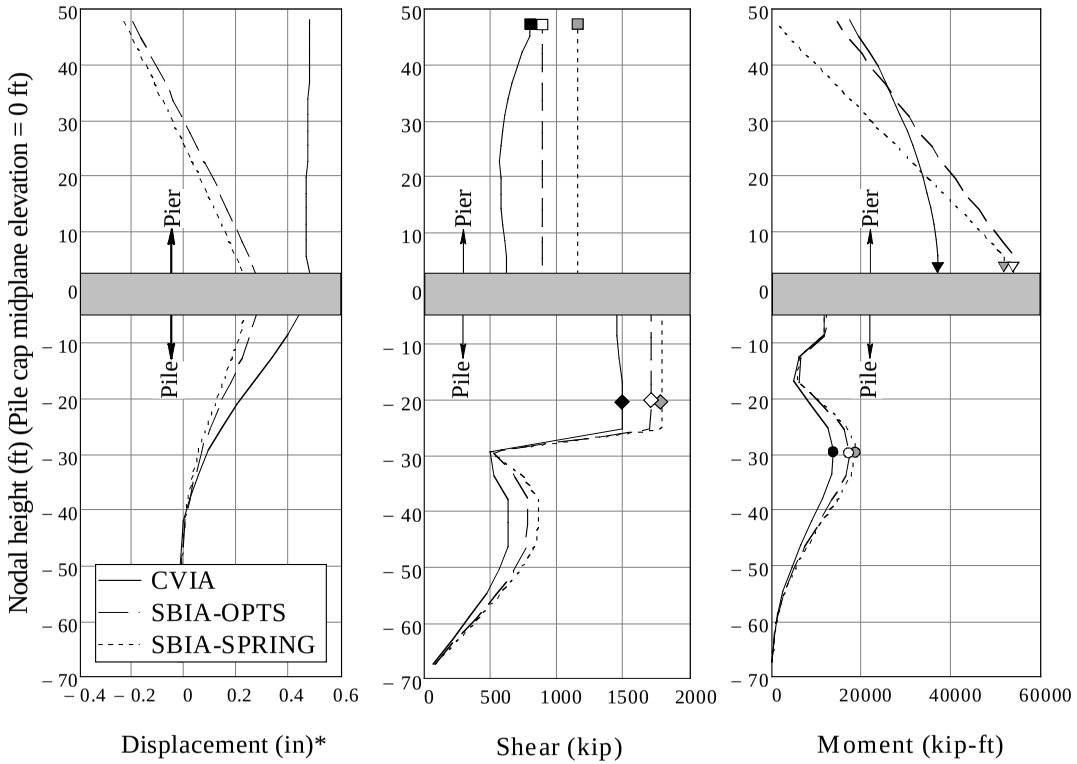

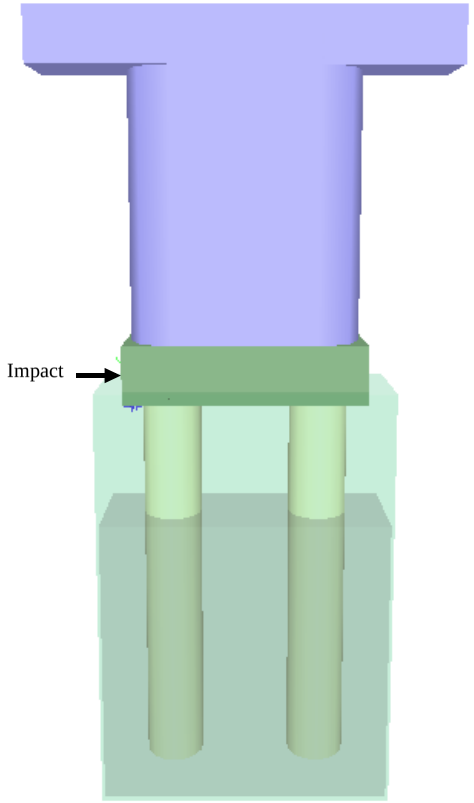

Peak Pier Demands	CVIA	SBIA OPTS	SBIA SPRING
Column moment:	37180 kip-ft	53783 kip-ft	51966 kip-ft
Column shear:	788 kips	881 kips	1160 kips
Pile Moment:	13818 kip-ft	17229 kip-ft	18760 kip-ft
Pile Shear:	1494 kips	1710 kips	1789 kips
Total Bearing Shear:	1199 kips	1219 kips	1667 kips

* SBIA displacement profiles shown were obtained using SBIA Load Case 1 with the moment IRF equation (Equation 5.15)

Figure A.16 Comparison of CVIA, SBIA-OPTS, and SBIA-spring results
Bridge: Ringling (RNG) channel pier; Impact condition: 5920 tons at 5.0 knots

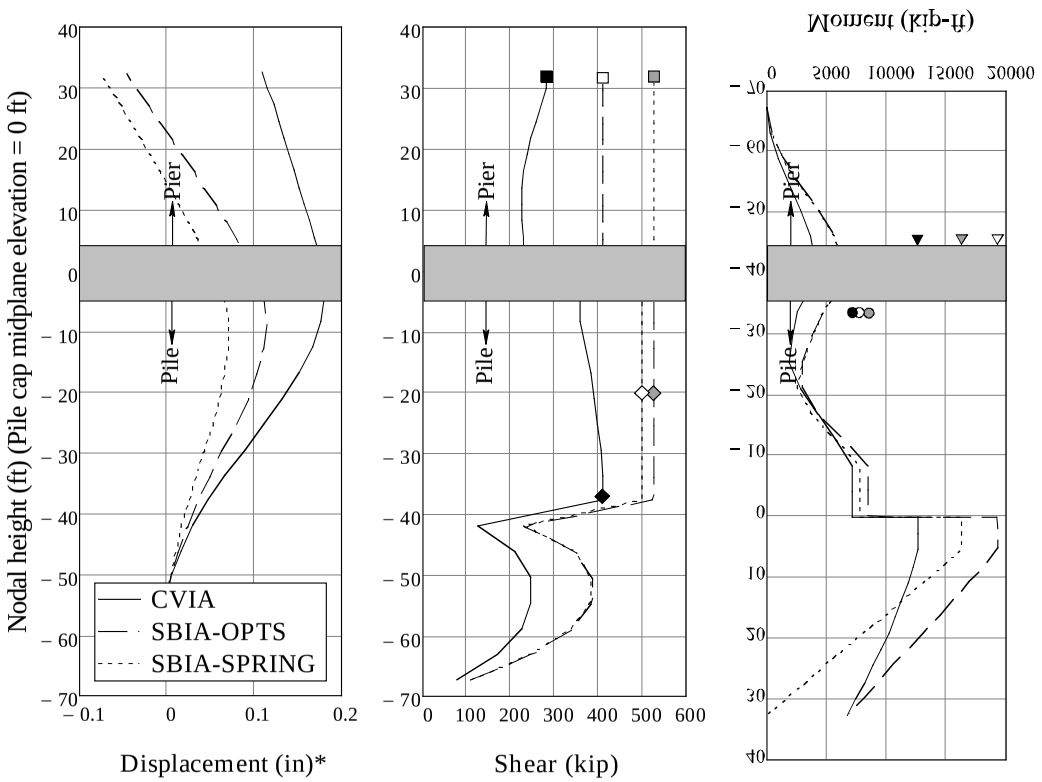

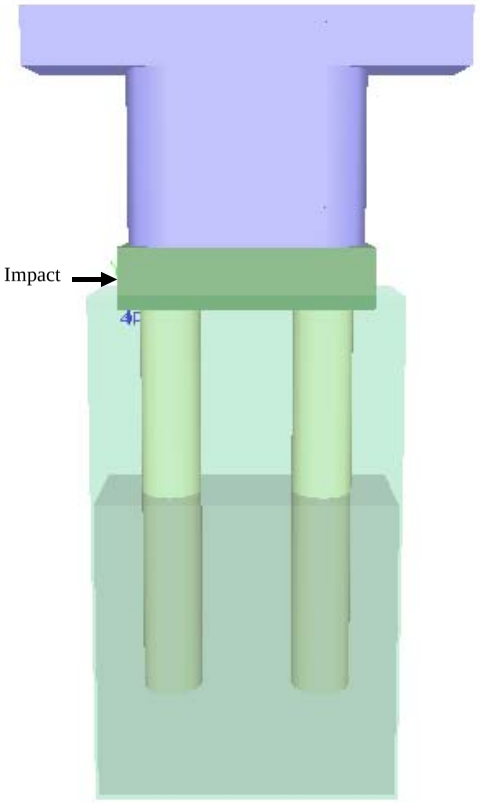

Peak Pier Demands	CVIA		SBIA OPTS		SBIA SPRING	
Column moment:	12678	kip-ft	19346	kip-ft	16233	kip-ft
Column shear:	282	kips	412	kips	528	kips
Pile Moment:	7134	kip-ft	8476	kip-ft	7766	kip-ft
Pile Shear:	410	kips	526	kips	500	kips
Total Bearing Shear:	428	kips	573	kips	759	kips

* SBIA displacement profiles shown were obtained using SBIA Load Case 1 with the moment IRF equation (Equation 5.15)

Figure A.17 Comparison of CVIA, SBIA-OPTS, and SBIA-spring results
Bridge: Ringling (RNG) off-channel pier; Impact condition: 200 tons at 1.0 knots

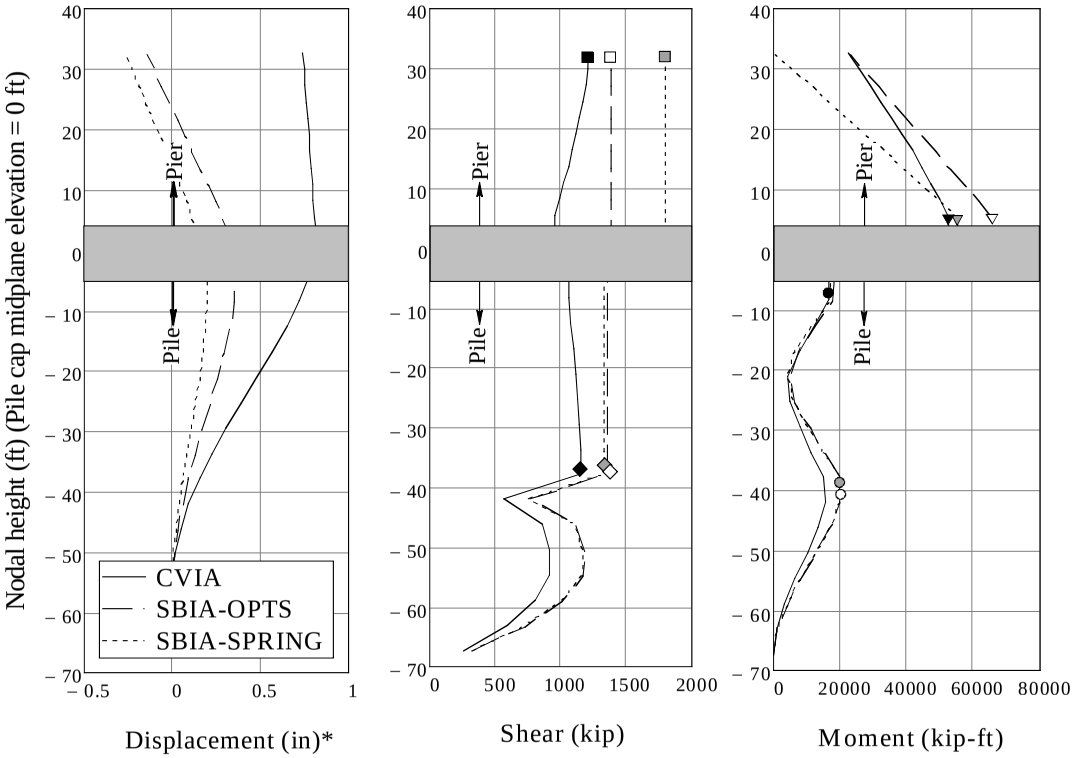

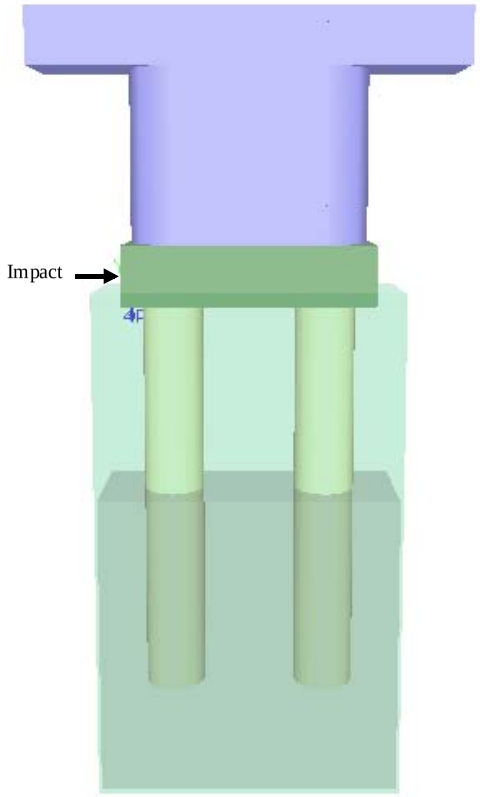

Peak Pier Demands	CVIA		SBIA OPTS		SBIA SPRING	
Column moment:	52823	kip-ft	65276	kip-ft	55154	kip-ft
Column shear:	1214	kips	1388	kips	1793	kips
Pile Moment:	16536	kip-ft	20116	kip-ft	19967	kip-ft
Pile Shear:	1156	kips	1361	kips	1322	kips
Total Bearing Shear:	1483	kips	1923	kips	2562	kips

* SBIA displacement profiles shown were obtained using SBIA Load Case 1 with the moment IRF equation (Equation 5.15)

Figure A.18 Comparison of CVIA, SBIA-OPTS, and SBIA-spring results
Bridge: Ringling (RNG) off-channel pier; Impact condition: 2030 tons at 2.5 knots

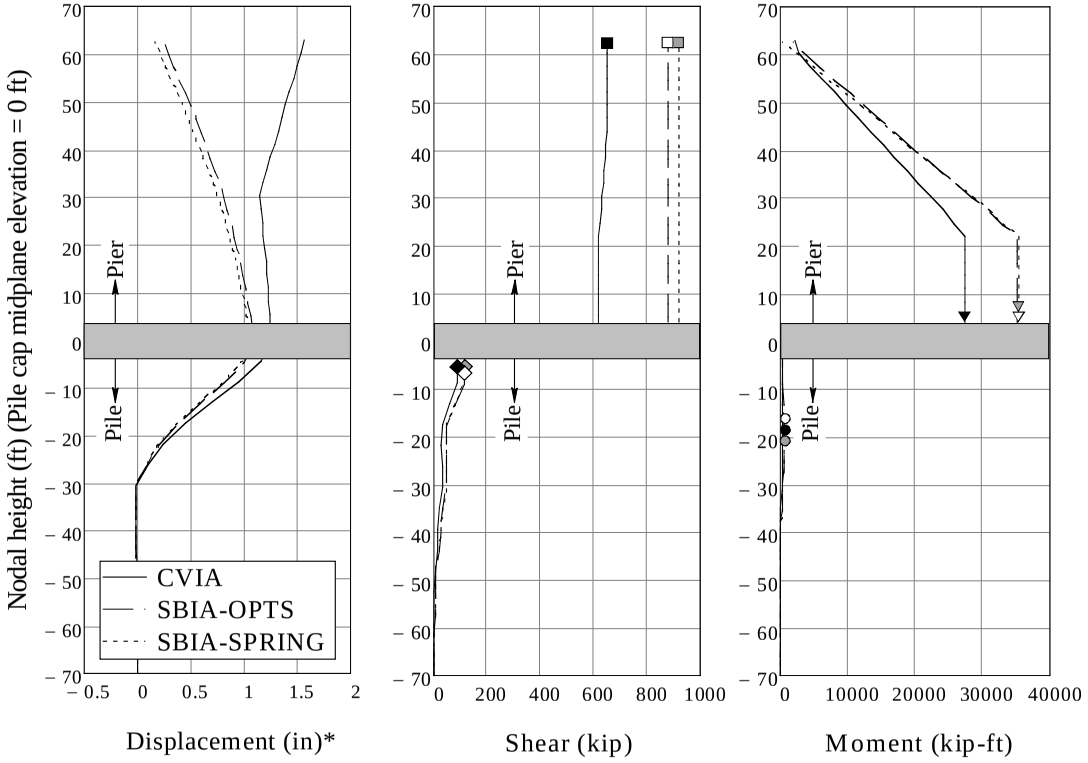

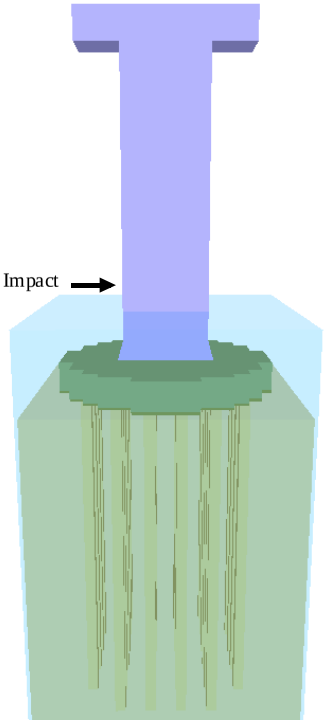

Peak Pier Demands	CVIA		SBIA OPTS		SBIA SPRING	
Column moment:	27487	kip-ft	35046	kip-ft	35467	kip-ft
Column shear:	654	kips	881	kips	918	kips
Pile Moment:	354	kip-ft	570	kip-ft	560	kip-ft
Pile Shear:	86	kips	114	kips	113	kips
Total Bearing Shear:	643	kips	1040	kips	1082	kips

* SBIA displacement profiles shown were obtained using SBIA Load Case 1 with the moment IRF equation (Equation 5.15)

Figure A.19 Comparison of CVIA, SBIA-OPTS, and SBIA-spring results
Bridge: Seabreeze (SBZ) channel pier; Impact condition: 2030 tons at 2.5 knots

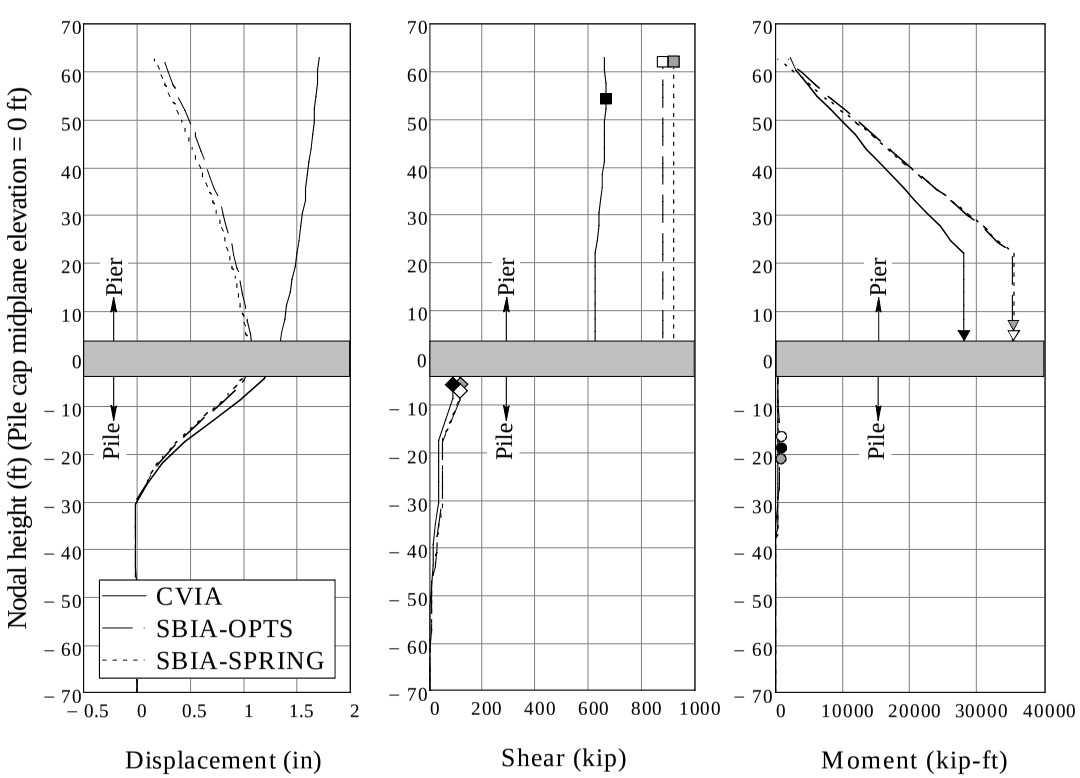

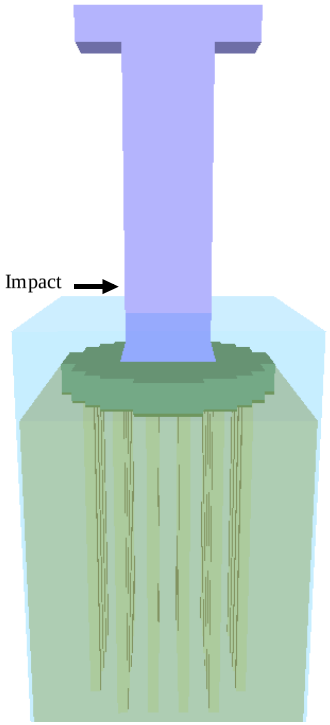

Peak Pier Demands	CVIA		SBIA OPTS		SBIA SPRING	
Column moment:	27807	kip-ft	35046	kip-ft	35467	kip-ft
Column shear:	661	kips	881	kips	918	kips
Pile Moment:	362	kip-ft	570	kip-ft	560	kip-ft
Pile Shear:	88	kips	114	kips	113	kips
Total Bearing Shear:	650	kips	1040	kips	1082	kips

* SBIA displacement profiles shown were obtained using SBIA Load Case 1 with the moment IRF equation (Equation 5.15)

Figure A.20 Comparison of CVIA, SBIA-OPTS, and SBIA-spring results
Bridge: Seabreeze (SBZ) channel pier; Impact condition: 5920 tons at 5.0 knots

APPENDIX B
DEMONSTRATION OF SBIA METHOD

B.1 Introduction

In this appendix, the SBIA method is demonstrated for the New Trammel Bridge, in northwestern Florida. For this example, a three-barge flotilla (5920 tons with tug) collides with the channel pier at 5.0 knots. Barge impact occurs near the top of a 30.5 ft tall shear wall that connects two 9 ft diameter drilled shafts (Figure B.1). Two circular pier columns (5.5 ft diameter), which are axially collinear with each foundation shafts, span from the foundation elements to the top of the pier.

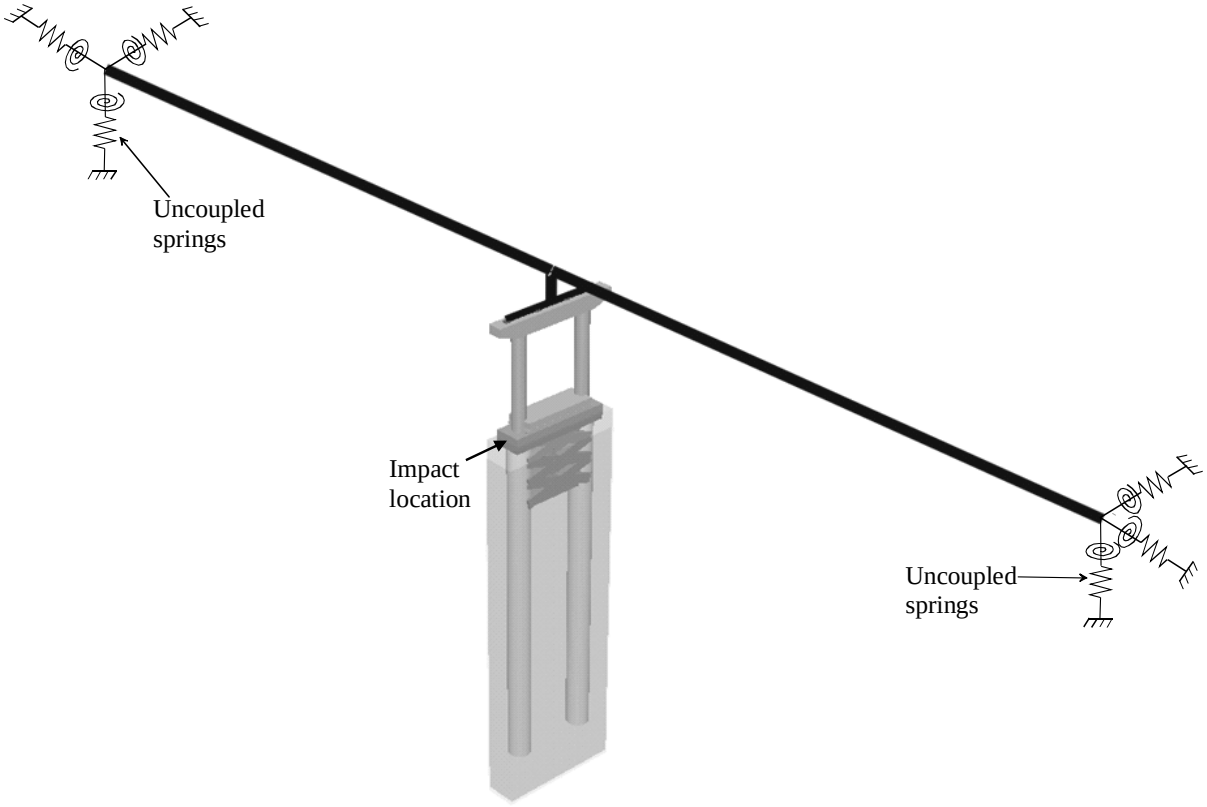

Figure B.1 Structural configuration for New Trammel Bridge

B.2 Demonstration of SBIA Procedure

Prior to constructing the SBIA load cases, the vessel impact force must be computed. For this bridge, impact occurs near the top of the shear wall, which has a 9-ft diameter round impact surface ($w_p = 9\,\text{ft}$). Thus, the barge yield force is determined in accordance with Figure B.2 and Equation B.1. Note that this yield force occurs at a crush depth (a_{BY}) of 2 in.

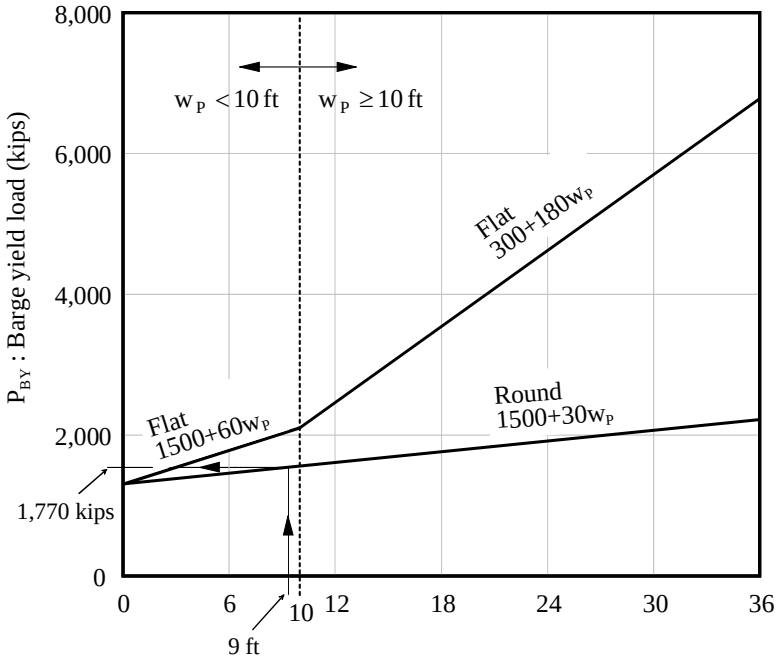

Figure B.2 Barge yield load determination for 9-ft round impact surface

$$P_{BY} = 1500 + 30 \cdot w_p = 1500 + 30 \cdot (9) = \boxed{1770\,\text{kips}} \tag{B.1}$$

With the yield force quantified, the impact force corresponding to the high-energy barge collision (5920-ton flotilla, traveling at 5.0 knots) is computed. First, the series stiffness of the barge and pier/soil system (k_S) is calculated per Equation B.3. Note that the stiffness of the pier/soil system for this bridge (k_P) must be quantified as shown in Figure B.3 and Equation B.2. For this example, P_{BY} is applied to the pier to quantify k_P; however, if the calculated impact load (P_B) is found to be less than P_{BY}, then this process should be repeated to obtain a more accurate estimate of k_P.

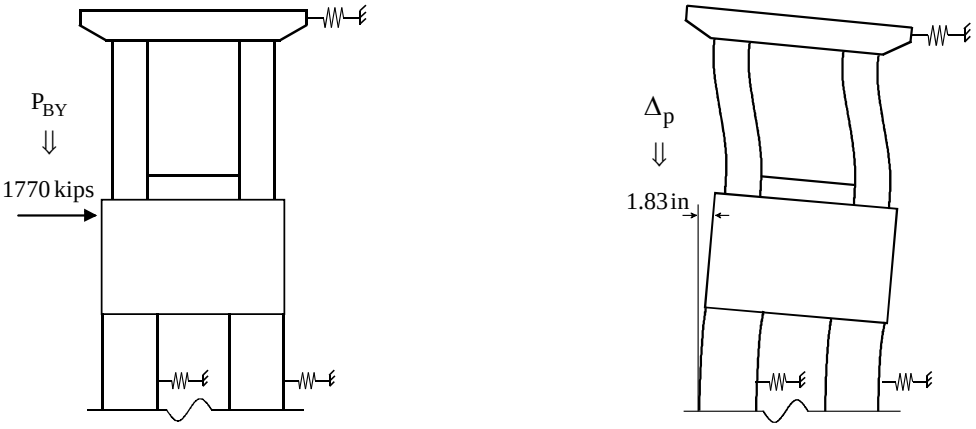

Figure B.3 Determination of pier stiffness (k_P)

$$k_P = \frac{P_{BY}}{\Delta_p} = \frac{1770}{1.83} = \boxed{963\,\text{kip/in}} \tag{B.2}$$

$$k_S = \left(\frac{a_{BY}}{P_{BY}} + \frac{1}{k_P}\right)^{-1} = \left(\frac{2}{1770} + \frac{1}{963}\right)^{-1} = \boxed{461\,\text{kip/in}} \tag{B.3}$$

Thus, the high-energy crush force is computed given the barge tow velocity (v_{Bi}) of 5.0 knots (101 in/s) and mass (m_B) of 5920 tons (30.7 kip/in/s^2):

$$\begin{aligned} &P_B = v_{Bi} \cdot \sqrt{k_S \cdot m_B} = (101) \cdot \sqrt{(461) \cdot (30.7)} = 12{,}015\,\text{kips} \\ &12{,}015\,\text{kips} > P_{BY} \\ &\therefore P_B = P_{BY} = \boxed{1{,}770\,\text{kips}} \end{aligned} \tag{B.4}$$

This calculation illustrates that the incoming kinetic energy of the barge tow is sufficient to yield the barge bow, generating the maximum crush force for this pier (1770 kips).

B.3.1 Load Case 1

With the barge impact load (P_B) quantified, the SBIA load cases are constructed. For Load Case 1, the amplified static impact load is computed:

$$1.45 \cdot P_B = 1.45 \cdot (1770) = \boxed{2567\,\text{kips}} \tag{B.5}$$

This amplified impact load is used for each part of Load Case 1, regardless of the demand type of interest. However, unique pier-top loads are computed, corresponding to pier moment, pier shear, and total bearing shear. To quantify these loads, corresponding IRFs are calculated, based on the bridge structural parameters illustrated in Figure B.4 and Figure B.5.

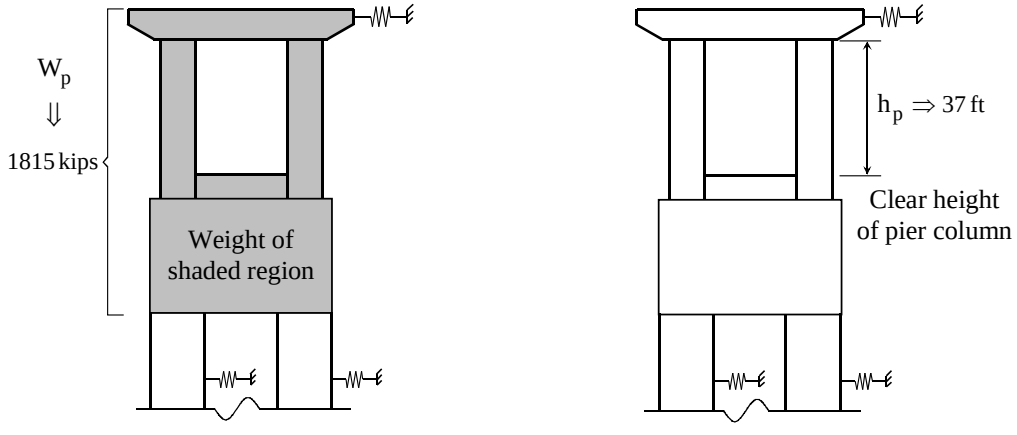

Figure B.4 Determination of pier weight (W_P) and pier height (h_p)

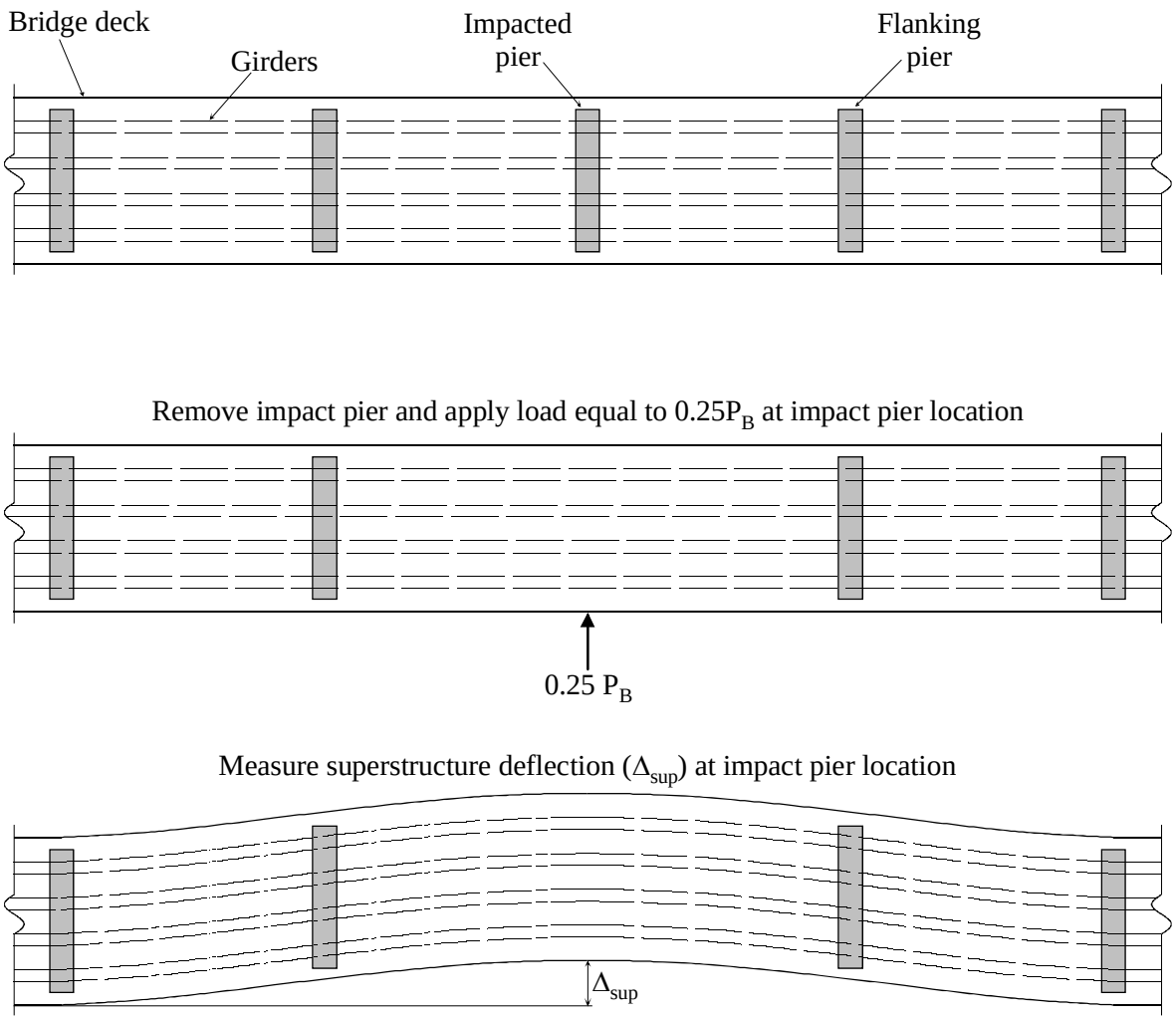

Figure B.5 Determination of superstructure stiffness (k_{sup})

As illustrated in Figure B.4, the total weight of this pier (W_p) is 1815 kips, and the height of the pier (h_p) is 37 ft. The lateral superstructure stiffness (k_{sup}) is 199 kip/in, as determined using the process shown in Figure B.5. Due to the empirical nature of the IRF equations, the units shown above must be used. Thus,

$$IRF_m = 0.22 + \frac{4.5}{h_p}\sqrt{\frac{k_{sup}}{\sqrt{W_p}}} = 0.22 + \frac{4.5}{(37)}\sqrt{\frac{(199)}{\sqrt{(1815)}}} = \boxed{0.48} \quad \text{(B.6)}$$

$$IRF_v = 0.36 + \frac{3.0}{h_p}\sqrt{\frac{k_{sup}}{\sqrt{W_p}}} = 0.36 + \frac{3.0}{(37)}\sqrt{\frac{(199)}{\sqrt{(1815)}}} = \boxed{0.54} \quad \text{(B.7)}$$

$$IRF_b = 0.37 + \frac{7.0}{h_p}\sqrt{\frac{k_{sup}}{\sqrt{W_p}}} = 0.37 + \frac{7.0}{(37)}\sqrt{\frac{(199)}{\sqrt{(1815)}}} = \boxed{0.78} \quad \text{(B.8)}$$

The amplified impact load (as computed in Equation B.5) is applied at the impact location for all three analyses. For each of the three analyses, the corresponding IRF (as calculated in Equations B.6, B.7, and B.8) is multiplied by the impact force (P_B), and this load is applied at the pier cap beam center of gravity, in the opposite direction of impact (Figure B.6).

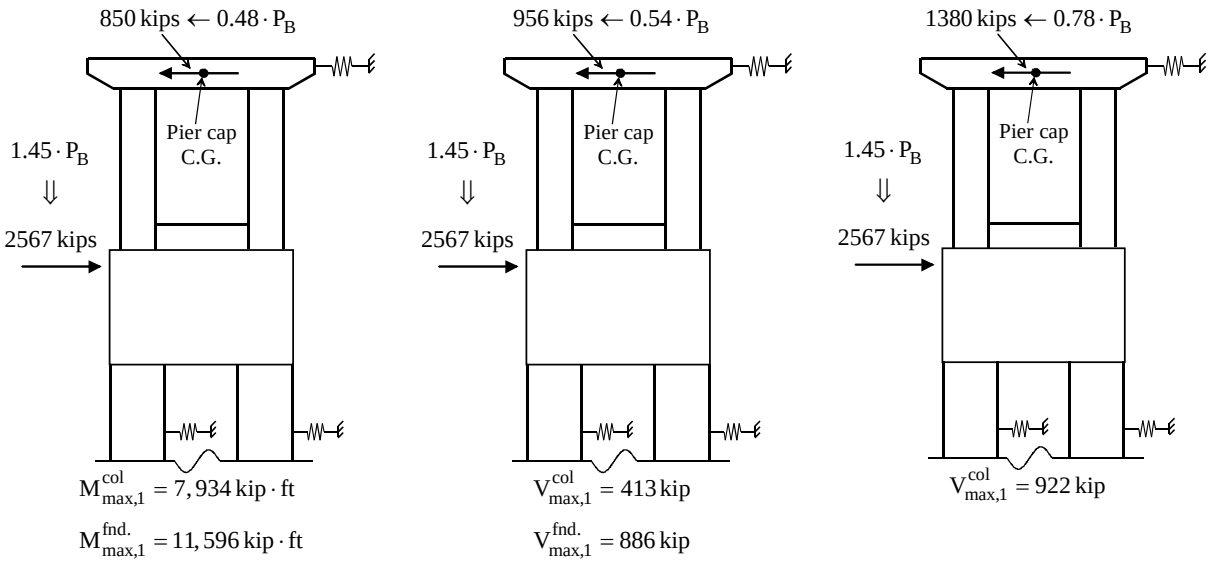

Figure B.6 Loading conditions and maximum demand predictions for Load Case 1

With the loading conditions for Load Case 1 developed, the structure is statically analyzed. Predictions of pier (column and foundation) moment, pier (column and foundation) shear, and total bearing shear demands are quantified using the respective analyses (Figure B.6). These design forces are additionally summarized in Table B.1.

B.4.1 Load Case 2

SBIA Load Case 2 is also analyzed as shown in Figure B.7. From this single analysis, all pertinent member forces are quantified—pier moments, pier shears, and total bearing shear. These demands are compared to those obtained from Load Case 1 in Table B.1. The amplified impact load for Load Case 2 is calculated as:

$$1.85 \cdot P_B = 1.85 \cdot (1770) = \boxed{3275\,\text{kips}} \tag{B.9}$$

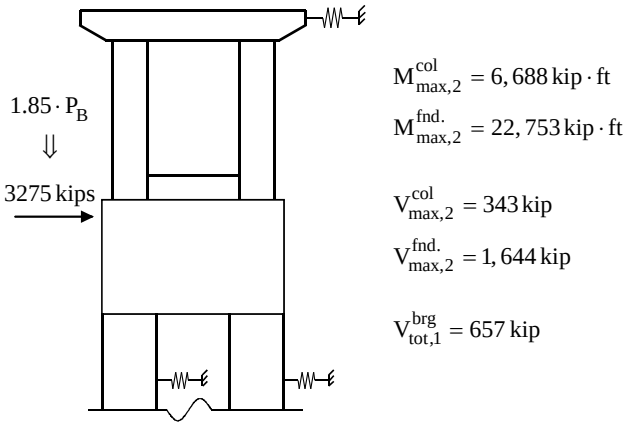

Figure B.7 Loading conditions and maximum demand predictions for Load Case 2

B.5.1 Results summary

Design forces predicted by Load Cases 1 and 2 are summarized in Table B.1. For each demand type, the maximum is selected for design. In this example, Load Case 1 controlled pier column and bearing design forces, while Load Case 2 controlled foundation design forces. This pattern is typical of the SBIA procedure; however, it is possible, given specific pier configurations and loading conditions, for either load case to dominate a given demand. Thus, the maximum demand predicted between both load cases must be considered for design.

Table B.1 SBIA demand prediction summary

	Load Case 1			Load Case 2	Maximum
	Calibrated to pier moment	Calibrated to pier shear	Calibrated to bearing shear		
Column moment (kip-ft)	7,934	--	--	6,688	7,934
Column shear (kips)	--	413	--	343	413
Foundation moment (kip-ft)	11,596	--	--	22,753	22,753
Foundation shear (kips)	--	886	--	1,644	1,644
Total bearing shear (kips)	--	--	922	657	922

APPENDIX C
SBIA PROCEDURE WITH NON-DIMENSIONAL PARAMETERS

C.1 Introduction

In this appendix, the development of a non-dimensional version of the SBIA method is presented. A modified methodology is employed to correlate pier-top inertial resistance factors (IRFs) to non-dimensional ratios of bridge structural parameters. In formulating the SBIA method presented earlier in this report (Chapter 5), discrete optimization was used to develop an optimal combination of structural parameters that correlates well with ideal IRF values (see Chapter 5, Section 5.4.3). In contrast, the methodology employed in this appendix uses a continuous optimization algorithm to find structural parameter combinations that correlate well with IRF values and are also non-dimensional (dimensionless).

C.2 Correlation of IRFs to bridge structural parameters

As discussed in Chapter 5, inertial restraint factors (IRFs) are developed for each bridge in the parametric study. It is assumed that IRF values should correlate well with bridge parameters that are associated with dynamic impact behavior, and that good correlations can be determined by means of optimization. The method described below employs a continuous optimization approach to find optimal correlations between IRF and dimensionless groupings of certain bridge structural parameters. The following quantities are considered:

- Span length (L_{sup})
- Pier height (h_p)
- Superstructure stiffness (k_{sup})
- Pier stiffness (k_p)
- Superstructure weight (W_{sup})
- Pier weight (W_p)

Length, stiffness, and weight parameters related to the superstructure and pier are paired to form non-dimensional ratios with arbitratry exponents (a, b, c) as follows:

$$\gamma = \left(\frac{L_{sup}}{h_P}\right)^a \left(\frac{k_{sup}}{k_P}\right)^b \left(\frac{W_{sup}}{W_P}\right)^c \tag{C.1}$$

The generalized non-dimensional parameter γ is a single scalar quantity that implicitly encapsulates the influences of all six individual structural parameters identified above. While IRF relationships for each demand type (pier moment, pier shear, and total bearing shear) could be correlated to separate forms of γ, each individually optimized, this is considered undesirable due the complexity it would introduce in the design process. Instead, a single functional form of γ is developed and optimized to be the best generalized fitting parameter (in an average sense) across all three demand types. To achieve this goal, a continuous

gradient-based optimization algorithm is used to arrive at optimal values of exponents a, b, and c. Specifically, the algorithm is used to maximize the expression:

$$r^2_{combined} = r^2_m \cdot r^2_v \cdot r^2_b \tag{C.2}$$

where,

$$\begin{aligned} r^2_m &= \text{corr}\left(\gamma, IRF^{ideal}_m\right)^2 \\ r^2_v &= \text{corr}\left(\gamma, IRF^{ideal}_v\right)^2 \\ r^2_b &= \text{corr}\left(\gamma, IRF^{ideal}_b\right)^2 \end{aligned} \tag{C.3}$$

r^2 values represent the coefficient of determination (i.e., square of the correlation coefficient) between γ and the ideal IRF values that have been calibrated to pier column moment, pier column shear, and total bearing shear (IRF^{ideal}_m, IRF^{ideal}_v, and IRF^{ideal}_b, respectively). Optimal exponent values of $a = 0.8$, $b = 0.4$, and $c = 0.6$ are computed with corresponding coefficients of determination of $r^2_m = 0.68$, $r^2_v = 0.41$, and $r^2_b = 0.77$. To develop a cleaner, more design-oriented expression, fractional exponents a, b, and c are rounded to the either 1 or ½ (square root) to obtain a simpler functional form for γ:

$$\gamma = \frac{L_{sup}}{h_P}\sqrt{\frac{k_{sup}}{k_P}\frac{W_{sup}}{W_P}} \tag{C.4}$$

Simplifying the expression in this way influences the strength of correlation only nominally between γ and IRF values for pier moment, pier shear, and total bearing shear, yielding coefficients of determination: $r^2_m = 0.66$, $r^2_v = 0.42$, and $r^2_b = 0.75$. Using this single, and simplified, functional form of γ, data from the parametric study are used to form best-fit linear regression expressions for each demand type:

$$IRF_m = 0.11 + 0.054 \cdot \gamma \tag{C.5}$$

$$IRF_v = 0.22 + 0.031 \cdot \gamma \tag{C.6}$$

$$IRF_b = 0.15 + 0.090 \cdot \gamma \tag{C.7}$$

where IRF_m (Fig. C.1), IRF_v (Fig. C.2), and IRF_b (Fig. C.3) are IRFs calibrated to pier moment, pier shear, and total bearing shear, respectively.

Note that because Eqns. C.5, C.6, and C.7 are best-fit trend lines (fitted through data from the parametric study), they produce static loading conditions that are conservative, when compared to dynamic analysis, in only approximately 50% of conceivable cases. Consequently, an upper bound envelope is needed that greatly increases the likelihood of conservatism. Envelopes are thus developed for each correlation, corresponding to a 99% upper-bound confidence level (using the Student's t-distribution). Envelopes of this form are described (for each demand type) by the following equations (shown also in Figs. C.1 - C.3):

$$IRF_m = 0.24 + \frac{L_{sup}}{14 \cdot h_P}\sqrt{\frac{k_{sup}}{k_P}\frac{W_{sup}}{W_P}} \tag{C.8}$$

$$IRF_v = 0.34 + \frac{L_{sup}}{19 \cdot h_P}\sqrt{\frac{k_{sup}}{k_P}\frac{W_{sup}}{W_P}} \tag{C.9}$$

$$IRF_b = 0.32 + \frac{L_{sup}}{8 \cdot h_P}\sqrt{\frac{k_{sup}}{k_P}\frac{W_{sup}}{W_P}} \tag{C.10}$$

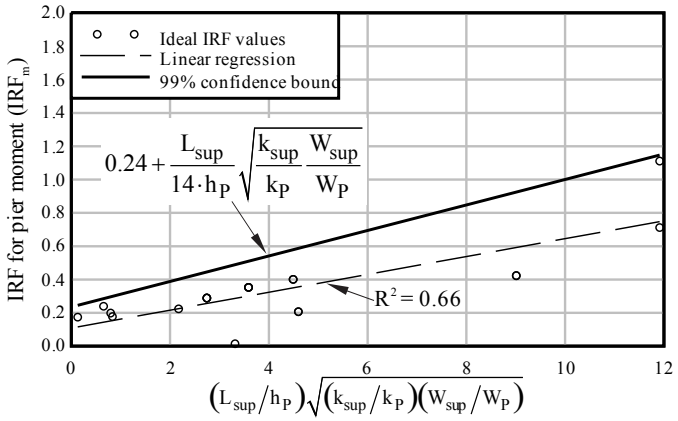

Figure C.1 Correlation of IRF to bridge parameters: calibrated to pier shear

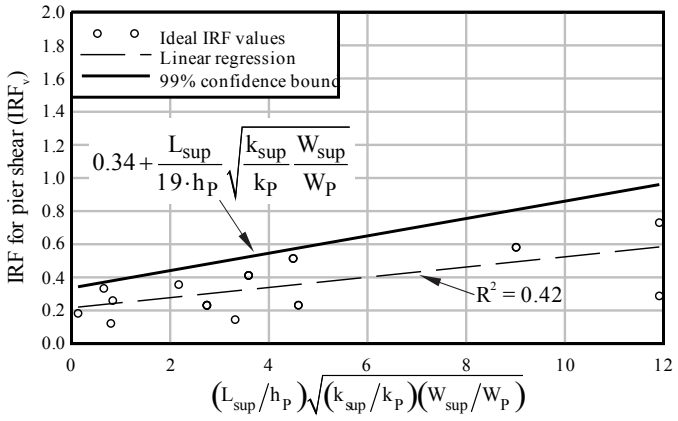

Figure C.2 Correlation of IRF to bridge parameters: calibrated to pier moment

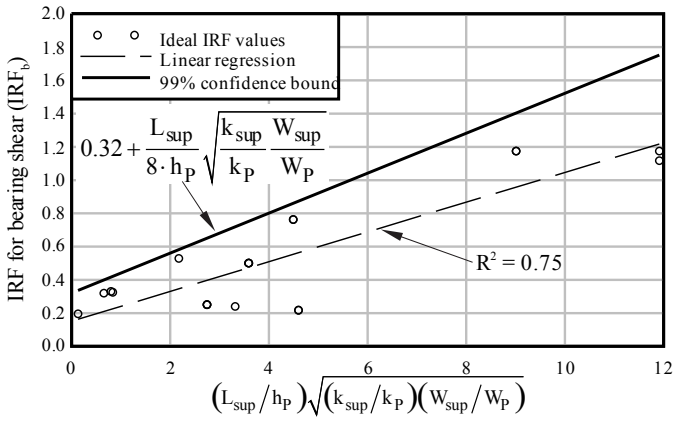

(c) Calibrated to total bearing shear

Figure C.3 Correlation of IRF to bridge parameters: calibrated to bearing shear

C.3 Summary of revised SBIA method

The non-dimensional SBIA procedure that is proposed for design (summarized in Fig. C.4) consists of two overarching load cases. Load Case 1 involves statically applying both an amplified impact load ($1.45 \cdot P_B$) and a static superstructure inertial load ($IRF \cdot P_B$). The magnitude of IRF depends on both bridge structural parameters and the desired pier demand type (pier moment, pier shear, or total bearing shear). Three distinct static analyses must be conducted as part of Load Case 1, each used to predict the pier demand corresponding to the chosen IRF. For example, when the structure is analyzed to predict pier moments—using the IRF corresponding to pier moment (IRF_m)—the column shear, foundation shear, and bearing shear forces predicted by this analysis case are not utilized. Typically, Load Case 1 controls the design of pier columns and bearing connections. Load Case 2 consists of the application of a single amplified impact load ($1.85 \cdot P_B$), and typically controls the design of foundation members (e.g., piles, drilled shafts).

C.4 Parametric study results using the non-dimensional SBIA method

The ability of the non-dimensional SBIA method to conservatively approximate dynamically amplified bridge design forces has been verified by analyzing each bridge and impact condition in the parametric study (see Chapter 4) using CVIA (dynamic analysis) and non-dimensional SBIA (equivalent-static analysis) and comparing the results. For each case, structural demands predicted by SBIA have been normalized by corresponding CVIA demands to form demand ratios. A ratio greater than 1.0 indicates that SBIA is conservative compared to CVIA; a ratio less than 1.0 indicates that SBIA is unconservative.

Based on the data presented in Figs. C.5 through C.7, it is observed that the non-dimensional SBIA method is universally conservative relative to CVIA for the cases studied. Not only is SBIA conservative relative to CVIA, but the overall level of conservatism is reasonably low, with mean values of demand ratios ranging from 1.32 to 1.45 for various demand types. Note that these mean ratios are consistent with the ratios (1.3 – 1.5) that were obtained from the SBIA method presented earlier in Chapter 5. Hence, the non-dimensional SBIA method is found to provide reasonably conservative estimates of

dynamically amplified bridge design forces using a process that involves only static structural analyses.

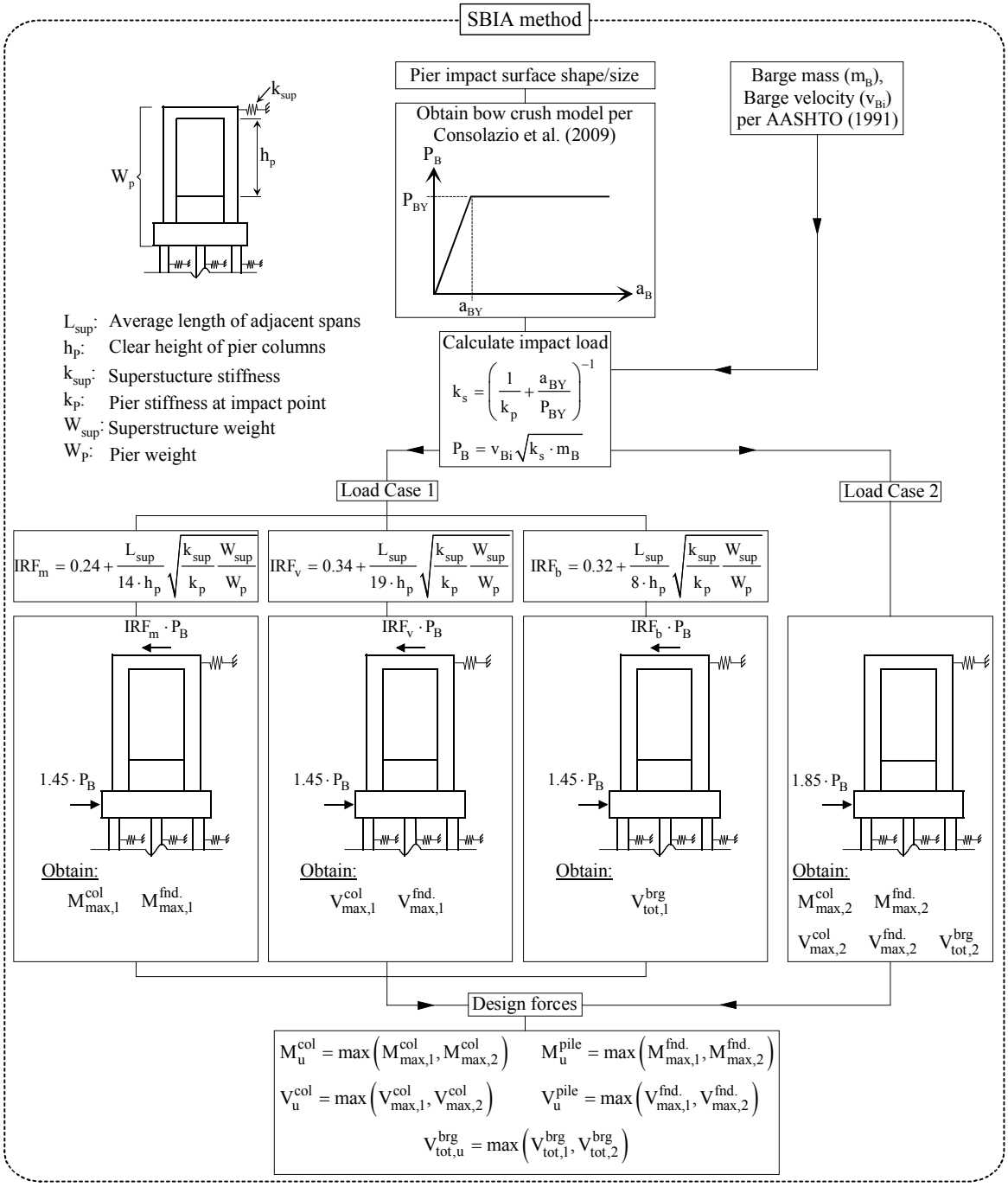

Figure C.4 Revised static bracketed impact analysis (SBIA) method

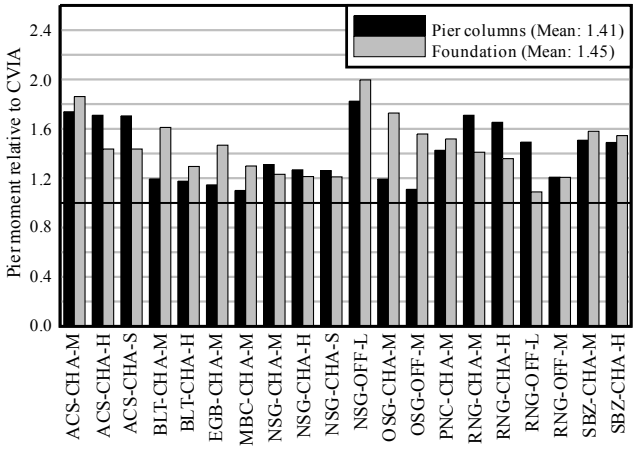

Figure C.5 Non-dimensional SBIA vs. CVIA demand comparison: pier moments

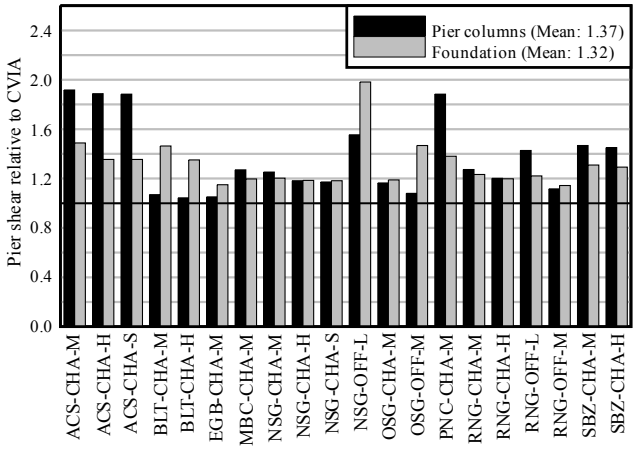

Figure C.6 Non-dimensional SBIA vs. CVIA demand comparison: pier shears

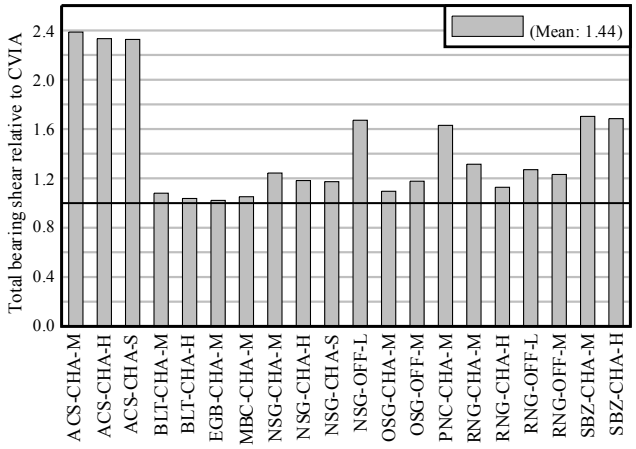

Figure C.7 Non-dimensional SBIA vs. CVIA demand comparison: total bearing shear

APPENDIX D
DEMONSTRATION OF NON-DIMENSIONAL SBIA METHOD

D.1 Introduction

In this appendix, the non-dimensional SBIA method (developed in Appendix C) is demonstrated for the New Trammel Bridge, in northwestern Florida. For this example, a three-barge flotilla (5920 tons with tug) collides with a channel pier at 5.0 knots. Barge impact occurs near the top of a 30.5 ft tall shear wall that connects two 9 ft diameter drilled shafts (Figure D.1). Two circular pier columns (5.5 ft diameter), which are axially collinear with each foundation shafts, span from the foundation elements to the top of the pier.

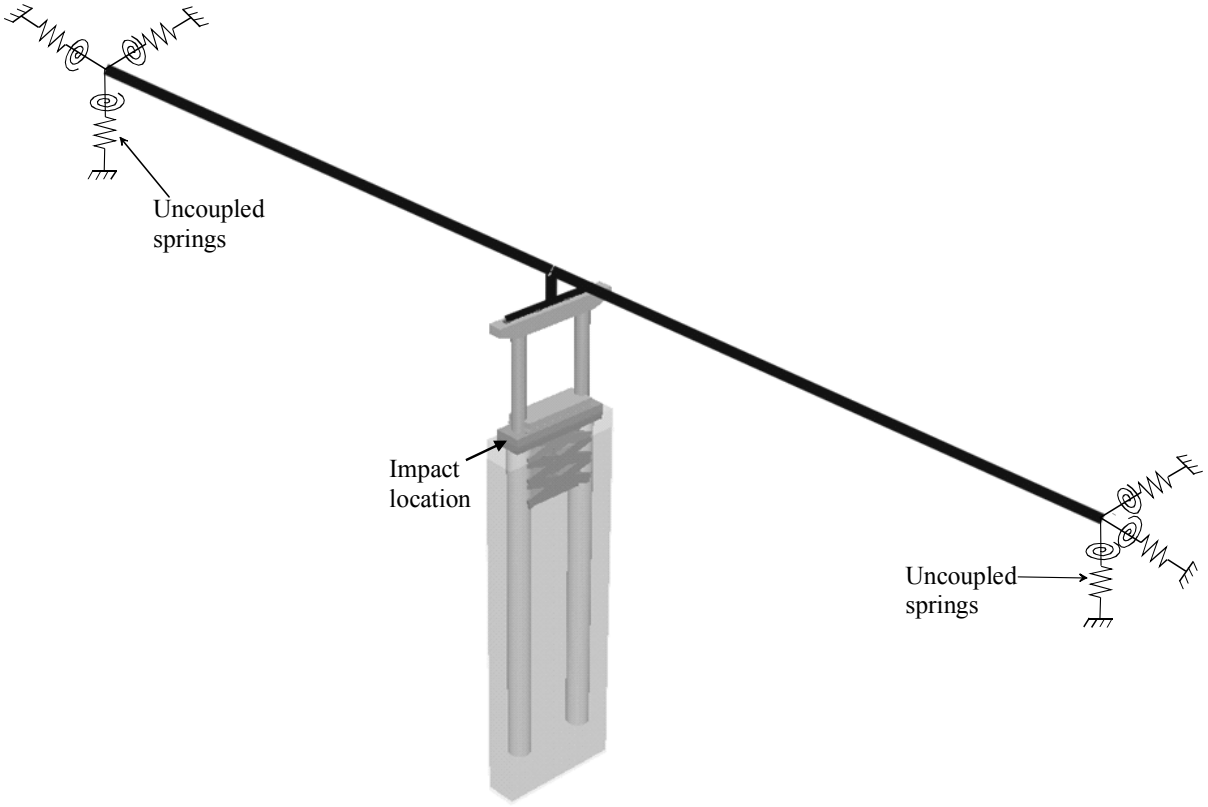

Figure D.1 Structural configuration for New Trammel Bridge

D.2 Demonstration of SBIA procedure

Prior to constructing the SBIA load cases, the vessel impact force must be computed. For this bridge, impact occurs near the top of the shear wall, which has a 9-ft diameter round impact surface ($w_p = 9\,\text{ft}$). Thus, the barge yield force is determined in accordance with Figure D.2 and Equation D.1. Note that this yield force occurs at a crush depth (a_{BY}) of 2 in.

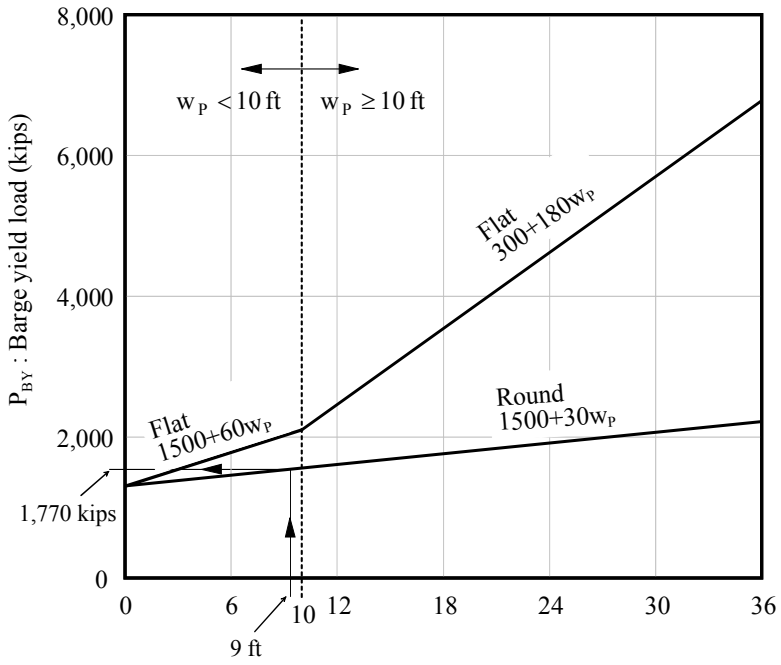

Figure D.2 Barge yield load determination for 9-ft round impact surface

$$P_{BY} = 1500 + 30 \cdot w_p = 1500 + 30 \cdot (9) = \boxed{1770\,\text{kips}} \tag{D.1}$$

With the yield force quantified, the impact force corresponding to the high-energy barge collision (5920-ton flotilla, traveling at 5.0 knots) is computed. First, the series stiffness of the barge and pier/soil system (k_S) is calculated per Equation D.3. Note that the stiffness of the pier/soil system for this bridge (k_P) must be quantified as shown in Figure D.3 and Equation D.2. For this example, P_{BY} is applied to the pier to quantify k_P; however, if the calculated impact load (P_B) is found to be less than P_{BY}, then this process should be repeated to obtain a more accurate estimate of k_P.

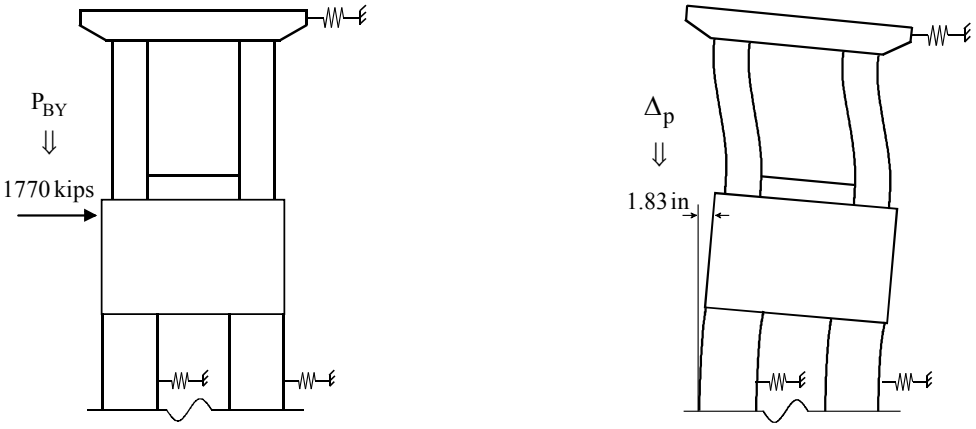

Figure D.3 Determination of pier stiffness (k_P)

$$k_P = \frac{P_{BY}}{\Delta_p} = \frac{1770}{1.83} = \boxed{963\,\text{kip/in}} \tag{D.2}$$

$$k_S = \left(\frac{a_{BY}}{P_{BY}} + \frac{1}{k_P}\right)^{-1} = \left(\frac{2}{1770} + \frac{1}{963}\right)^{-1} = \boxed{461\,\text{kip/in}} \tag{D.3}$$

Thus, the high-energy crush force is computed given the barge tow velocity (v_{Bi}) of 5.0 knots (101 in/s) and mass (m_B) of 5920 tons (30.7 kip/in/s^2):

$$\begin{aligned} &P_B = v_{Bi} \cdot \sqrt{k_S \cdot m_B} = (101) \cdot \sqrt{(461) \cdot (30.7)} = 12{,}015\,\text{kips} \\ &12{,}015\,\text{kips} > P_{BY} \\ &\therefore P_B = P_{BY} = \boxed{1{,}770\,\text{kips}} \end{aligned} \tag{D.4}$$

This calculation illustrates that the incoming kinetic energy of the barge tow is sufficient to yield the barge bow, generating the maximum crush force for this pier (1770 kips).

D.3.1 Load Case 1

With the barge impact load (P_B) quantified, the SBIA load cases are constructed. For Load Case 1, the amplified static impact load is computed:

$$1.45 \cdot P_B = 1.45 \cdot (1770) = \boxed{2567\,\text{kips}} \tag{D.5}$$

This amplified impact load is used for each part of Load Case 1, regardless of the demand type of interest. However, unique pier-top loads are computed, corresponding to pier moment, pier shear, and total bearing shear. To quantify these loads, corresponding IRFs are calculated, based on the bridge structural parameters illustrated in Figure D.4 and Figure D.5.

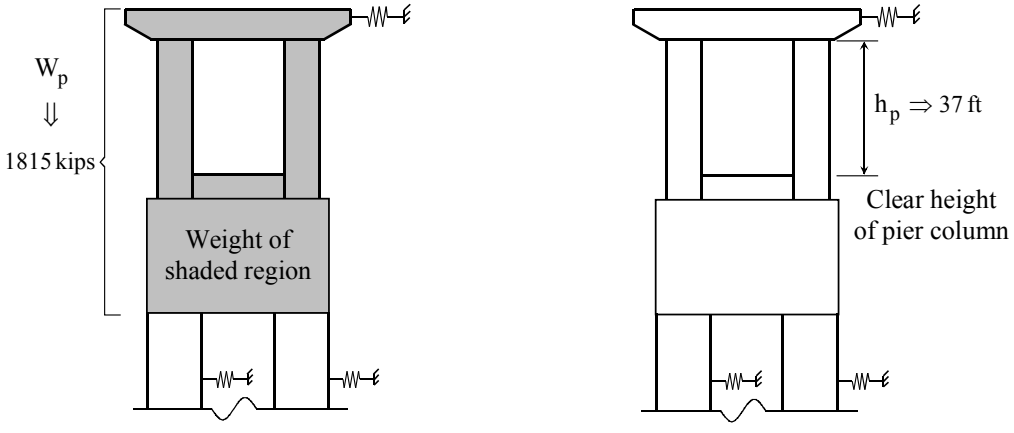

Figure D.4 Determination of pier weight (W_P) and pier height (h_p)

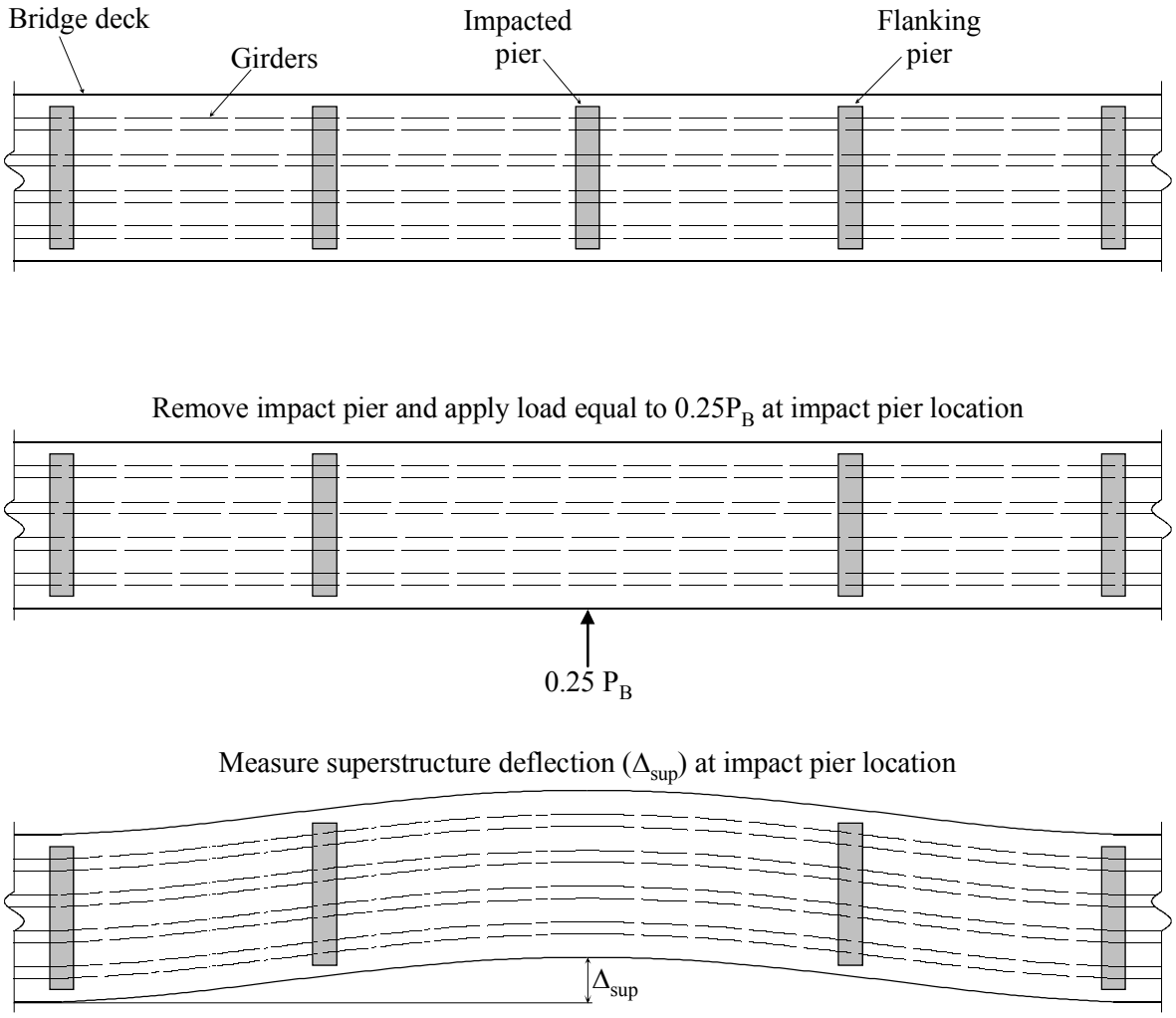

Figure D.5 Determination of superstructure stiffness (k_{sup})

For this bridge, the average span length adjacent to the impacted pier (L_{sup}) is 252 ft, and the weight of this length of span (W_{sup}) is 2521 kip. As illustrated in Figure D.4, the total weight of this pier (W_p) is 1815 kips, and the height of the pier (h_p) is 37 ft. The lateral superstructure stiffness (k_{sup}) is 199 kip/in, as determined using the process shown in Figure D.5, and the lateral pier stiffness (K_P) is (1770 kip / 1.83 in.) = 963 kip/in, as shown in Figure D.3. Thus,

$$IRF_m = 0.24 + \frac{L_{sup}}{14 \cdot h_P}\sqrt{\frac{k_{sup}}{k_P}\frac{W_{sup}}{W_P}} = 0.24 + \frac{(252)}{14 \cdot (37)}\sqrt{\frac{(199)}{(963)}\frac{(2521)}{(1815)}} = \boxed{0.50} \quad (D.6)$$

$$IRF_v = 0.34 + \frac{L_{sup}}{19 \cdot h_P}\sqrt{\frac{k_{sup}}{k_P}\frac{W_{sup}}{W_P}} = 0.34 + \frac{(252)}{19 \cdot (37)}\sqrt{\frac{(199)}{(963)}\frac{(2521)}{(1815)}} = \boxed{0.53} \quad (D.7)$$

$$IRF_b = 0.32 + \frac{L_{sup}}{8 \cdot h_P}\sqrt{\frac{k_{sup}}{k_P}\frac{W_{sup}}{W_P}} = 0.32 + \frac{(252)}{8 \cdot (37)}\sqrt{\frac{(199)}{(963)}\frac{(2521)}{(1815)}} = \boxed{0.78} \quad \text{(D.8)}$$

The amplified impact load (as computed in Equation D.5) is applied at the impact location for all three analyses. For each of the three analyses, the corresponding IRF (as calculated in Equations D.6, D.7, and D.8) is multiplied by the impact force (P_B), and this load is applied at the pier cap beam center of gravity, in the opposite direction of impact (Figure D.6).

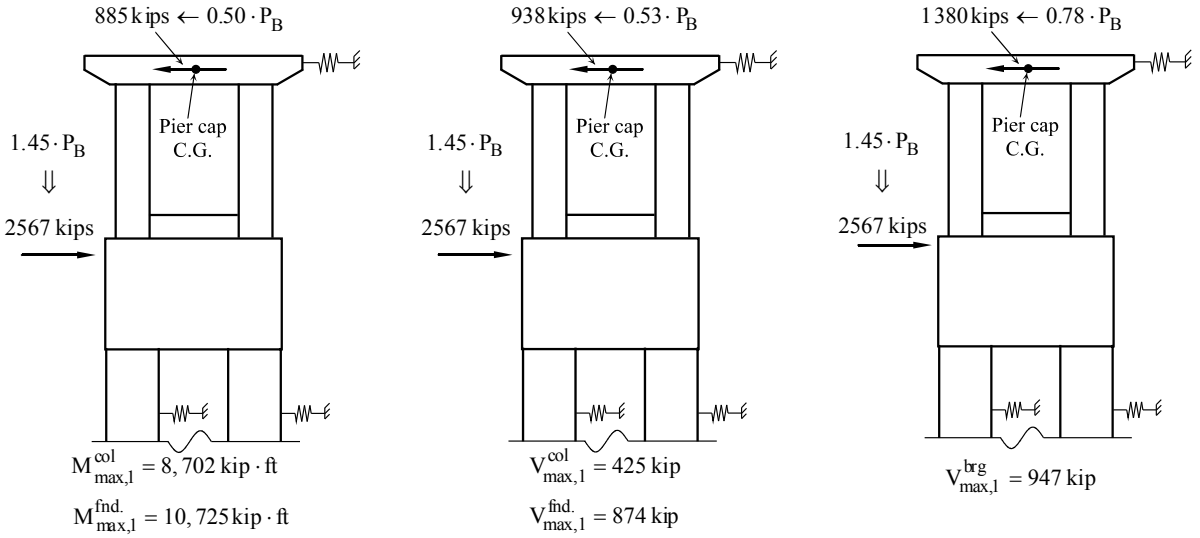

Figure D.6 Loading conditions and maximum demand predictions for Load Case 1

With the loading conditions for Load Case 1 developed, the structure is statically analyzed. Predictions of pier (column and foundation) moment, pier (column and foundation) shear, and total bearing shear demands are quantified using the respective analyses (Figure D.6). These design forces are additionally summarized in Table D.1.

D.4.1 Load Case 2

SBIA Load Case 2 is analyzed as shown in Figure D.7. From this single analysis, all pertinent member forces are quantified—pier moments, pier shears, and total bearing shear. These demands are compared to those obtained from Load Case 1 in Table D.1. The amplified impact load for Load Case 2 is calculated as:

$$1.85 \cdot P_B = 1.85 \cdot (1770) = \boxed{3275\,\text{kips}} \quad \text{(D.9)}$$

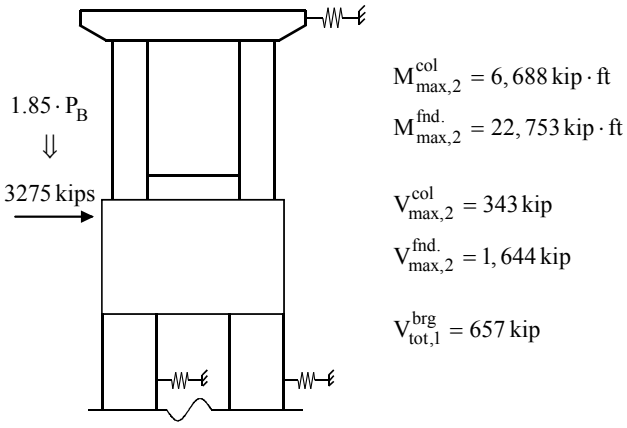

Figure D.7 Loading conditions and maximum demand predictions for Load Case 2

D.5.1 Results summary

Design forces predicted by Load Cases 1 and 2 are summarized in Table D.1. For each demand type, the maximum is selected for design. In this example, Load Case 1 controlled pier column and bearing design forces, while Load Case 2 controlled foundation design forces. This pattern is typical of the SBIA procedure; however, it is possible, given specific pier configurations and loading conditions, for either load case to dominate a given demand. Thus, the maximum demand predicted between both load cases must be considered for design.

Table D.1 SBIA demand prediction summary

	Load Case 1			Load Case 2	Maximum
	Calibrated to pier moment	Calibrated to pier shear	Calibrated to bearing shear		
Column moment (kip-ft)	8,702	--	--	6,688	8,702
Column shear (kips)	--	425	--	343	425
Foundation moment (kip-ft)	10,725	--	--	22,753	22,753
Foundation shear (kips)	--	874	--	1,644	1,644
Total bearing shear (kips)	--	--	947	657	947